Travail de fin d'études et stage[BR]- Travail de Fin d'Etudes : Modelling waste heat recovery systems applied to heavy duty vehicles[BR]- Stage d'insertion professionn

Auteur : Lambrechts, Sébastien
Promoteur(s) : Lemort, Vincent
Faculté : Faculté des Sciences appliquées
Diplôme : Master en ingénieur civil mécanicien, à finalité spécialisée en technologies durables en automobile
Année académique : 2019-2020
URI/URL : http://hdl.handle.net/2268.2/10265

MASTER THESIS

Modelling waste heat recovery systems applied to heavy duty vehicles

Sébastien Lambrechts

Master thesis conducted with the aim of obtaining the Master's degree in Mechanical Engineering (Sustainable automotive engineering)

Academic supervisor: Vincent Lemort
Industrial supervisor: Thomas Reiche

INTERNSHIP AT VOLVO - GROUP TRUCKS TECHNOLOGY LYON
(POWERTRAIN STRATEGIC DEVELOPMENT)

University of Liège - Faculty of Applied Sciences
Academic year 2019-2020

Abstract

Future European regulations imposing large decrease in CO_2 emissions force the manufacturers of heavy-duty vehicles to implement innovative solutions to achieve these challenging targets. In this context, waste heat recovery systems represent a suitable solution to exploit thermal energy lost to the ambient by diesel engines. To this end, waste heat recovery by means of an Organic Rankine cycle (ORC) is considered as a promising technology. This thermodynamic bottoming cycle aims to recover thermal power in order to produce electricity on-board, that can be injected into mild-hybrid drivelines.

Volvo Trucks is studying for many years this fuel-saving technology. In the scope of their current project in which this internship takes part, exhaust gases downstream the exhaust after treatment system are exploited as heat source. The heat sink is simply the ambient air, driven towards the condenser placed behind the cab by two fans. A piston expander is used to produce mechanical power, which is in turn converted into electricity to charge a 48V battery of a mild-hybrid truck.

The modelling of an ORC is a major aspect of the system design methodology. Indeed, simulations are used in the early design phase to compare several system architectures and to select the most appropriated working fluid. At a later stage, the plant model can be exploited to design the controller of the ORC system. It is thus essential to develop a precise and efficient model integrating all the components of the Rankine cycle (heat exchangers, expander, pump, etc.) as well as an accurate procedure to compute working fluid properties. In this context, the present work aims to improve the ORC simulation tool developed by *Volvo Trucks* on *Matlab-Simulink*.

At first, a new moving boundaries (MB) model of heat exchanger is developed to replace the previous one, based on a finite volumes (FV) approach. This new model is as accurate as the FV model, but it is computationally faster. This robust model takes the form of a *Simulink* library and is exploited to model the exhaust boiler as well as the air condenser in the complete Rankine system model. It is validated regarding both steady-state and transient simulations. Thanks to this new approach of heat exchanger modelling, the computational time required to perform simulations of the ORC during a road driving cycle is drastically reduced (-72%).

Secondly, this master thesis is dedicated to the modelling of the lubricant added to the working fluid performing the Rankine cycle. This oil is needed in practice to ensure the lubrication of the piston expander, but its presence was neglected up to now in the Rankine simulation tool where pure working fluid properties are assumed. However, a brief literature review shows that it could have a significant impact on ORC performances. To this end, an empirical solubility model is exploited to compute thermodynamic properties of the mixture composed of working fluid (cyclopentane) and Polyalkylene Glycol (PAG) synthetic oil. In addition, all the components of the Rankine model are revised to take into account the presence of lubricant. This study concludes that the net ORC power is clearly impacted by the presence of lubricant. This decrease in net power depends on the exhaust conditions, the ambient air temperature and the oil circulation rate.

Keywords: waste heat recovery, organic Rankine cycle, automotive, modelling, heat exchanger, moving boundaries model, heat transfer, PID controller, lubricant, solubility model.

Acknowledgements

Firstly, I would like to thank my two supervisors: Thomas Reiche from Volvo Trucks and Vincent Lemort from the Thermodynamic laboratory of the University of Liège. This master thesis would have been much more difficult without their daily support and their help to solve practical and theoretical issues. I also express all my gratitude to them for their guidance during the Covid-19 pandemic, which made my internship more difficult than expected.

I also want to thank the other members of the examination committee, Pierre Duysinx and Olivier Dumont, for the time they spent to read this manuscript and to evaluate my master thesis. Furthermore, my colleagues from Volvo Trucks are thanked, as well as Prof. Jader Barbosa from the Federal University of Santa Catarina for his help and the experimental data he shared with me to improve this work.

I am also infinitely grateful to my family for their encouragements and unfailing support all along my studies. I know that they greatly facilitated these five years at the University.
Special thanks to all my friends and colleagues for the moments spent working together before and during this master thesis, especially François, Astrid and Nicolas.

Last but not least, I have to thank my sweet Manon for her unconditional and lovely support in every situation. Even if I don't often say it, I am aware that this is a chance to have you by my side.

List of abbreviations

- BDC: Bottom Dead Center
- BSFC: Break-Specific Fuel Consumption
- CAC: Charge Air Cooling
- COR: Cut-off Ratio
- EATS: Exhaust After Treatment System
- EGR: Exhaust Gas Recirculation
- EU: European Union
- FEM: Finite Element Method
- FK: Frankfurt-Koblenz (road cycle)
- FV: Finite Volume
- GSP: Global Simulation Platform
- GWP: Global Warming Potential
- HDV: Heavy-Duty Vehicle
- HTC: Heat Transfer Coefficient
- ICE: Internal Combustion Engine
- ISO: International Organization for Standardization
- MB: Moving Boundary
- NEDC: New European Driving Cycle
- ODP: Ozone Depletion Potential
- ORC: Organic Rankine Cycle
- PAG: Polyalkylene Glycol synthetic oil
- PID: Proportional Integral Derivative (controller)
- SC: Sub-cooling
- SH: Super-heating
- SP: Set-point
- TDC: Top Dead Center
- TEG: Thermo-Electric Generator
- VG: ISO viscosity grade
- WF: Working Fluid
- WHR: Waste Heat Recovery
- WLTP: Worldwide harmonized Light vehicles Test Procedures

Contents

Manuscript contents

This manuscript is organized in three main parts:

1. The first part contains the report of the internship carried out at *Volvo Trucks* (Lyon) in the scope of this master thesis (Chapter 1). The company is briefly presented and the internship environment is described.
   After introducing current challenges of the automotive industry, Chapter 2 is dedicated to the state of the art on waste heat recovery by means of Organic Rankine Cycle. An overview of the different system architectures is presented, and several important aspects are discussed: fluid selection, interaction with the vehicle cooling system, control challenges, limiting factors, etc. The Rankine system developed currently by *Volvo Trucks* is also introduced.

2. The second part corresponds to Chapter 3. After a literature review on heat exchanger modelling, the moving boundary heat exchanger model developed on *Matlab-Simulink* during this internship is presented in detail. Once the new model is integrated into the complete model of the Rankine system, steady-state and transient simulations along a driving cycle are performed to assess the quality of this exchanger model, in comparison with the previous one developed by *Volvo Trucks*.

3. Chapter 4 forms the third part, which is devoted to the simulation of the Rankine system while taking into account the presence of lubricant added to the working fluid performing the Rankine cycle. The chosen solubility model fitted with empirical data is presented and discussed, in order to compute thermodynamic properties of the mixture composed of working fluid and oil. After that, required modifications of the component models are highlighted to deal with the presence of lubricant in the Rankine system model. Simulation results are then discussed and compared to the system performances obtained by assuming a pure working fluid.

Finally, a global conclusion of this master thesis as well as perspectives are proposed in Chapter 5.

1 | Internship report

The *Volvo Group* (also called *AB Volvo*) is a Swedish manufacturer of heavy vehicles, whose headquarters are situated in Gothenburg. Volvo Group sells trucks, buses, construction equipment as well as marine and industrial engines in 190 markets. It was founded in 1927 by Assar Gabrielsson and Gustav Larson. The group is now a multinational company represented by more than 100,000 employees all around the world, holding production facilities in 18 different countries. Martin Lundstedt is currently the Volvo group president and CEO. It was the world's second-largest heavy-duty trucks manufacturer in 2016.

Volvo Group activities in heavy vehicles are divided into five brands: *Volvo Trucks* (Europe and South America), *Renault Trucks* (Europe and Africa, integrated to Volvo Group in 2002), *Mack Trucks* (North America), *UD Trucks & JVs* (Asia) and *Arquus* (armored vehicles, previously called *Renault Trucks Defense*). In addition, other brands are responsible for the sales of buses, marine engines, construction equipment, etc. The automobile manufacturer *Volvo Cars* was part of the Volvo Group until its sale to the *Ford Motor Company* in 1999.
Three main divisions are defined in the truck activity of Volvo Group, and are common to all truck brands. Group Trucks Technology (GTT) is the division in charge of research and development for powertrain, complete vehicles and components. Group Trucks Operations (GTO) is responsible for the manufacturing of engines, transmissions and cabs, as well as the assembly of whole trucks. The third division is called Group Trucks Purchasing (GTP) and is in charge of the products purchase and aftermarket.

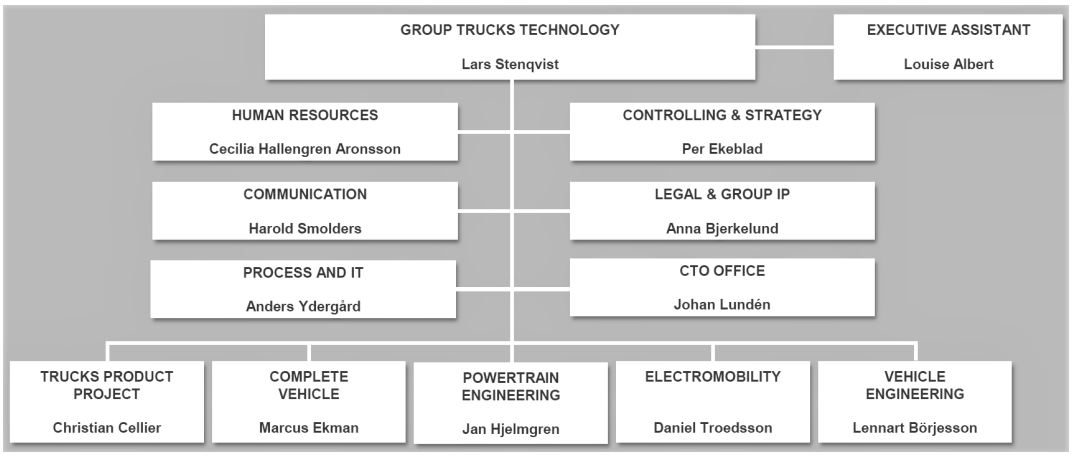

Figure 1.1: Organization of Volvo GTT (Group Trucks Technology).

My internship at Volvo has lasted 6 months, between the 3rd of February to the 24th of July 2020. It took place in Lyon (Saint-Priest), which is the historic industrial site of Renault Trucks. I have worked in the GTT division (8,300 employees including 1575 people working in Lyon), more precisely in the Powertrain Engineering department (Fig. 1.1). This department is divided into different teams, and I was integrated to the Concept Creation team of the Powertrain Strategic Development. This R&D team

is composed of a dozen engineers working on new powertrain concepts developed to reduce fuel consumption and CO_2 emissions of trucks: hybrid systems, innovative combustion engines, fuel cells and waste heat recovery systems. These concepts are modelled, designed and finally tested experimentally. Prototypes are also built for the proof of concept.

My internship was devoted to the modelling of a waste heat recovery system by means of Organic Rankine cycle (ORC). Basically, this system aims to recover thermal energy from exhaust gases to produce electricity using a thermodynamic cycle. The research project dedicated to this system is called *Rankine Generation 3*, and is led by Thomas Reiche which was my direct supervisor. This project is also carried out in collaboration with industrial partners, subcontractors and research laboratories.

The ORC system is simulated on *Matlab-Simulink 2017b*. This model aims to be integrated to a global simulation platform (called GSP) created by assembling all the numerical models of truck components (engine, gear box, cooling system, etc.). Then, this platform is used to simulate road driving cycles. As part of my internship, I was focused on the improvement of the Rankine simulation tool, without performing simulation on GSP.
My first goal was the development of a new heat exchanger model, to represent the three heat exchangers integrated to the Rankine system (exhaust boiler, air condenser and recuperator). The main objective of this model is to be computationally faster than the one previously developed by *Volvo Trucks*, without loss in precision. To this end, a moving boundary approach is preferred to model heat exchangers, instead of the finite volume method that was chosen for the previous model.
The second part of my internship was devoted to the simulation of the Rankine system in steady conditions and during transient cycles, taking into account the impact of lubricant added to the working fluid. In fact, the presence of oil was not modelled so far in the Rankine simulation tool, but its impact could be significant. This second task was not initially planned at the beginning of my internship, but it was important to improve the quality of my master thesis, knowing that a 6-month internship allowed me to increase my workload.

In order to perform these two personal tasks, I have worked alone with little interaction with other members of the team. Thomas Reiche was my sole supervisor at *Volvo Trucks*, and regular meetings were organized via Skype with Vincent Lemort, my supervisor from the University of Liège. I have worked with a lot of autonomy, and other small tasks that are not reported in this manuscript were entrusted to me during my internship. Beyond my personal work, I have regularly participated in project presentations, Matlab training and pulse meetings where all the team members present the status of their work.

The Covid-19 pandemic had a significant impact on my internship. Firstly, Thomas Reiche and a majority of the team were temporarily unemployed during about 3 months (from mid-March to mid-June). It was thus difficult for me to continue to progress on my work in these circumstances, as I was not directly supervised. However, I have kept in touch with Thomas Reiche, and Vincent Lemort took a closer look at my work during this period.
Then, the return to work was done by teleworking until the end of my internship, without going back to the office more than a few days. Despite this situation, I am nevertheless satisfied with my work, and grateful to my supervisors who did their best to help me during this very particular period.

2 State of the art on ORC power systems for waste heat recovery

2.1 Introduction

According to the European Union (EU), duty vehicles are nowadays responsible for a quarter of CO_2 emissions originating from the road-transport sector in Europe [1]. It corresponds to 6% of total European emissions. In the past few years, even with improvements of diesel engines integrated to duty vehicles, these emissions have not been reduced because of the increasing road freight traffic. As a result, the European Commission has fixed new regulations limiting the CO_2 emission standards for duty and heavy-duty vehicles. From 2025, average emissions of the fleet of new lorries put on the market by a given manufacturer have to be reduced by 15%, with respect to the level of 2019. And this target will be further increased to 30% from 2030. Other emission standards, including very stringent American targets are shown in Fig. 2.1.
European manufacturers consider that the 2025 objective would be achieved thanks to improved systems and technologies that are already or nearly put on the market today. However, the 2030 target needs to develop new technologies to reduce CO_2 emissions. In fact, it seems that diesel engine's efficiency is reaching a physical limitation around 40% for duty vehicles, which means that further improvements have to emerge from other technical breakthroughs. For this purpose, but also to face the increase of fuel prices, trucks manufacturers are developing waste heat recovery (WHR) systems for diesel engine applications.

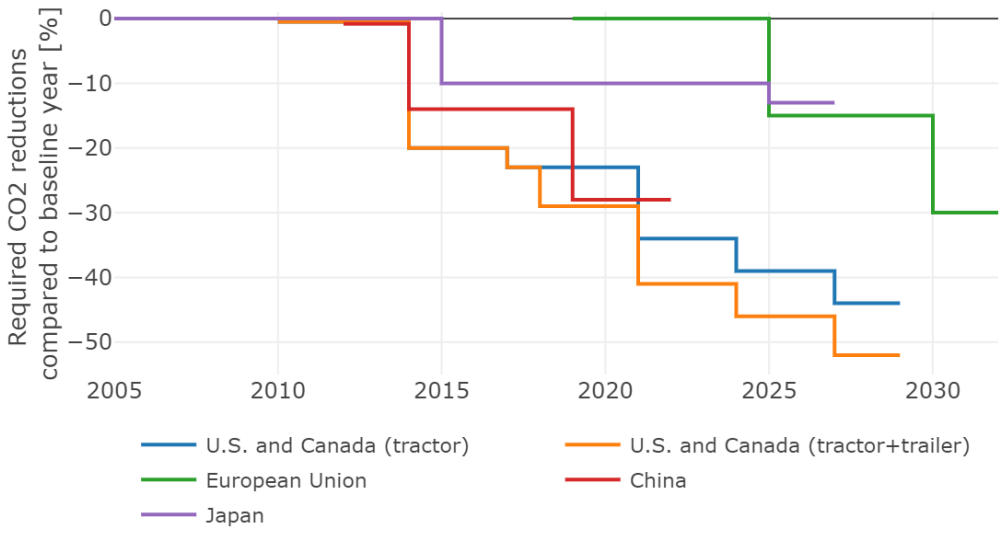

Figure 2.1: CO_2 reduction standards imposed by several countries to tractor trucks manufacturers with respect to the baseline year (data from *Rodriguez and Delgado* [2]).

2.2 Waste heat recovery technologies

It is well known that for internal combustion engines (ICE), roughly one third of the energy contained in the fuel and released during the combustion process is effectively transformed into mechanical work to propel the vehicle. Another third of this energy is wasted in the coolant system, required to maintain the engine around its optimal working temperature. Finally, the last third of the fuel energy is released in the exhaust gases. A more precise distribution between these energy fluxes is presented by *Xu et al.* in [3] and reported in Fig. 2.2. This distribution corresponds to averaged steady-state results obtained with two heavy-duty diesel engines, considering different operating points (engine speed and torque). In this experimental study, the energy wasted due to the cooling processes is divided into three contributions: the engine coolant, the exhaust gas recirculation (EGR) system and the charge air cooling (CAC).

One of the waste heat recovery technologies developed for duty vehicles are thermoelectric generators (TEGs). From the temperature difference between a hot source (commonly the exhaust pipe or EGR) and the engine coolant, semiconductor materials are able to produce directly electric energy thanks to the *Seebeck effect*. Even if this phenomenon was discovered in 1821, this technology is not yet mature. However, the main benefits are the easy packaging of TEGs and the lack of moving part [4]. Thermoelectricity has always a very low efficiency, characterized by the low figure of merit (ZT) of semiconductor materials. It is also important to highlight that a given material is not able to effectively recover energy independently of the heat source temperature.

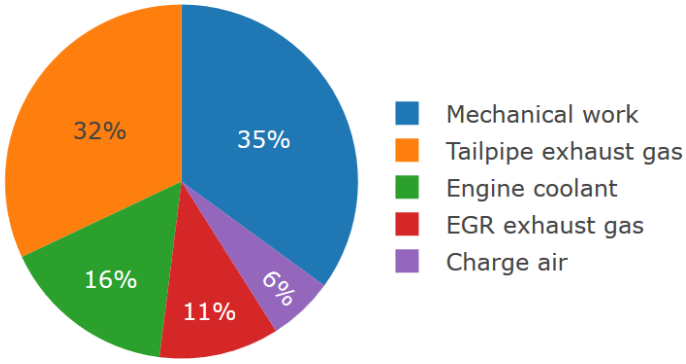

Figure 2.2: Experimental results of heavy-duty vehicles waste energy distribution based on two heavy-duty diesel engines: 2006MY 10.8L Cummins ISX and 2004MY 10.8L Mack MP7-355E (data from *Xu et al.* [3]).

Espinosa et al. in [5] have modelled a TEG composed of Mg_2Si/Zn_4Sb_3 and Bi_2Te_3. Using two different semiconductor materials aims to recover energy for both high (Mg_2Si/Zn_4Sb_3) and low temperatures (Bi_2Te_3) heat sources. The potential sources on a long-haul truck diesel engine are the following: the coolant water (90°C-110°C), the exhaust gases (250°C-350°C), the EGR gases (400°C-500°C) and the charge air cooler outlet gases (∼150°C). In this study, the exhaust gases are chosen as heat source even if the EGR gases are warmer due to the energy loss in the turbocompressor. In fact, exergy calculations show that exhaust gases offer more available energy thanks to their higher mass flow rate. The recovered electric power varies between 100 and 1200 W, depending on the number of Mg_2Si/Zn_4Sb_3 thermoelements along the TEG. However, experiments were conducted in optimistic situations. Generally, it is considered that the thermal efficiency of TEG is between 2% and 4% according to [3] and [6].

In [7], *Saidur et al.* introduce the six-stroke internal combustion engine as another type of WHR system. The working principle is similar to a typical four-stroke engine (intake stroke, compression stroke,

combustion stroke and exhaust stroke). In addition, two added cycles aim to increase the efficiency and/or decrease emissions by recovering energy from expanded exhaust gases. Two types of 6-strokes engines can be distinguished: those benefiting from the thermal energy of exhaust gases (to generate steam from liquid water injected into the cylinder) and the others taking advantage of the relatively high pressure of exhaust gases. A lot of patents have been awarded for such engines; nevertheless these technical solutions were never put on the market due to their too high complexity.

The study conducted by *Liu et al.* in [6] is only focused on technologies recovering energy from exhaust gases called *direct or indirect bottom cycles*. Direct recovery cycles are defined as methods based on a secondary expansion of exhaust gases (i.e. downstream of the engine). A turbocharger or turbocompressor, defined in [7] as a supercharger that is driven by exhaust energy, is an example of direct recovery. Heat and pressure contained in the exhaust gases are exploited to drive a gas turbine, from which mechanical energy is retrieved to compress the air that supplies the engine. Another direct recovery technology from exhaust gases is turbocompounding. In this case, the mechanical energy produced by the gas turbine is either directly transferred mechanically to the driveline, either transformed into electricity using a generator. In any case, the increase in backpressure and pumping losses for the ICE limits the interest for direct recovery cycles. Moreover, the gas turbine produces mechanical power only during relatively high load engine conditions, when the exhaust mass flow and pressure are sufficient to drive effectively the turbine.

On the other hand, indirect recovery is defined in [6] as methods based on heat transfer between exhaust gases and a working fluid performing a thermodynamic cycle, such as Rankine steam cycle and Brayton air cycle. In this case, it is the thermal energy of gases that is recovered, while direct recovery cycles recover part of the mechanical energy of the exhaust mass flow. As a result, the working pressure of the bottom cycle is decoupled from the exhaust engine pressure.
Indirect recovery cycles mainly depends on the selected working fluid. With a liquid working medium, little compression work is needed to reach high working pressure. A high volume flow rate is obtained by increasing the working medium volume during the phase change process (evaporation). Mechanical energy is then produced using an expander, which can also be connected to a generator to create electricity. In addition to the heat source, a heat sink is needed according to the second law of thermodynamics formulated by Kelvin-Planck, to retrieve the working medium in liquid state. If this liquid fluid is water, the well-known Rankine steam cycle is recovered.
On the other hand, when air is used as working medium, the bottom cycle does not exhibit any phase transition (Brayton air cycle). In this case, an open cycle is possible and would be more convenient for transport applications, without using a condenser.

Liu et al. conclude in [6] that direct bottom cycle by secondary gas expansion (turbocompound) has a little potential for gasoline engine. The interest would be even negative regarding the increased backpressure for the ICE. For diesel engine, turbocompound is an efficient technical solution, especially at full load when the exhaust pressure is elevated. On the other hand, indirect bottom cycles are suitable in terms of energy recovery potential thanks to their relatively good functioning at part load. The Rankine cycle is much more efficient than Brayton cycle, even if a cycle with phase transitions is even more challenging in terms of packaging and integration into the vehicle.

A comparison of waste heat recovery technologies in terms of several indicators (efficiency, costs, maturity and packaging) is presented by *Legros et al.* in [4] for automotive application. Their results are summarized in Fig. 2.3. They conclude that turbocompouding and Rankine cycle are the best suited technologies to be integrated into a car in the near future, thanks to their good efficiency and a relatively high level of maturity. Joule and Stirling cycles are considered as not suitable for automotive applications and are not addressed in the present document, likewise thermophotovoltaic applications that are in their early development phase.

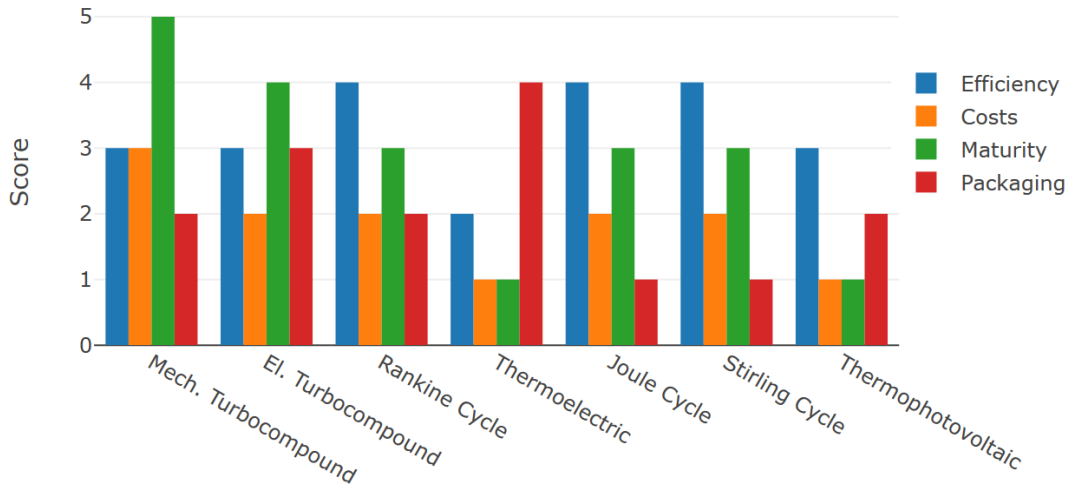

Figure 2.3: Performance indicators of waste heat recovery technologies in the transport sector (*data from Legros et al. [4]*).

Legros et al. have developed models to compare TEGs, Rankine cycles and electrical turbocompound from vehicle data during two different road cycles: the New European Driving Cycle (NEDC) and the Worldwide harmonized Light vehicles Test Procedures (WLTP). The Rankine system model is calibrated with experimental measurements, while the models describing TEG and turbocompound are much simpler. The principal interest of these simulations is that they are performed in a complete mid-size hybrid vehicle environment, where the additional weight induced by these waste heat recovery technologies is taken into account (10 kg for thermoelectricity and turbocompound, 20 kg for Rankine cycle). To simplify the comparison, in any case the produced electrical energy is directly transferred to the vehicle shaft, reducing the power needed from the thermal engine. For both atmospheric or turbocharged engines, the turbocompound exhibits the best reduction in break-specific fuel consumption (BSFC). However, this model does not take into account the additional counterpressure acting at the engine exhaust due to the gas turbine, resulting in an overestimated decrease in BSFC. The Rankine system is the second most efficient technology, and exhibits nearly the same benefits than turbocompound during WLTP test. The thermoelectric generator is far behind due to its very low efficiency.
The peak power produced by the turbocompound is much higher than the Rankine system power, but the recovery is possible during only 19% of the time for the NEDC (and 35% for the WLTP), when the exhaust mass flow is sufficient to drive the gas turbine (acceleration phases). By contrast, the Rankine system is used during 64% of the time during the NEDC test (and 71% for the WLTP), so that the decrease in peak power with respect to the turbocompound is balanced when the comparison is performed from averaged power results. Finally, the TEG is used almost all the time.

From the different aspects mentioned above, waste heat recovery by Rankine cycle integrated to heavy-duty vehicles is a suitable technical solution to further enhance diesel engine efficiency and achieve the goals of the EU in terms of CO_2 emissions. Despite major problems of packaging and limiting factors when integrated to road vehicles, Organic Rankine cycle is a heavily researched topic and will be undoubtedly one of the technologies shaping the future of some truck manufacturers.

2.3 Organic Rankine Cycle

2.3.1 Generalities

Waste heat recovery by Organic Rankine Cycle (ORC) is very similar to the well-known steam Rankine cycle, based on two pressure levels: a liquid working fluid (WF) is vaporized at high pressure in a boiler and then expanded to generate mechanical power. After that, the working fluid is condensed in a second heat exchanger and the cycle is closed by a pump to bring back the fluid at the high-pressure level (Fig. 2.4).

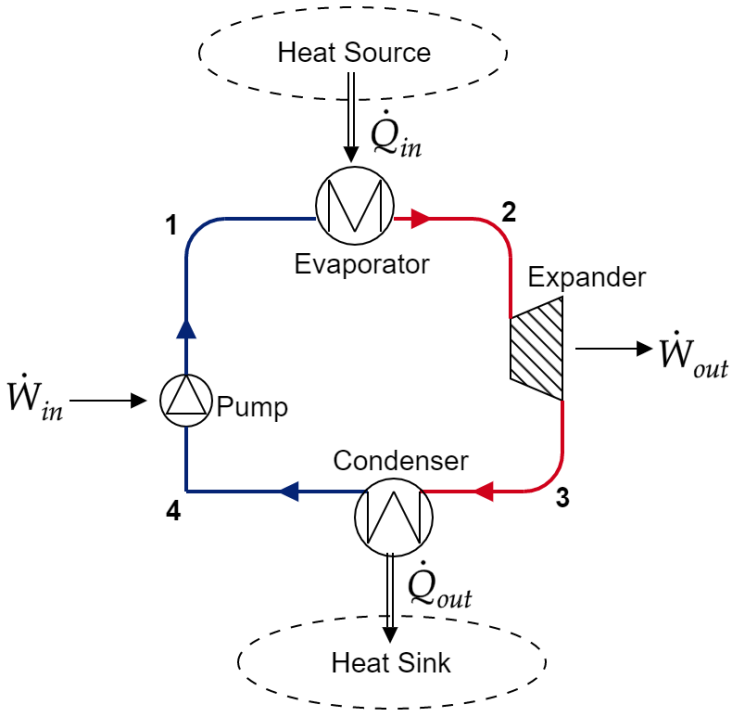

Figure 2.4: Main components of the Rankine cycle.

The temperature-entropy diagram of an ORC is shown in Fig. 2.5. The main components are basically the same than a steam power plant, successively: boiler (1→2), expander (2→3), condenser (3→4) and pump (4→1). By contrast, such a cycle is qualified as *organic* because the working fluid is an organic compound, which can be a pure fluid or a mixture. Such a fluid exhibits sometimes a lower ebullition temperature than water, making possible to recover thermal energy from low temperature heat sources.

Using water as working fluid could be cheap, simpler and very efficient due to its high heat of vaporization and good transport properties. However, its use for automotive applications is compromised by obvious freezing issues in case of cold external conditions. And mixing water with an additive to reduce the freezing point is often very harmful for the thermodynamic performance and the prediction of the WF behavior. In addition to that, the use of water causes a lubrication issue since separating oil from water is very difficult. Regardless these problems, some authors as *Arias et al.* in [8] have designed a Rankine cycle working with water, using two different heat sources: the exhaust gases and the engine cooling system.

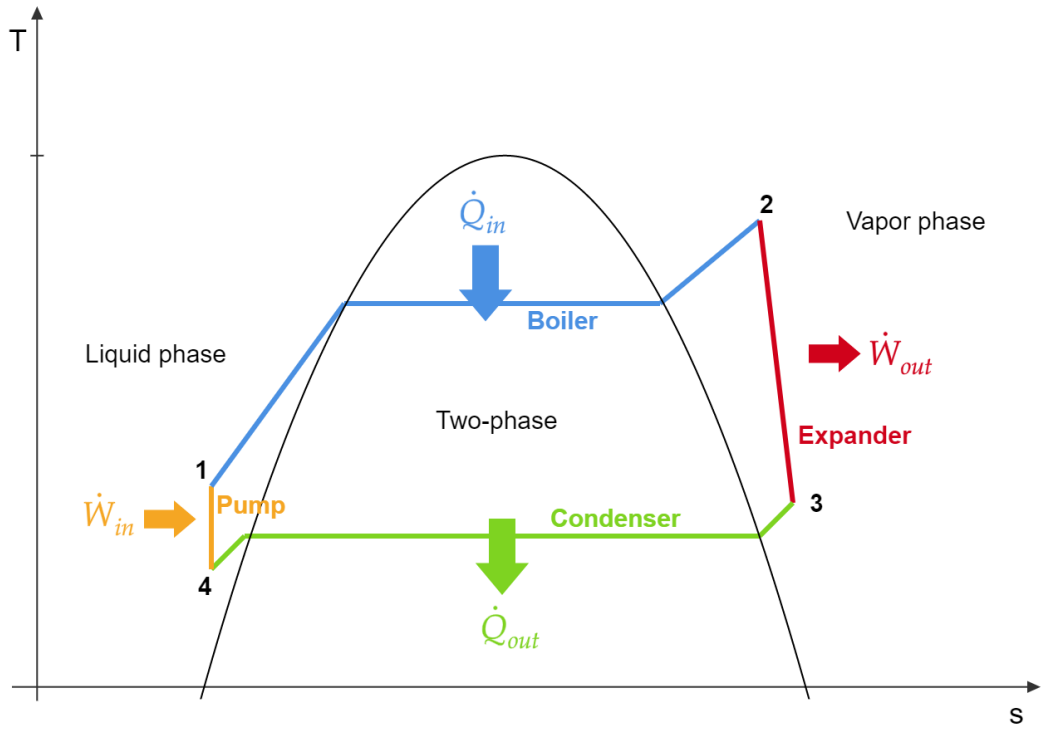

Figure 2.5: Temperature-entropy diagram of the Rankine cycle.

According to Fig. 2.5, the analysis of the Rankine cycle from the first principle of thermodynamics states that:

$$\dot{Q}_{in} + \dot{W}_{in} - \dot{Q}_{out} - \dot{W}_{out} = 0 \tag{2.1}$$

where $\dot{Q}_{in}$ refers to the heat flow rate transferred to the fluid in the boiler, $\dot{W}_{in}$ is the pumping power, $\dot{Q}_{out}$ depicts the heat flow rate removed from the fluid to the ambient in the condenser, and $\dot{W}_{out}$ is the useful power produced by the working medium while expanding.

The market of ORC is growing exponentially since the end of the 20th century and its development is not expected to decline in the near future. Recovering low-grade heat in low to medium-power applications is important in numerous fields of activities. In [9] and [10], *Quoilin et al.* present a techno-economic survey of ORC systems, mainly exploited for decentralized low-capacity power plants. It is concluded that ORC is more appropriate than conventional steam cycles for low and moderate power ranges, as well as for low temperature waste heat recovery. Geothermal application is a good example of stationary utilization where ORC are promising for the future. Nevertheless, the size of current plants is characterized by a minimum output power below which the plant efficiency is no more satisfactory.

2.3.2 Integration to road vehicles

An ORC integrated to a road vehicle takes benefit from one or more heat source(s). In the literature, the most often studied heat source is the exhaust mass flow. To assess the potential of this source, a reference exhaust gas heat flow is introduced:

$$\dot{Q}_{exh,ref} = \dot{m}_{exh} \times \left(h_{exh}(T_{exh,in,boiler}) - h_{exh}(T_{amb}) \right) \tag{2.2}$$

where $\dot{m}_{exh}$ is the exhaust mass flow rate and h_{exh} its specific enthalpy, function of the temperature. This reference heat flow is a maximum feasible limit since it considers that the exhaust gases would be cooled down until the ambient temperature T_{amb} after recovery.

In the study of *Horst et al.* [11], a counter-flow exhaust boiler is added on a turbo diesel engine downstream the exhaust after treatment system (EATS). In fact, this position avoid influencing the performance of EATS in emission control: a boiler placed upstream the gas treatment system would extend the time needed to reach the elevated working temperature of the catalyst. Simulations along several road cycles are performed to assess the benefits of an ORC integrated to a passenger car. It highlights the need for evaluating the impact of the WHR system, often considered as an add-on device, in the whole vehicle environment in order to characterize the potential negative impact on the ICE. For this ORC, an *indirect condensation* strategy is chosen: the working fluid is cooled down by an additional loop of engine coolant, aiming to chill the condenser in parallel with the engine block. This type of ORC layout is represented schematically in Fig. 2.6.

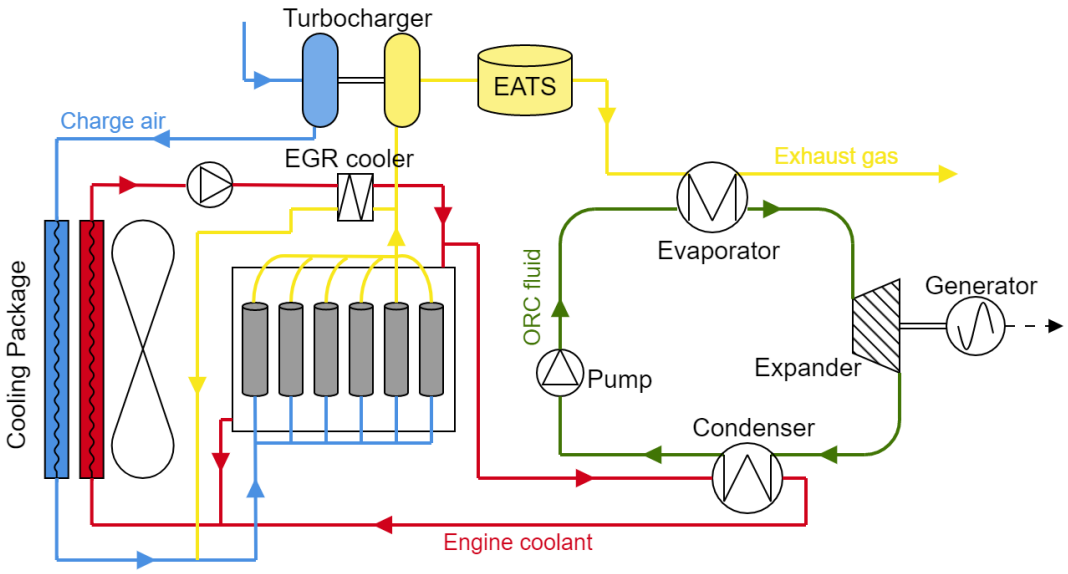

Figure 2.6: Example of ORC layout: heat recovery from exhaust gases, indirect condensation loop with the engine coolant and electrical power output.

This type of condensation increases the necessary heat transfer from the front-end cooling package to the environment. It is demonstrated that the overall heat transfer area must be increased by 20%-30% to ensure good operating conditions for the ORC during extreme conditions, without altering the cooling capacities for the ICE [11]. However, for moderate engine loads, it is often assumed that the ICE cooling system is oversized and exhibits a sufficient heat rejection potential remaining for the ORC. In the modelling of *Horst et al.*, the working fluid mass flow rate pumped from low to high-pressure level and the volumetric flow rate through the expander are controlled to maintain the maximum WF temperature (at the outlet of the exhaust boiler) below 300°C ($p_{ev} = 7$ bars), and the WF temperature at the outlet of the condenser below 90°C. This paper based on numerical simulations concludes that the heat-up of the ORC takes between 5 and 6 minutes, which is 3 minutes more than the time required to reach the minimum operating temperature of exhaust gases (350°C). Neglecting the interactions with the engine, the average net electric power output of the ORC is 980 W during a road cycle. But this value reduces to 500 W while considering negative impacts of WHR on the vehicle: the increase in car weight and backpressure for the ICE, but also the increase in air resistance coming from the additional load on the cooling package ($\Delta c_{x,agv} = 0.0024$). As a result, the fuel economy is only 1.3% but the author concludes that it would be increased up to 4% with an optimized ORC control and enhanced electrification of engine auxiliaries.

The study of *Bettoja et al.* [12] is dedicated to the European *NoWaste Project* devoted to the development of ORC for long-haul trucks, by recovering energy from exhaust and EGR gases. This experimental

study is partially based on a Volvo diesel engine (6 cylinders, 317 kW). Two configurations are studied to combine these two heat sources: parallel or serial configuration. In any case, the EGR function has to be satisfied such that the outlet gas temperature is sufficiently low before being reintroduced towards the ICE. This constraint determine the distribution between WF mass flow going through the EGR boiler or through the exhaust boiler in the parallel configuration. On the other hand, the EGR exchanger is placed upstream the exhaust boiler in the serial configuration to maintain a large temperature gradient between exhaust gases and WF in the EGR cooler.
In this experimental study, the serial configuration is chosen to minimize the complexity of the ORC as well as the price of the system, since the parallel configuration requires a larger number of sensors and actuators. The heat rejection is ensured by an indirect loop using the engine coolant, similarly to the ORC presented above [11]. The final ORC layout of the *NoWaste Project* is shown in Fig. 2.7. The obtained cycle efficiency is around 10% (turbine efficiency = 65%) without altering the engine cooling, demonstrating the interest of using both EGR and exhaust gases as heat sources.

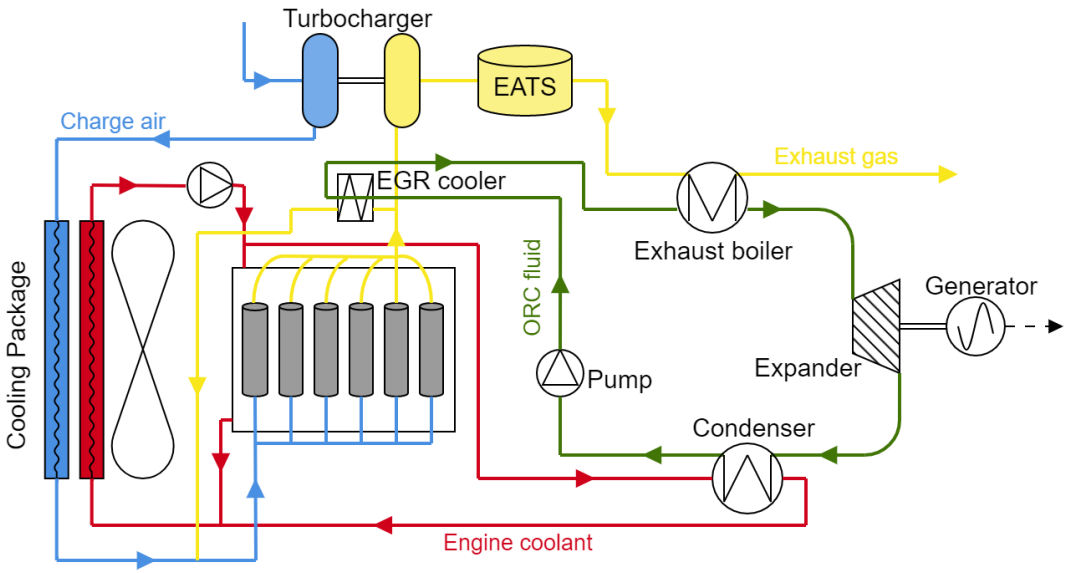

Figure 2.7: Example of ORC layout: heat recovery from EGR gases and exhaust gases (serial configuration), indirect condensation loop with the engine coolant and electrical power output.

Other studies derive a maximum thermal efficiency between 10% and 25% [13]. However, large differences are observable between results obtained by simulations and experimental studies. For example, *Arias et al.* [8] obtain a cycle efficiency equal to 7% by simulations. However, this value reduces to 5.5% in real conditions on a test bench. It highlights the importance of simulation assumptions and the difficulty to put into practice ORC with relatively low power output, where some losses are far to be negligible.

In addition to the different configuration regarding the heat source of the ORC, several layouts are also possible towards the WF condensation. A comprehensive review of all the ORC architectures is presented by *Grelet et al.* in [14]. An alternative to the indirect condensation with the engine coolant loop is shown in Fig. 2.8. In this case, a low temperature radiator dedicated to the ORC is added to the cooling package, with an additional coolant loop equipped with a pump. As a result, the WF condensation is less intrusive for the ICE and the ORC control is easier. However, this solution requires an additional space in the frontal module, and would generally lead to an oversizing of this additional radiator designed for high load conditions.
If the powertrain architecture is not hybridized, the whole mechanical power delivered by the expander

can be directly transferred to the driveline, using a mechanical coupling and possibly a reducer (Fig. 2.9). This solution increases the field of application of ORC systems and needs one less energy conversion, but reduces its flexibility and control capacities due to the inherent coupling with the engine (running the expander at an optimized speed is impossible), while preventing from energy storage in a battery.

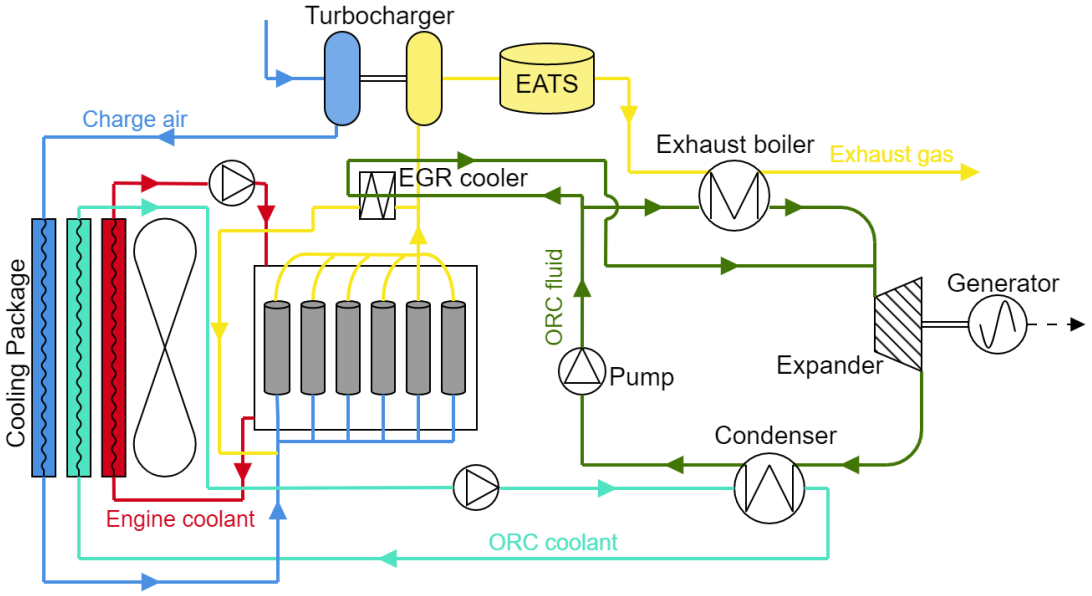

Figure 2.8: Example of ORC layout: heat recovery from EGR gases and exhaust gases (parallel configuration), indirect condensation loop with low temperature radiator dedicated to the ORC and electrical power output.

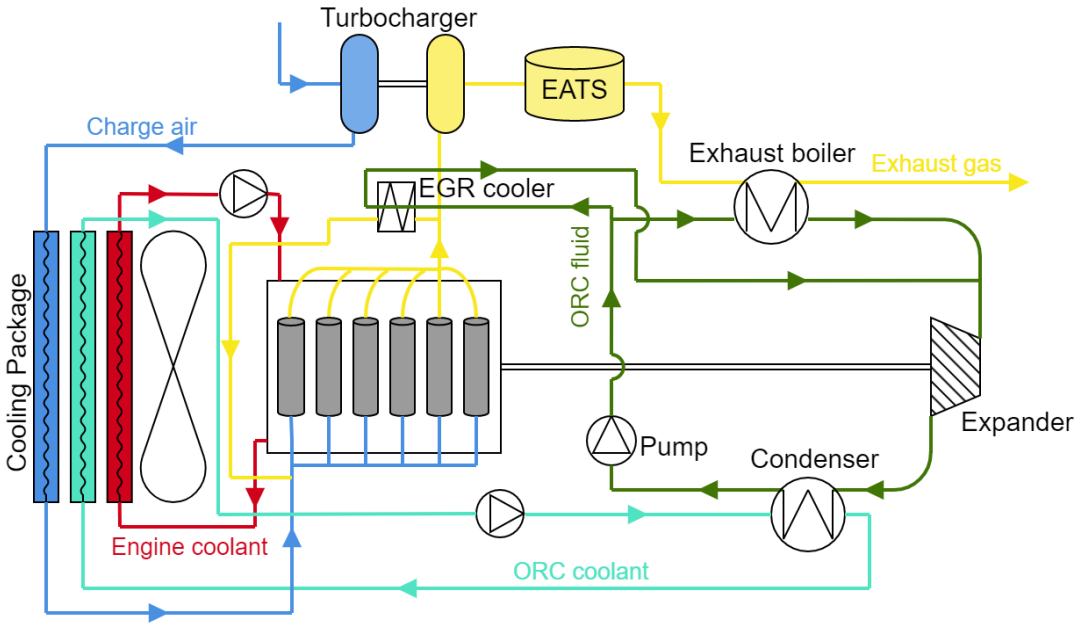

Figure 2.9: Example of ORC layout: heat recovery from EGR gases and exhaust gases (parallel configuration), indirect condensation loop with low temperature radiator dedicated to the ORC and mechanical power output injected into the driveline.

Another possible ORC layout is presented in Fig. 2.10. In this case, the heat source is still the exhaust mass flow. However, a *direct condensation* strategy is chosen: the heat sink is the air flow ensured by an electrically driven fan. Any RAM effect is applicable since this condenser is not placed in the front-end

module. This solution is less intrusive for the engine because the only interaction with the vehicle is the exhaust boiler, and only one heat exchanger is needed for the condensation. However, it requires energy to drive the fan, so that the gross power produced by the ORC is partially exploited for the condensation, but also to feed the WF pump. Moreover, it reinforces the uncertainty on the heat rejection due to variable ambient conditions. The pressurization of the WF tank placed after the condenser makes possible to control the condensation pressure. For heavy-duty vehicles, the direct condenser can be placed behind the cab, as suggested by *Galuppo et al.* [15]. By contrast, this layout is obviously more difficult to put into practice for passenger cars.

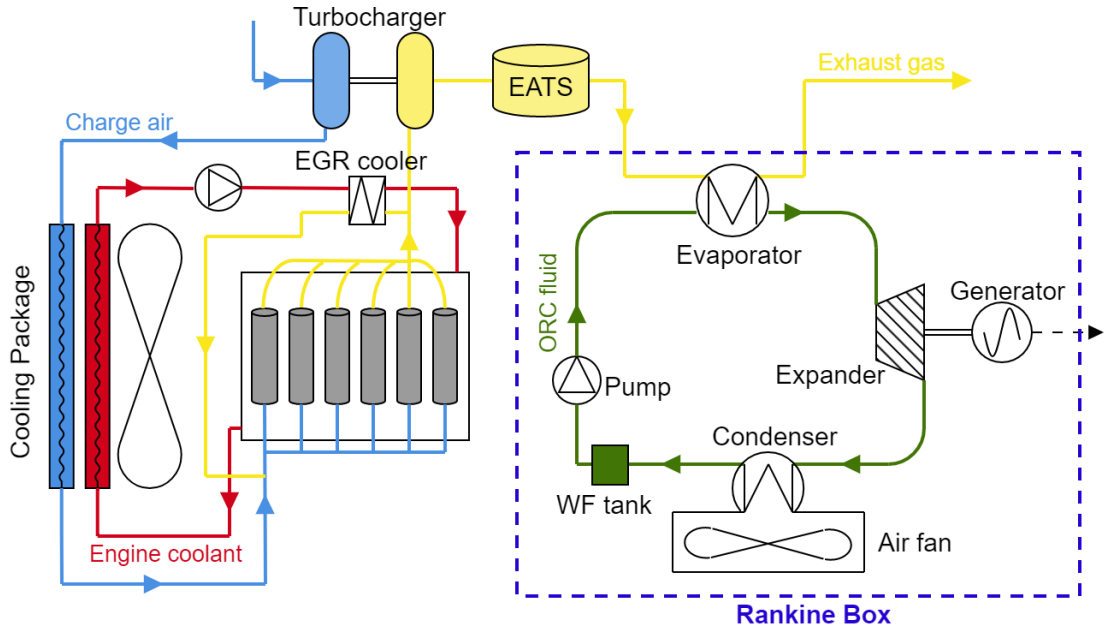

Figure 2.10: Example of ORC layout: heat recovery from exhaust gases, direct condensation with an electrically propelled air fan and electrical power output.

Figure 2.11: Modular waste heat recovery system called *Rankine Box* with electric power output (*Marlok et al. - Mahle* [16]).

The configuration shown in Fig. 2.10 also opens the door to add-on ORC systems under the form of a *Rankine box*, without direct interface with the ICE or the cooling module, also reducing the complexity of integration. This type of product is developed by *Marlok et al. (Mahle)* [16], and placed instead of a part of the fuel tank of a heavy-duty vehicle (Fig. 2.11). The corresponding reduction in fuel capacity is one of the main problems for customer acceptance, especially if it is not compensated by the decrease in fuel consumption thanks to the ORC, resulting in a lower range in kilometers. In [16], the box weighs 150 kg and uses cyclopentane as working fluid. The electrical output energy feeds 48V auxiliaries as

well as an e-motor mounted to the power takeoff of the ICE. A control strategy is developed to drive the fan in order to ensure a complete WF condensation in the air-cooled condenser. The average net power output is around 3.4 kW and the ORC efficiency achieves 3%. In addition, the authors consider that this efficiency could reach 3.6% with optimized components, and the resulting fuel economy would enable an amortization time below two years.

The working fluid selection is also an important subject of study in the ORC field. *Quoilin et al.* present in [9] a complete review of the different working fluids used in other studies. They highlight that a WF would be chosen regarding other aspects in addition to the sole thermodynamic performance: fluid cost, global warming potential (GWP), Ozone depletion potential (ODP), impact on the size of ORC components, etc. Obviously, the temperature of the heat source is one of the major parameters to select the best working fluid.
Xu et al. in [3] recalls the three types of pure working fluids, depending on their vapor saturation curve in a temperature-entropy diagram (Fig. 2.12). If the slope of this curve is negative, the fluid is called a *wet fluid*. From the analysis of the T-s diagram in Fig. 2.5, it is clear that if a wet fluid has a too small saturation slope, a large superheat at the boiler outlet is needed to avoid condensation during the expansion. By contrast, a *dry fluid* is characterized by a positive slope, so that a large condenser is often needed to ensure liquid conditions at the pump inlet. Unfortunately, requiring large cooling capacities results traditionally in lower cycle efficiency. Finally, an *isentropic fluid* with an infinite slope (vertical vapor saturation curve) is the best choice since a dry expansion is ensured while minimizing the superheat at the condenser inlet.

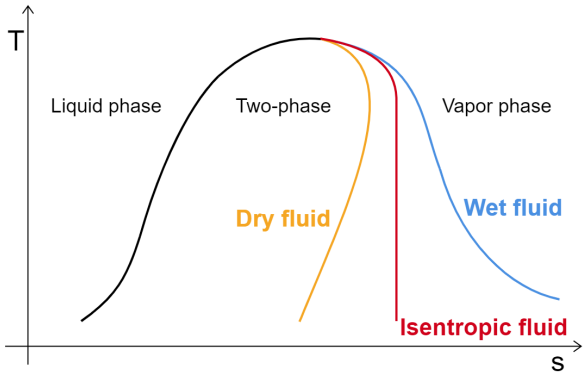

Figure 2.12: Temperature-entropy diagrams of the three working fluid types: wet, dry and isentropic fluids.

To sum up, the criteria determining the working fluid selection are the following, classified by decreasing order of importance:

1. Thermodynamic performance
2. Dry or isentropic fluid (positive or infinite slope of the vapor saturation curve)
3. Elevated vapor density and low volume ratio, to limit the expander size
4. Cost and security
5. Condensing pressure higher than 1 bar and evaporating pressure lower than 30 bar
6. Moderate backwork ratio
7. Availability and environmental impact

Ethanol-based cycles are often found in the literature but a water-ethanol mixture is preferable to decrease flammability and corrosivity with respect to pure ethanol [12]. The chosen WF by *Grelet et al.* in [17] is composed of ethanol (80% wt) and water (20% wt). In accordance with *Chintala et al.*, the R245fa is also a very good organic working fluid for ORC application, regarding availability, environmental and performance parameters [13]. Despite an important interest for ethanol, *Marlok et al.* have finally chosen cyclopentane as working fluid for their add-on Rankine box, due to better transport properties [16].

2.3.3 ORC in heavy-duty vehicles: control and limiting factors

For road vehicles where energy is recovered from exhaust gases, the heat source power profile is dynamic and characterized by large time variations acting as disturbances for the WHR system, so that the need for robust and performing control is easily understood. However, for heavy-duty vehicles this heat source tends to be more stable than for passenger cars, especially in the case of long-haul vehicles driving mainly on highways. Moreover, the action of EATS filters partially the variations in exhaust temperature due to its a high thermal inertia [15]. These two aspects make high-duty vehicles more adapted for ORC applications than passenger cars.

Galuppo et al. [18] analyze an ORC cycle integrated to a mild-hybrid driveline of heavy-duty vehicle, using two different condensation strategies (direct and indirect), operating with two types of proportional–integral–derivative (PID) controller. A *Matlab-Simulink* 1D vehicle model developed internally by *Volvo Trucks* is exploited to simulate transient road cycles. Two main control issues to guarantee safe ORC operations are characterized, and translated into physical values that have to be controlled. At first, the *super-heating* (SH) at the outlet of the exhaust boiler (i.e. at the inlet of the expander):

$$SH_{in,exp} = T_{in,exp} - T_{sat}(p_{in,exp}) \tag{2.3}$$

is defined as the difference between the inlet temperature of the expander and the saturation temperature of the working fluid, depending on the outlet boiler pressure. This high-pressure level has also a direct impact on the pressure ratio and the expander power. *Espinosa et al.* conclude in [19] that the net power increases with p_{ev}, irrespective of the selected working fluid.
The superheat has always to be positive in order to guarantee that the expansion is performed in vapor state (considering a dry WF, see Fig. 2.12). In practice, the PID controller is designed to keep $SH_{in,exp}$ as close as possible to a given set-point (SP), typically between 5 and 40 K, by acting on the WF pump speed. The second controlled physical value is the *sub-cooling* (SC) at the condenser outlet:

$$SC_{in,exp} = T_{sat}(p_{out,cond}) - T_{out,cond} \tag{2.4}$$

which corresponds to the difference between the WF saturation temperature in the condenser, and the WF temperature at the inlet of the pump. This value has to be kept over zero (5-15 K) to guarantee a fluid in the subcooled liquid state at the beginning of the compression in the pump (to avoid cavitation). In the case of an indirect condensation, the actuator that is controlled to manage the value of $SC_{in,exp}$ is the speed of the coolant pump dedicated to the ORC cooling loop. With a direct condensation system the fan speed is the manipulated variable, as well as the pressure in the reservoir, which is equal to the condensation pressure p_{cond} (Fig. 2.10). In fact, the fan power is limited to 500 W in [18] to limit the difference between gross and net ORC output power. When this limit is reached, the ambient air mass flow is kept constant and the WF condensation pressure is increased by varying the WF tank pressurization. As a result, the saturation temperature $T_{sat}(p_{out,cond})$ and the temperature gradient between the fluid and the ambient air also increase, so that the heat transfer in the condenser is improved. However, this solution decreases the gross power due to the reduced pressure ratio. The exact control strategy in case of direct condensation is thus the result of an optimization problem.

An additional heat exchanger, called *recuperator*, can be used to preheat the WF flow at the inlet of the exhaust boiler thanks to the remaining energy that can be extracted from the working fluid at the expander outlet. The overall weight of ORC is increased by around 15% with a recuperator, but it could reduce the frontal area up to 17% in the case of indirect condensation with a dedicated coolant loop and additional radiator [20]. In [15], *Galuppo et al.* report that up to 25% of the recovered heat from exhaust gases can be exchanged by the WF in the recuperator.

The limiting factors of ORC systems for the transport sector are summarized in a comprehensive manner by *Di Battista et al.* in [20]. At first, the recovered electrical energy must have a final use on-board (hybrid driveline and/or electrified auxiliaries). A mechanical coupling between the expander and the driveline eliminates this problem, but considerably reduces the flexibility of ORC. Using an exhaust boiler to recover thermal energy from the tailpipe increases engine backpressure, which could be very harmful for the fuel consumption. The evaporator should be designed to minimize the flow resistance on the gas side, without altering too much the heat transfer capabilities. However, an exhaust boiler placed downstream the EATS would not impact the catalysis process.
The strong fluctuations in exhaust mass flow and temperature is another challenge during ICE operation, requiring a safe and robust control. Some components that are the actuators managed by the controller have to be able to withstand sudden variations in operating conditions (the pump regarding its rotation speed for example).

According to *Katsanos et al.* [21], the heat rejection from the ORC condenser is one of the main technical challenges. As shown above, different cooling strategies are possible, and each of them has advantages and disadvantages. A direct condensation is not possible without an electrically propelled fan if the ORC system is placed behind the cab (Fig. 2.11), which causes an important decrease in net output power. In this case, the condensation also depends on the ambient conditions (air temperature). By contrast, an indirect condensation makes use of the ICE coolant: it induces potential interaction problems with the engine in case of saturation of the front-end cooling package. A dedicated ORC coolant loop can be used, if the integration of an additional low-temperature radiator in the frontal module is possible. In any case, it could have a non-negligible impact on the internal aerodynamics.

Other aspects concerning the working fluid selection have to be addressed: flammability, toxicity, environmental impact, etc. The WF cost is primordial, and can be an important part of the total ORC system cost. The system durability is also important, taking into account that during its lifetime the Rankine cycle is exposed to vibrations from the engine and the transmission.
The geometric integration to a passenger car is a real challenge, which remains difficult for heavy-duty vehicles. The weight of an ORC is also a major limiting factor, resulting in a decrease of the useful load. It is due to the multiple components and heat exchangers that are needed, contrary to TEGs and turbocompounds that are less intrusive.

2.4 Rankine box developed by Volvo Trucks

Volvo Trucks has been studying WHR systems by ORC for many years, with the purpose of reducing the fuel consumption of their heavy-duty vehicles. Some demonstrators have been developed since 2014, but at the present time this technical solution is not yet commercially available. Several architectures of the Rankine system have been studied using different heat sources (exhaust gases, EGR, engine cooling system) and condensation strategies (direct air condenser or indirect condensation with the engine coolant), associated to different working fluids.
The current project conducted by *Volvo Trucks* and dedicated to ORC systems is called *Rankine Generation 3*. This master thesis and the corresponding internship are associated to this project.

The *Rankine Generation 3* project is dedicated to an ORC architecture similar to the one presented in Fig. 2.10 and Fig. 2.11. The unique heat source is the exhaust gases, and the heat sink is the ambient air mass flow (direct condensation) ensured by two electrically driven fans. This ORC system is called *Rankine box* and is placed behind the cab to limit the installation impact. The detailed architecture of this box is shown in Fig. 2.13.

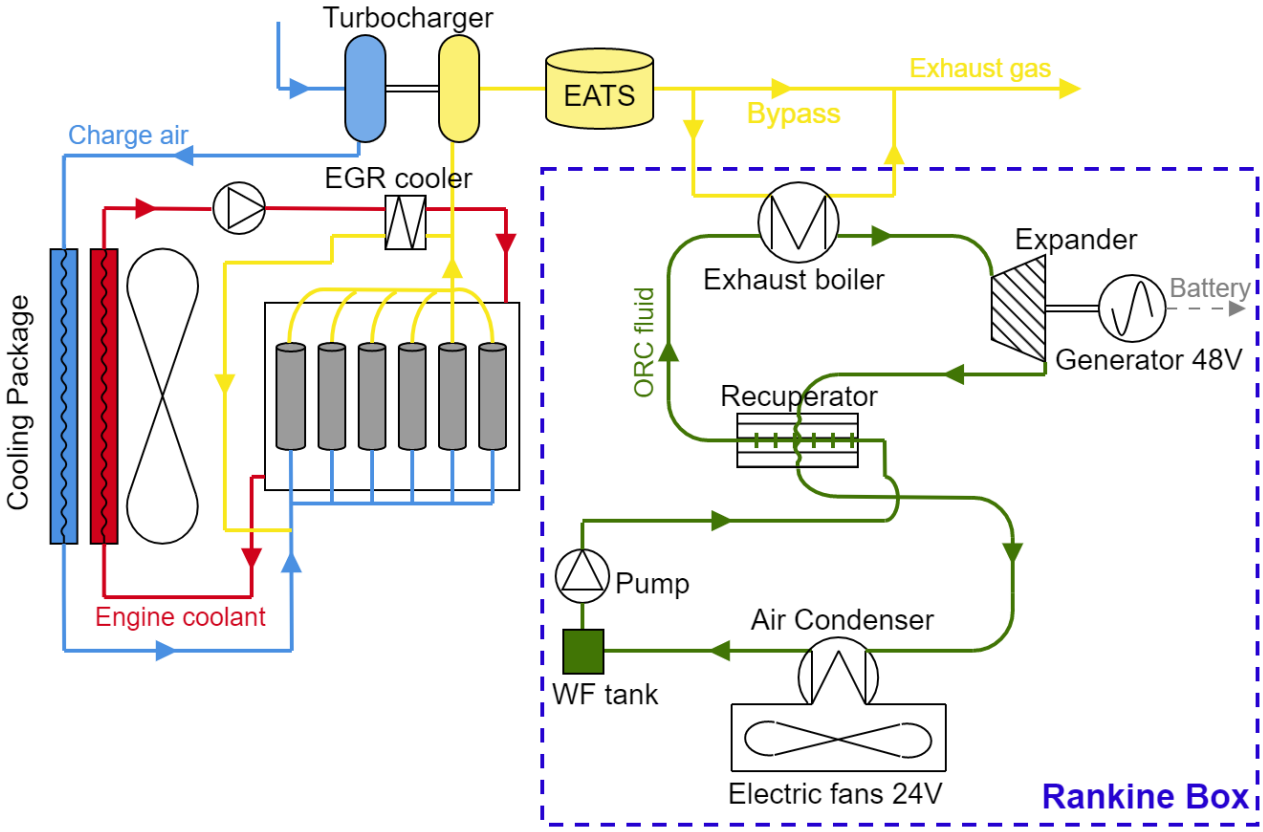

Figure 2.13: Architecture of the Rankine box currently developed by *Volvo Trucks*.

This Rankine box is designed to be a completely autonomous, safe and simple add-on solution. It is equipped with a volumetric expander connected via a belt to a 48V generator. The electrical power output is used to charge a battery, which supplies electrified auxiliaries and/or a hybrid powertrain. The two fans are propelled by electrical 24V motors to cool the condenser made of aluminum. The exhaust boiler is placed downstream the EATS and can be partially or totally bypassed via the exhaust bypass valve. The pump is either coupled mechanically to the expander, or has a own electrical motor.
A recuperator is also used to transfer thermal energy from the working fluid at the expander outlet to the working fluid going to the exhaust boiler. The selected working fluid is cyclopentane (C_5H_{10}), which is not conventional in the field of low-scale ORC power systems. However, hydrocarbons are increasingly being used for large geothermal applications since these fluids simplify the design of large turbines (*Tartière et al.* [22]). A Polyalkylene Glycol (PAG) synthetic oil or a Polyalphaolefin (PAO) oil is used as lubricant, depending on the expander supplier. The total weight of this box would be below 140 kg, and it is expected to decrease the truck BSFC by 3%.

3 | Moving boundaries heat exchangers modelling

3.1 Literature review

3.1.1 Finite volume and moving boundary models

The simulation of WHR systems integrated to road vehicles is a difficult topic, mainly due to the variable conditions such as engine operating point, vehicle speed, waste heat flow and ambient conditions. The dynamic behavior of an organic Rankine cycle during transients mainly depends on the heat exchangers. This observation is true for most of the unsteady low capacity systems. Therefore, a good ORC simulation tool requires an accurate and robust model to represent the evaporator, the condenser as well as the recuperator, if applicable. Three specific challenges associated to the modelling of thermophysical systems are identified by *Desideri* in [23]:

- Computing the thermophysical substance properties of working fluids
- Computational efficiency
- Robustness during initialization and integration

In the case of heat exchanger modelling, these two last points are of primary importance. Two different methods are commonly adopted to model heat exchangers involving phase changes: the *finite volume* (FV) approach and the *moving boundary* (MB) approach. In the two cases, the conservation laws (mass, energy and momentum) are applied in distinct control volumes and characteristic physical quantities are chosen as nodal values connecting two adjacent volumes. As a result, FV and MB methods are considered as 1-D dynamic models.

The FV approach is based on a spatial discretization of the heat exchanger into a constant number of control volumes. These finite volumes have commonly the same size, without any time variation, which facilitates the application of conservation laws. This method is comparable to finite element models (FEM) used in mechanical engineering, and the number of control volumes is a key parameter. The main advantage of a FV model is its good accuracy associated to a high stability [3]. However, the price to pay is a large computational cost. More precisely, a trade-off has to be found between accuracy and CPU time, depending on the number of finite elements.

By contrast, in a MB model, the heat exchanger is divided into a number of elements equal to the number of different states in the fluid flow (vapor, liquid or two-phase). As a result, at most three distinct zones are defined, whose volume varies during unsteady simulations. The exact points where occur phase transitions (saturated liquid and vapor boundaries) are captured to define the volumes; it is a result that the FV approach is not able to compute precisely. Obviously, the moving boundary modelling is able to deal with heat exchangers where only one of the two fluids is evaporated or condensed: the control

volumes are computed from the exchanger side where phase change occurs. However, applications where phase changes occur on both sides of the exchanger are less usual. It is the case for example with cascade refrigeration cycles.
From a computational point of view, the MB method is lighter and more efficient than FV models, even if a MB model is generally less accurate [23]: the decrease in CPU time due to the lower number of elements counteracts sufficiently the small loss of accuracy. MB models are thus a good trade-off between accuracy and computational cost [24]. However, in their comparison between moving boundary and finite volume modelling, *Desideri et al.* highlights that MB models are usually less robust and suffer from stability issues for highly transient simulations [25]. The calculation of zone boundaries is also a source of complexity. By contrast, *Majumdar et al.* [26] states that quasi-steady state moving boundary models are as reliable as finite volume tools.

It is also important to outline that moving boundary models can also be adapted to capture multiple fluid phase transitions. For example, *Feru et al.* present in [27] their modelling of an EGR evaporator integrated to a Rankine cycle mounted on a heavy-duty diesel engine. In this case, ethanol is chosen as working fluid and the boiler is not a simple counter-flow exchanger, but is divided into 3 modules to avoid too high wall temperatures (Fig. 3.1). From the working fluid side, the modules 2 and 3 would be inverted to recover a classical counter-flow configuration. The maximum wall temperature corresponds generally to the outlet of the working fluid flow (inlet of the exhaust gas flow) with a counter-flow boiler. However, this modular exchanger reduces the maximum wall temperature because the module containing the working fluid in vapor state (central volume in Fig. 3.1) is associated to a lower exhaust gas temperature. As a result, *Feru et al.* have developed a model able to track multiple phase transitions that could occur with this particular layout.

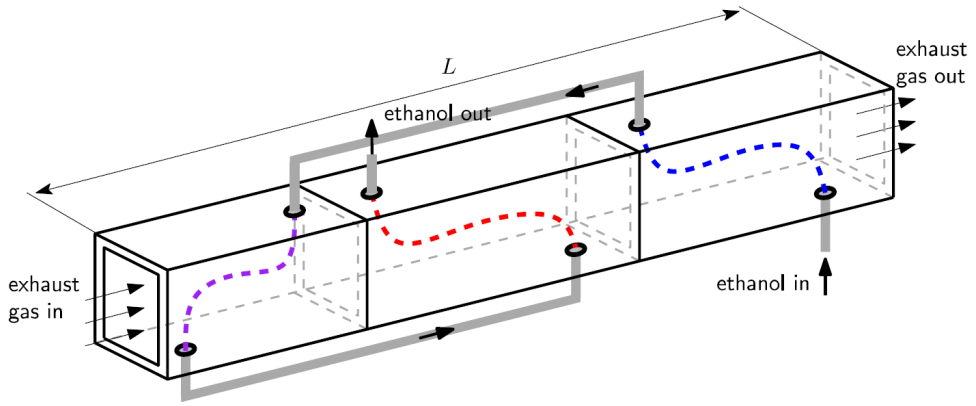

Figure 3.1: Diagram of an exhaust gas recirculation heat exchanger modular design (*Feru et al.* [27]).

As introduced by *Rasmussen et al.* in [28], modelling heat exchangers with a combined FV and MB approach is also possible. The phase changes are tracked similarly to moving boundary models, then each of the three volumes is divided into a fixed number of finite volumes. As shown by *Sangi et al.* [29], coupling these two methods results in a very complex model with an elevated computational cost, but the gain in accuracy can be considerable. Furthermore, these two methods are both modifiable to take into account a binary mixture exhibiting phase transitions, instead of a pure fluid (*Kim et al.* in [30]).

3.1.2 Model developed by Volvo and objective of this study

Cuevas et al. have identified in [31] two ways to simulate heat exchangers. The first one is called the *deterministic* approach, used when the exchanger geometry is completely known or for exchanger sizing. The second one is the *theoretical-experimental* approach: in this case, the lack of knowledge about the

heat exchanger geometry is compensated by empirical results giving the performance of the exchanger for several operating conditions. Furthermore, some parameters are required to fit the simulations with these empirical results coming generally from a supplier.
The model of heat exchanger developed previously by *Volvo Trucks* corresponds to the deterministic approach. This model is used currently in their in-house *Matlab-Simulink* ORC modelling tool integrated to a global simulation platform (GSP), which represents the whole truck. This heat exchanger model is based on a finite volume discretization, and is presented in detail by *Grelet et al.* in [17] and [32]. The same formulation is used for the boiler and the condenser; in this review, the example of the exhaust boiler is chosen.

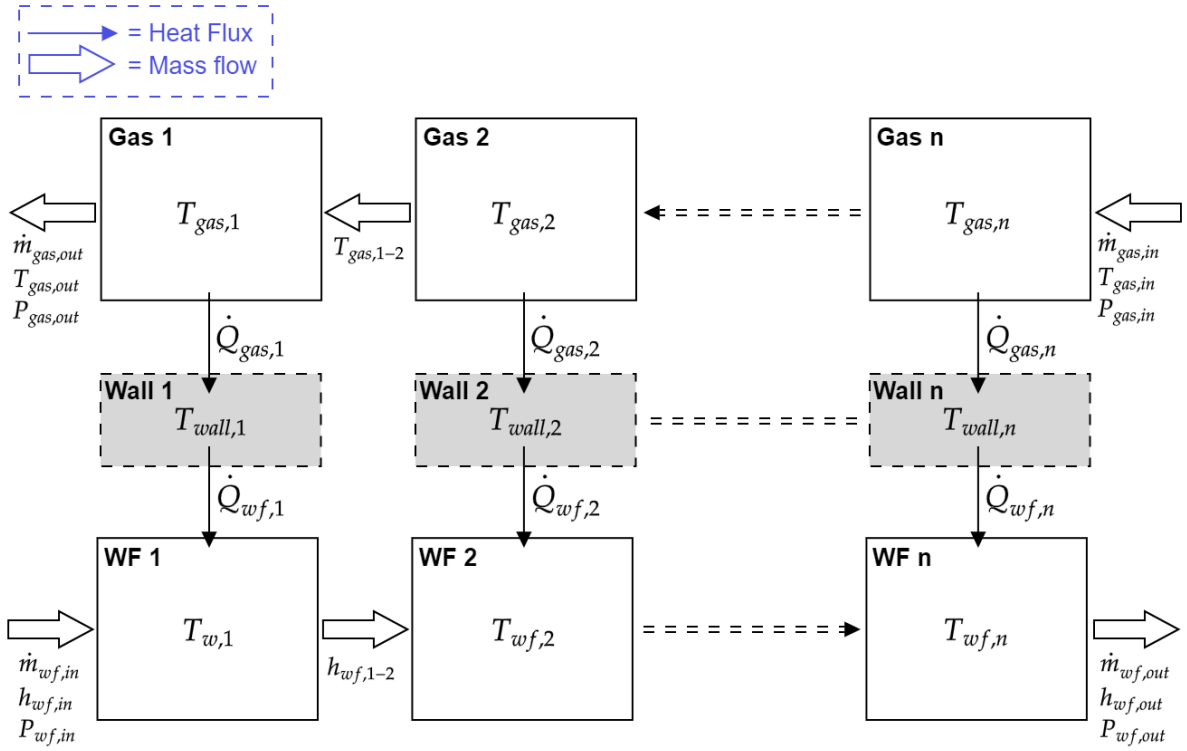

Figure 3.2: Block diagram of the FV exhaust boiler model ($n = 10$).

This boiler is modelled as a simple straight pipe in a counter-flow heat exchanger and divided into 10 control volumes in the longitudinal direction (Fig. 3.2). A uniform cross-section in the flow direction is assumed, resulting in a simplified 1-D modelling. As a result, the exchanger wall and both fluids (WF and exhaust gases) are represented by 10 finite elements. The other assumptions are listed below:

- The heat transfer by conduction is neglected because the dominating transfer mode is the convection.
- Fluid properties are evaluated at the outlet of each control volume.
- No phase change of the transfer fluid is taken into account (i.e. no condensation of the exhaust gas in the case of the exhaust boiler).
- The temperature gradient across the wall thickness is neglected and a uniform wall temperature is considered in a given wall element. The conductive heat transfer along the exchanger length is also neglected.
- Thermal losses to the ambient are neglected.

- The pressure drops are neglected on both sides of the exchanger (WF and transfer fluid).
- Pressure dynamics is neglected during transients, because the corresponding time scales are very small in comparison to the relevant thermal phenomena (i.e. no equation for momentum conservation is necessary). As a result, the variations of WF specific energy Δu_{wf} are assumed to be equal to specific enthalpy fluctuations Δh_{wf}.

The last two assumptions are commonly adopted for dynamic modelling of exchanger with phase change (*Feru et al.* [27], *Vaja* [33]). However, pressure dynamics could also be taken into account (*Gräber et al.* [34]), and pressure losses are sometimes included in the model (*Qiao et al.* [35]).
In Fig. 3.2, the FV model developed by *Volvo Trucks* is represented schematically. The counter-flow exhaust boiler is divided into n volumes, and each of them is composed of three elements: the gas side, the fluid side and the wall representing the heat exchanger mass. Thermal power is firstly transferred from the hot gas mass flow to the separation wall ($\dot{Q}_{gas,i}$). Then, this energy is partially transferred to the working fluid ($\dot{Q}_{wf,i}$). The wall temperature of each finite volume is thus the link between the two exchanger sides; there is no direct interaction between WF and gas control volumes.

The governing equations of this FV model are based on the mass and energy conservation applied in each control volume j:

$$A_{cross}\,\frac{\partial \rho_j}{\partial t}+\frac{\partial \dot{m}_j}{\partial z}=0 \tag{3.1}$$

$$A_{cross}\,\frac{\partial \rho_j h_j}{\partial t}+\frac{\partial \dot{m}_j h_j}{\partial z}+\dot{Q}_{j-wall}=0 \tag{3.2}$$

where ρ, $\dot{m}$ and h stands respectively for the density, the mass flow and the specific enthalpy, z represents the longitudinal direction and A_{cross} is the uniform cross section of the considered side of the exchanger. The flux $\dot{Q}_{j-wall}$ is the heat flux between the studied control volume (gas or WF side) and the corresponding wall element:

$$\dot{Q}_{j-wall}=\alpha_j\,A_{exch,j}\,(T_{wall_j}-T_j) \tag{3.3}$$

where α_j is the convective heat transfer coefficient (HTC), and $A_{exch,j}$ is the exchange area corresponding to element j. This heat flux depends on the uniform temperature of the wall element T_{wall_j} and the temperature of the fluid T_j. This formulation is valid for the WF side as well as the exhaust gas side. As a result, temperature T_j in Eq. (3.3) corresponds either to $T_{wf,j}$ or $T_{gas,j}$ in Fig. 3.2. However, the specific enthalpy h_j appearing in Eq. (3.2) can be replaced on the gas side by the product of the specific heat capacity and the gas temperature, since no phase change is taken into account.
The assumptions listed above specify that the fluid properties are evaluated at the outlet of each FV. In accordance with this choice, the temperature T_j corresponds to the *outlet* temperature of the studied control volume, and not to the average temperature.

The model was validated and its accuracy demonstrated in [32]. The number of finite volumes (10) comes from a trade-off between accuracy and computational time. Because the ORC model developed by *Volvo Trucks* is composed of three heat exchangers (boiler, condenser and recuperator), the time required to perform ORC simulations mainly depends on the exchanger model. Moreover, the models used for the expander and the pump are computationally lighter.
As a result, the interest for a simpler and faster HEX model is easily understood. One of the goals of this master thesis is thus the development of a moving boundary model that will replace the current FV approach, since the MB method would be more efficient than FV models in terms of computational cost, without loss in precision of results.

In order to develop this moving boundary simulation tool, a literature review of scientific publications dealing with MB models were performed. The relevant topics, assumptions and simulation choices that

are used in this study are mainly coming from the studies of *Gräber et al.* [34], *Horst et al.* [36], *Bell et al.* [37] and *Li et al.* [38]. These articles are referenced in the next section of this document, where the complete formulation of the developed moving boundary model is presented in detail.

3.2 Presentation of the MB condenser model

In this section, the moving boundaries heat exchanger model developed on *Matlab-Simulink* is presented in detail. More precisely, it is the condenser model that is chosen to illustrate the more important aspects of this MB approach. Of course this model is very similar to the one representing the exhaust boiler of the Rankine box. The particularities of the boiler model are discussed later in the text.

3.2.1 Generalities and assumptions

The air condenser is made of aluminum, with extruded flat tubes and corrugated louvered fins (Fig. 3.3). A cross-flow configuration is considered by assuming a perfect distribution on the condenser surface of the cooling air flow supplied by the two electrically propelled fans. This exchanger is characterized by the volume, the flow section and the exchange area on both sides (WF and air sides), the mass of the separation wall, the number of tubes and the fin density.

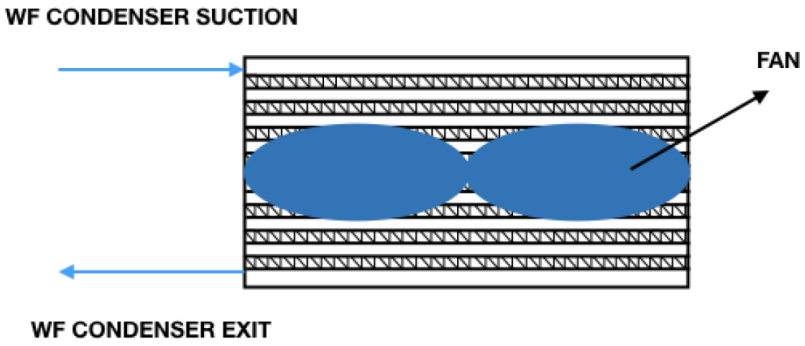

Figure 3.3: Schematic representation of the direct air condenser (tube and fin heat exchanger).

In the Rankine box, the working fluid (cyclopentane) is cooled down by direct condensation in this cross-flow air condenser. The MB model consists in a representation of the heat exchanger by considering the working fluid side (which is condensed), the air side and the wall separating these two fluids. This condenser in normal operating conditions is divided into 3 distinct zones (Fig. 3.4).

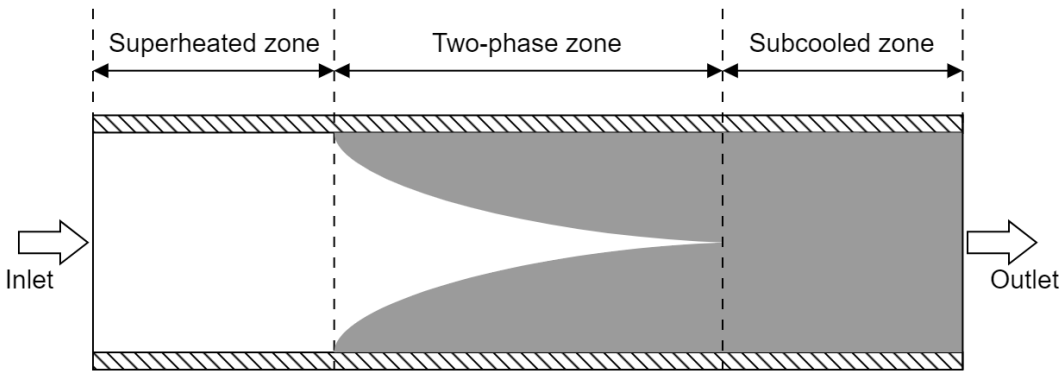

Figure 3.4: MB condenser model involving 3 zones.

Assuming that the working fluid enters the condenser in vapor state, the first zone corresponds to the cooling until the vapor saturation point is reached (superheated zone). After that, the second zone depicts the condensation of the working fluid from the vapor saturation to the liquid saturation point (two-phase zone). It corresponds to the main goal of the condenser. If the WF is a pure fluid, the condensation process occurs at a constant temperature. Finally, the third zone makes use of the remaining part of the exchanger to cool down the liquid fluid below the saturation temperature (subcooled zone). From a control-oriented point of view, this zone which enables the sub-cooling is of primary importance to guarantee that the WF is completely liquid at the inlet of the feed pump.
These three zones are effectively involved in the model if two conditions are satisfied:

- The working fluid enters the condenser in vapor state.
- The heat exchange between the working fluid and the coolant is large enough to ensure a complete condensation of the fluid as well as an additional sub-cooling.

In other words, the three zones would not be always necessary during simulations. In fact, one can distinguish 6 configurations according to the presence/absence of each zone:

1. Three zones are necessary: superheated zone, two-phase zone and subcooled zone, as shown above.
2. Two zones are present since the working fluid enters the condenser in a two-phase state and not in the vapor state: two-phase and subcooled zones are sufficient to model the exchangeur (Fig. 3.5).
3. Two zones exist because the heat transfer is not large enough to ensure a complete condensation of the working fluid: vapor and two-phase zones are only used (Fig. 3.6). In this case, the condenser function is not achieved since the working fluid is not in the liquid state at the outlet.
4. One zone is sufficient (vapor zone) because the working fluid enters the condenser in the vapor state and the heat exchange is so small that the vapor saturation point is not even reached at the outlet.
5. One zone is used (two-phase zone) because the working fluid enters the condenser in two-phase state and the heat transfer is so small that the fluid remains above the liquid saturation point at the outlet.
6. One zone is present (liquid zone) because the working fluid is already in the liquid state at the inlet of the condenser.

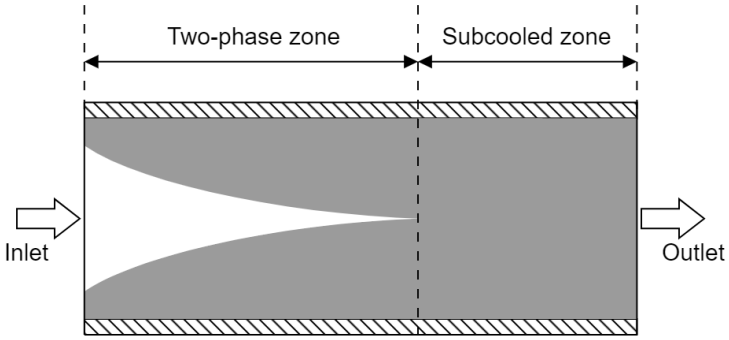

Figure 3.5: MB condenser model involving 2 zones (two-phase and liquid zones).

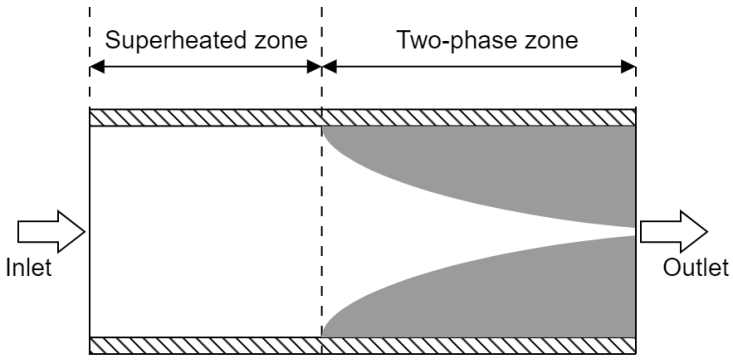

Figure 3.6: MB condenser model involving 2 zones (vapor and two-phase zones).

It is clear that the MB model needs to represent all the 6 possible configurations listed above, even if some of them represent extreme cases and would only be encountered during transients and/or short periods. However, the MB model is more focused on the standard configuration (Fig. 3.4) which corresponds to the ordinary operating conditions of the condenser. As a result, a certain lack of accuracy on results obtained in abnormal configurations (especially the last three configurations listed above) is acceptable.

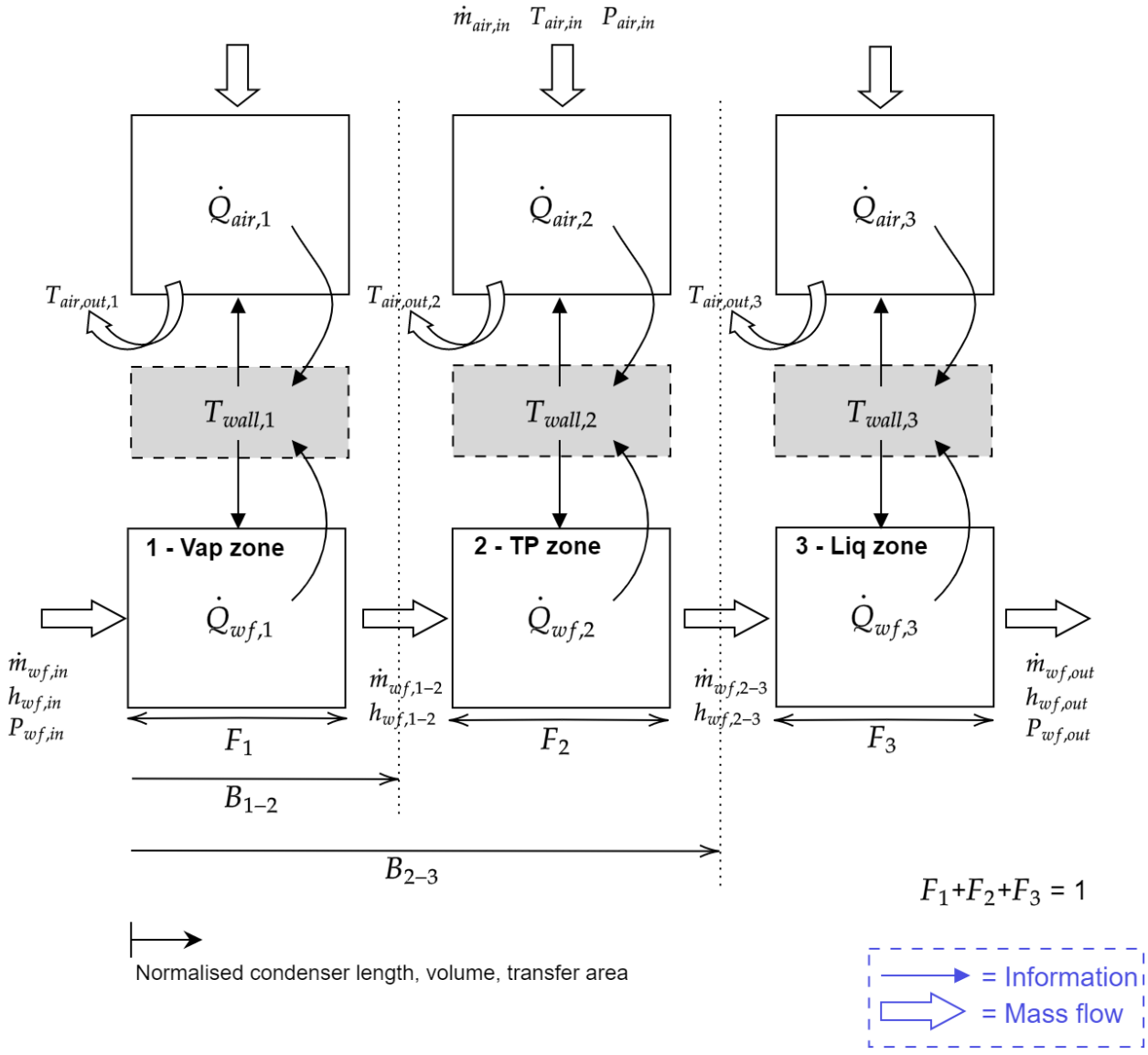

Figure 3.7: Block diagram of the moving boundaries condenser model.

The outline block diagram of the condenser MB model is shown in Fig. 3.7. One can distinguish the working fluid side and the air (coolant) side in cross flows; the wall representing the exchanger mass is placed in between. This diagram represents the basic configuration where all the 3 zones (vapor, two-phase and liquid zones) are employed. The heat exchanger is modelled with a constant flow cross-section for each fluid as well as a uniform distribution of the total heat exchange area and the wall mass along the condenser length. As a result, all the geometric parameters describing a given zone only depend on the length of this zone in the direction of the working fluid flow. The variables F_1, F_2 and F_3 depict respectively the fractions corresponding to the lengths of zones 1 (vapor), 2 (two-phase) and 3 (liquid) with respect to the total length:

$$F_i = \frac{L_{zone,i}}{L_{hex,tot}} \tag{3.4}$$

By definition, their sum is always equal to one:

$$F_1 + F_2 + F_3 = 1 \tag{3.5}$$

The parameter noted B_{1-2} in Fig. 3.7 corresponds to the position of the boundary between zones 1 and 2 along the exchanger length. As a result, one has directly:

$$B_{1-2} = F_1 \tag{3.6}$$

In the same way, B_{2-3} depicts the position of the boundary separating zones 2 and 3, so that:

$$B_{2-3} = F_1 + F_2 \tag{3.7}$$

As shown in Fig. 3.7, the cross-flow configuration means that the inlet air temperature $T_{air,in}$ is the same for each control volume on the air side. The total air flow is divided between the three zones in proportion to these fractions. Solid arrows depict the basic transfer of information between blocks of the *Simulink* model: each control volume on the WF and air sides aims to compute the heat flux ($\dot{Q}_{wf,i}$ or $\dot{Q}_{air,i}$) that is received or released by the fluid flow, knowing the corresponding wall temperature $T_{wall,i}$.

The governing equations defining each element of the MB model are described in the following. However, it is already important to highlight that, even if configurations encountering less than 3 zones are possible (depending on the states of the working fluid along the exchanger), the MB model developed in this study *always* recovers the basic configuration with 3 zones. In fact, these zones are always taken into account to avoid singularities: a volume whose size could be zero (i.e. no exchange area, no WF mass in the control volume, etc.) is impossible to manage with this model. As a result, if a zone should disappear, its size is fixed to a negligible minimal length $F_{min} = 0.001\%$ ($1/10^5$ of the total length). For example, if the fluid enters the condenser already in the two-phase state, the model will set F_1 to F_{min}, and the heat flux corresponding to this *virtual* vapor zone is negligible.
As a result, the existence of a minimum zone length induces that the maximum length fraction cannot be equal to 1. The maximum zone length is fixed to $F_{max} = 99.998\%$ in order to retrieve:

$$F_{max} + 2 \times F_{min} = 1 \tag{3.8}$$

when the condenser model considers only one zone (and the two others are virtually set to the minimum length). This method is inspired from the work of *Horst et al.* presented in [36].

The main hypotheses of the MB model are listed below. Some assumptions are obviously similar to those of the FV model listed above, in order to obtain comparable results with the new MB model.

- The heat transfer by conduction is neglected because the dominating transfer mode is convection.

- Contrary to the FV approach where properties are evaluated at the outlet of finite volumes, *average* fluid properties are taken into account for the MB model (mean value between inlet and outlet of the control volume). In fact, choosing outlet properties would be meaningless with only 3 zones to model the whole exchanger.

- No phase change of the transfer fluid is taken into account.

- The temperature gradient across the wall thickness is neglected and a uniform wall temperature is considered in a given wall element. The conductive heat transfer along the exchanger length is also neglected.

- Thermal losses to the ambient are neglected.

- The pressure drops are neglected on both sides of the exchanger (WF and transfer fluid).

- Pressure dynamics is neglected during transients, because the corresponding time scales are very small in comparison to the relevant thermal phenomena, meaning that pressure changes are assumed to occur instantly (i.e. no equation for momentum conservation). Similarly to the FV model, it means that $\Delta u_{wf} = \Delta h_{wf}$.

3.2.2 WF side of the condenser and calculation of zone boundaries

In the literature, different methods are employed to compute the length of the three zones. In [37], *Bell et al.* present a steady-state moving boundary model based on the analysis of internal and external pinch points. Starting from guesses on the exchange areas corresponding to the different zones, an iterative method is implemented to compute the total heat flux. This solution verifies the equality between the sum of the three assumed zone areas and the real exchange area of the whole condenser. For transient simulations, *Gräber et al.* in [34] use the evolution of an extended vapor fraction along the exchanger length to track zone boundaries. In their work, the inlet and outlet vapor fractions determine the lengths of control volumes for the *following* time step.
Horst et al. present in [36] a dynamic exchanger model for automotive waste heat recovery systems by ORC. This method is well suited for highly transient simulations, and adapted to be implemented on *Matlab-Simulink*. As a result, the new model elaborated in this study to replace the previous FV model developed by *Volvo Trucks* is partially inspired from the work of *Horst et al.*.

The zone boundaries are determined from the working conditions encountered on the WF side of the exchanger. Equations governing each WF control volume are thus explained in the first instance. As said before, no equation for the momentum conservation is taken into account. The mass conservation writes:

$$\frac{dm}{dt} = \dot{m}_{in} - \dot{m}_{out} \tag{3.9}$$

With a backward time derivative:

$$\frac{dm}{dt} = \frac{m(t) - m(t-1)}{\Delta t} \tag{3.10}$$

Considering a simple backward time derivative is motivated by the constraints associated to *Matlab-Simulink*. In addition, the derivatives of the previous FV model are also computed in this way. Knowing the value of the WF mass contained in the control volume at the previous time step $m(t-1)$, the time

derivative only depends on $m(t)$.
The energy conservation equation is:

$$\dot{Q}_{wf} = \dot{m}_{in} \cdot h_{in} - \dot{m}_{out} \cdot h_{out} - \left[\frac{d(m \cdot h_{avg})}{dt} - V \cdot \cancel{\frac{dP_{cd}}{dt}} \right] \tag{3.11}$$

where $\dot{Q}_{wf}$ is the heat transfer between the working fluid and the wall. The derivative of the condensation pressure P_{cd} is neglected in accordance with the assumptions listed above. The mean WF enthalpy is simply defined as:

$$h_{avg} = \frac{h_{in} + h_{out}}{2} \tag{3.12}$$

And the backward time derivative of the transient term writes:

$$\frac{d(m \cdot h_{avg})}{dt} = \frac{m(t) \cdot h_{avg}(t) - m(t-1) \cdot h_{avg}(t-1)}{\Delta t} \tag{3.13}$$

In Eq. (3.11), the signs before each term are chosen to have $\dot{Q}_{wf} > 0$ in normal conditions (i.e. when the fluid is cooled down in the case of the condenser). Defining this term as positive is of primary importance for the set of equations presented below.

From the knowledge of the WF mass flow and fluid properties at the inlet of a control volume (P_{in}, h_{in}, T_{in} and ρ_{in}), the model is based on the calculation of two heat fluxes at each time step: the quantity named *total* heat flow $\dot{Q}_{wf,tot}$, and the *desired* heat flow $\dot{Q}_{wf,des}$.
The total heat flow is the one that would occur if the zone of interest took the whole remaining available length of the exchanger. If it is the case with the vapor zone for example, it corresponds to an extreme case where the working fluid would be still in the vapor state at the output of the condenser, without any condensation. This total heat flow is directly computed from the heat transfer coefficient α_{wf} (W/m^2K) and the temperature gradient between the working fluid and the corresponding wall element:

$$\dot{Q}_{wf,tot} = F_R \cdot A_{wf,tot} \cdot \alpha_{wf} \cdot (T_{wf,avg} - T_{wall}) \tag{3.14}$$

In this equation, $A_{wf,tot}$ is the total exchange area on the WF side of the condenser. The quantity F_R is the remaining fraction of the exchanger length that can be occupied by the zone of interest. The average WF temperature is simply computed from the inlet and outlet temperatures of the zone:

$$T_{wf,avg} = \frac{T_{wf,in} + T_{wf,out}}{2} \tag{3.15}$$

One can verify that $\dot{Q}_{wf,tot}$ is defined as positive in Eq. (3.14) when the wall temperature is below the average fluid temperature, which is the case in normal operating conditions of the condenser.
The desired heat flow corresponds to the one that is required to reach the desired state of the working fluid (i.e. the desired enthalpy $h_{out,des}$) at the output of the considered zone. For the vapor zone (superheated zone), the desired state is reached when the outlet enthalpy verifies: $h_{out,des} = h_{sat,vap}$, so that the working fluid is at the vapor saturation point at the output of the zone. From Eq. (3.11), this heat flux is computed as:

$$\dot{Q}_{wf,des} = \dot{m}_{in} \cdot h_{in} - \dot{m}_{out} \cdot h_{out,des} - \frac{d(m \cdot h_{avg})}{dt} \tag{3.16}$$

Inserting Eq. (3.13) into Eq. (3.16) to replace the transient term gives:

$$\dot{Q}_{wf,des} = \dot{m}_{in} \cdot h_{in} - \dot{m}_{out} \cdot h_{out,des} - \frac{m(t) \cdot h_{avg}(t) - m(t-1) \cdot h_{avg}(t-1)}{\Delta t} \tag{3.17}$$

By definition, $\dot{Q}_{wf,des}$ is the required heat flux to obtain $h_{out} = h_{out,des}$, but also to modify the average WF enthalpy from a given value at the previous time step $h_{avg}(t-1)$ to the value $h_{avg}(t)$ corresponding to the mean between h_{in} and $h_{out,des}$. Hence Eq. (3.17) becomes:

$$\dot{Q}_{wf,des} = \dot{m}_{in} \cdot h_{in} - \dot{m}_{out} \cdot h_{out,des} - \frac{m(t) \cdot \dfrac{h_{in} + h_{out,des}}{2} - m(t-1) \cdot h_{avg}(t-1)}{\Delta t} \tag{3.18}$$

Finally, the heat flux that really corresponds to the zone of interest is logically the minimum of these two values:

$$\dot{Q}_{wf} = min\ \left(\dot{Q}_{wf,tot}\ ;\ \dot{Q}_{wf,des} \right) \tag{3.19}$$

Once the desired and total heat fluxes are known, the non-dimensional quantity χ is introduced:

$$\chi = \frac{\dot{Q}_{wf,des}}{\dot{Q}_{wf,tot}} \tag{3.20}$$

From this definition, the fraction of the heat exchanger length that corresponds to the studied zone would be simply: $F = F_R \cdot \chi$, due to the presence of the remaining disponible length fraction F_R in Eq. (3.14). However, F cannot be larger than F_R, which could be the case if $\chi > 1$. In addition, one has to remind that a non-zero minimum length fraction F_{min} must always be considered. As a result, F is computed by:

$$F = max\ \left[F_{min}\ ;\ min\ \left(F_R\ ;\ F_R \cdot \chi \right) \right] \tag{3.21}$$

If $\chi < 1$, Eq. (3.19) gives $\dot{Q}_{wf} = \dot{Q}_{wf,des}$: the desired fluid state is reached at the end of the zone, and $F = F_R \cdot \chi$. On the other hand, $\chi > 1$ means that the total heat flux is lower than the desired heat flux. In this case, one has $\dot{Q}_{wf} = \dot{Q}_{wf,tot}$ and $F = F_R$: the fluid leaves the zone without reaching the desired state point, even if this zone takes the whole remaining exchanger volume.

	Zone 1 (vapor zone F_1)	**Zone 2** (two-phase zone F_2)	**Zone 3** (liquid zone F_3)
$\mathbf{h_{out,des}}$	$h_{sat,vap}(P_{cd})$	$h_{sat,liq}(P_{cd})$	/
$\mathbf{F_R}$	F_{max}	$F_{max} - F_1$	$F_{max} - F_1 - F_2$

Table 3.1: Desired outlet enthalpy $h_{out,des}$ and expression of the remaining disponible fraction of the condenser length F_R for each zone of the condenser MB model.

The case $F = F_{min}$ is encountered to avoid singularities if the studied zone is not necessary due to the fluid state at the inlet of the condenser. For example, the first (vapor) zone is set to F_{min} if the fluid is already below the vapor saturation point before entering the exchanger. In addition, one has $F = F_{min}$ is there is no more remaining volume for the zone of interest.

One could highlight that the maximum exchanger fraction F_{max} is not taken into account in Eq. (3.21). In fact, this quantity appears implicitly because F_R depends on F_{max}. The value of F_R is obviously different for each zone, as shown in Tab. 3.1.

Regarding the last zone (liquid zone in the case of the air condenser), the definition of $\dot{Q}_{wf,des}$ is meaningless because there is no desired outlet enthalpy below the liquid saturation point that is associated to this volume. This zone provides only a sub-cooling below the WF saturation temperature. As a result, one can fix $\dot{Q}_{wf,des} = \infty$ in Eq. (3.20) so that $F = max(F_{min} ; F_R)$ for the last zone.

The key parameter that is important to compute is thus the quantity χ, equal to the ratio between desired and total heat fluxes. However, the expression of $\dot{Q}_{wf,des}$ (Eq. 3.18) is itself implicitly dependent on χ. In fact, the WF mass $m(t)$ contained in the control volume is a function of the zone length computed at time t. Assuming that $\chi < 1$ (i.e. $\dot{Q}_{wf,des} < \dot{Q}_{wf,tot}$), one has:

$$m(t) = \chi \cdot F_R \cdot V_{hex} \cdot \rho_{avg} \tag{3.22}$$

where V_{hex} is the total exchanger volume on the WF side, and ρ_{avg} is the mean density of the fluid between the zone inlet and outlet. By definition of the desired heat flux, the outlet density has to correspond to the required saturation point, so that ρ_{avg} writes:

$$\rho_{avg} = \frac{\rho_{in} + \rho_{out,des}}{2} \tag{3.23}$$

with $\rho_{out,des} = \rho_{sat,vap}$ for the first condenser zone, and $\rho_{out,des} = \rho_{sat,liq}$ for the second zone. By conservation of the WF mass, the mass flow that leaves a control volume is also a function of χ, and is obtained by inserting Eqs. (3.22) and (3.23) into Eq. (3.9):

$$\begin{aligned} \dot{m}_{out} &= \dot{m}_{in} - \frac{m(t) - m(t-1)}{\Delta t} \\ &= \dot{m}_{in} - \frac{1}{\Delta t} \cdot \chi \cdot F_R \cdot V_{hex} \cdot \frac{\rho_{in} + \rho_{out,des}}{2} + \frac{m(t-1)}{\Delta t} \end{aligned} \tag{3.24}$$

where $m(t-1)$ is the mass of the fluid at the preceding time step, calculated previously with Eq. (3.22). This expression is of primary importance, because it highlights the relation between the mass flow and the moving boundaries.

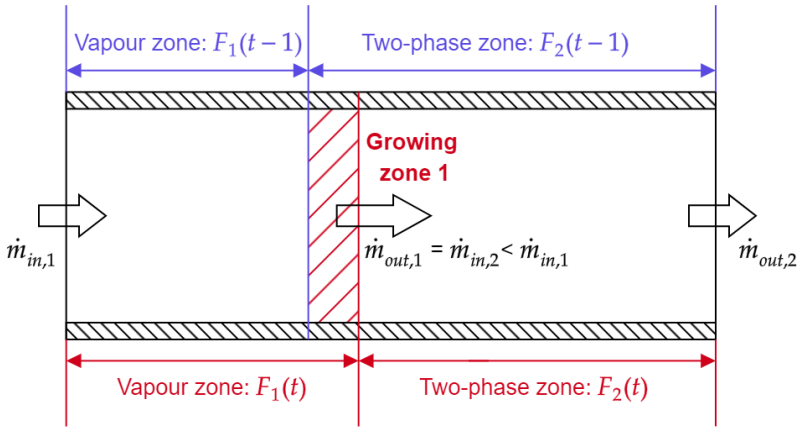

Figure 3.8: Illustration of the impact of moving boundaries on the mass conservation equation.

If zone boundaries and fluid densities inside control volumes do not change overtime, one has simply $\dot{m}_{in} = \dot{m}_{out}$ for the three zones. However, if for example the length of the first zone (vapor zone of the condenser) suddenly increases for some reasons, the boundary between zones 1 and 2 moves as a consequence. This situation is illustrated in Fig. 3.8, where the third (liquid) zone is not represented for the sake of simplicity. Assuming a constant inlet mass flow in the first zone $\dot{m}_{in,1}$ (i.e. the WF mass flow entering the condenser), the mass contained into the first control volume increases while the boundary between vapor and two-phase zones moves to the right. In other words, $F_1(t)$ is greater than $F_1(t-1)$ so that $m_1(t) > m_1(t-1)$. The mass flow that leaves the first control volume $\dot{m}_{out,1}$ (whose enthalpy is equal to $h_{sat,vap}$) is computed by Eq. (3.24), and is thus lower than the entering flow $\dot{m}_{in,1}$ while the zone expands. Furthermore, $\dot{m}_{out,1}$ is equal to the inlet mass flow of the second control volume $\dot{m}_{in,2}$. As a result, one can observe that $\dot{m}_{in,2} < \dot{m}_{in,1}$ when the boundary is moving to the right. The opposite situation ($\dot{m}_{in,2} > \dot{m}_{in,1}$) is observed if the boundary is moving to the left (decreasing length of zone 1). The complexity of the mass conservation equation in the case of MB modelling is largely discussed by *Li et al.* in [38]. In his study, the authors conclude rightly that the mass flow going from one zone to another is a question of *relative* velocities between boundaries and working fluid going through the exchanger, in accordance with the example of Fig. 3.8.

In order to compute the quantity χ, one has to begin from the definition of $\dot{Q}_{wf,des}$ in Eq. (3.18). Knowing that $\dot{Q}_{wf,des} = \chi \cdot \dot{Q}_{wf,tot}$:

$$\chi \cdot \dot{Q}_{wf,tot} = \dot{m}_{in} \cdot h_{in} - \dot{m}_{out} \cdot h_{out,des} - \frac{m(t) \cdot \dfrac{h_{in} + h_{out,des}}{2} - m(t-1) \cdot h_{avg}(t-1)}{\Delta t} \tag{3.25}$$

Inserting Eqs. (3.22) and (3.24) into Eq. (3.25) gives:

$$\begin{aligned} \chi \cdot \dot{Q}_{wf,tot} = \dot{m}_{in} \cdot h_{in} - \overbrace{\left[\dot{m}_{in} - \frac{1}{\Delta t} \cdot \chi \cdot F_R \cdot V_{hex} \cdot \frac{\rho_{in} + \rho_{out,des}}{2} + \frac{m(t-1)}{\Delta t}\right]}^{\dot{m}_{out}} \cdot h_{out,des} \\ - \frac{\overbrace{\left[\chi \cdot F_R \cdot V_{hex} \cdot \dfrac{\rho_{in} + \rho_{out,des}}{2}\right]}^{m(t)} \cdot \dfrac{h_{in} + h_{out,des}}{2} - m(t-1) \cdot h_{avg}(t-1)}{\Delta t} \end{aligned} \tag{3.26}$$

From this result, all the terms where χ appears can be moved to the left-hand side of the equation, while the terms independent of χ are placed in the right-hand side:

$$\begin{aligned} &\chi \cdot \dot{Q}_{wf,tot} - \frac{1}{\Delta t} \cdot \chi \cdot F_R \cdot V_{hex} \cdot \frac{\rho_{in} + \rho_{out,des}}{2} \cdot h_{out,des} + \frac{\chi \cdot F_R \cdot V_{hex} \cdot \dfrac{\rho_{in} + \rho_{out,des}}{2} \cdot \dfrac{h_{in} + h_{out,des}}{2}}{\Delta t} \\ &= -\left[\dot{m}_{in} + \frac{m(t-1)}{\Delta t}\right] \cdot h_{out,des} + \dot{m}_{in} \cdot h_{in} + \frac{m(t-1) \cdot h_{avg}(t-1)}{\Delta t} \end{aligned} \tag{3.27}$$

Finally, solving Eq. (3.27) for χ gives:

$$\chi = \frac{\dot{m}_{in} \cdot h_{in} - \left[\dot{m}_{in} + \dfrac{m(t-1)}{\Delta t}\right] \cdot h_{out,des} + \dfrac{m(t-1)}{\Delta t} \cdot h_{avg}(t-1)}{F_R \cdot V_{hex} \cdot \dfrac{\rho_{in} + \rho_{out,des}}{2} \cdot \dfrac{h_{in} + h_{out,des}}{2 \cdot \Delta t} + \dot{Q}_{wf,tot} - F_R \cdot V_{hex} \cdot \dfrac{\rho_{in} + \rho_{out,des}}{2} \cdot \dfrac{h_{out,des}}{\Delta t}} \tag{3.28}$$

In a control volume, the quantity χ is computed with Eq. (3.28) because all the terms appearing in this equation are calculated *before* knowing the zone length at the current time step t. In fact, the total heat flux $\dot{Q}_{wf,tot}$ is computed beforehand with Eq. (3.14) considering the temperature gradient between WF and wall at the *previous* time step. It is necessary because the *Matlab-Simulink* model developed by *Volvo Trucks* is not able to deal with *algebraic loops*. These loops occur when an input port of a given *Simulink* block is driven by the output of the same block[1]. Using the fluid temperature computed at time t, which is an output of a WF control volume, to calculate $\dot{Q}_{wf,tot}$ at the same time step is thus impossible. As a result, a *memory block* is needed on *Simulink* to store the temperature at the previous time step, in order to reuse it to compute $\dot{Q}_{wf,tot}$ at the next time step.
More precisely, implicit algorithms are able to solve models containing algebraic loops on *Simulink*, but it increases drastically the computational costs. Therefore, it is more efficient to disable the implicit solver and to use memory blocks to avoid algebraic loops.

Once the value of χ is known, the zone length fraction is calculated with Eq. (3.21) and the mass contained in the control volume is computed with:

$$m(t) = F \cdot V_{hex} \cdot \frac{\rho_{in} + \rho_{out,des}}{2} \tag{3.29}$$

One has to highlight an hypothesis of the model: to simplify the computation, the average density in Eq. (3.29) is calculated by considering that the fluid reaches the desired saturation point at the outlet of the control volume, which is not always the case. After that, the WF outlet mass flow is computed and becomes the inlet mass flow of the following zone:

$$\dot{m}_{out} = \dot{m}_{in} - \frac{m(t) - m(t-1)}{\Delta t} \tag{3.30}$$

Finally, the outlet enthalpy of the fluid leaving the control volume is equal to the desired one if and only if $\dot{Q}_{wf} = \dot{Q}_{wf,des}$, meaning that the required zone fraction to reach $h_{out,des}$ is lower than the remaining length F_R. However, if $\dot{Q}_{wf} = \dot{Q}_{wf,tot}$ the outlet enthalpy is computed by solving Eqs. (3.11), (3.12) and (3.13) for h_{out}:

$$h_{out} = \frac{\left(\dot{m}_{in} \cdot h_{in} - \dot{Q}_{wf,tot}\right) \cdot \Delta t - \frac{m(t)}{2} \cdot h_{in} + m(t-1) \cdot h_{avg}(t-1)}{\dot{m}_{out} \cdot \Delta t + \frac{m(t)}{2}} \tag{3.31}$$

This equation is also used to compute the outlet enthalpy of the last control volume, taking into account that $\dot{Q}_{wf}$ is always equal to $\dot{Q}_{wf,tot}$ in this zone.

In this section, equations governing the working fluid side of the exchanger model were described. By definition of a moving boundary model, it is on this side that the lengths of the different zones are defined (F_1, F_2 and F_3). For this purpose, Eq. (3.28) really corresponds to the heart of the problem.
To complete the description of this new exchanger model, the wall and the air side of the exchanger are described later in the text.

3.2.3 Computation of the heat transfer coefficient

The heat transfer coefficient α_{wf} appearing in Eq. (3.14) represents the heat transfer by convection from the working fluid flow to the wall of the condenser. To compute this coefficient, different empirical

[1] https://nl.mathworks.com/help/simulink/ug/algebraic-loops.html

correlations are employed, depending on the WF state. It means that a different correlation is used for each zone of the new MB model (liquid, two-phase or vapor). These correlations are the same than the ones chosen for the previous FV model, where the switching between correlations inside a given control element depends on the WF state at the *outlet* of the volume.

One can highlight here a major difference between FV and MB models. Regardless the switching strategies between HTC correlations, the value of the transfer coefficient that is computed in a certain control volume of a FV model can be inaccurate if phase change occurs inside this volume. For example, in the FV condenser model developed by *Volvo Trucks*, the fact that the fluid is in the two-phase state at the outlet of a control volume does not mean that the major part of this element contains two-phase WF. For example, the correlation adapted to vapor WF would be more relevant if the transition from vapor to two-phase state occurs close to the outlet of the control volume. This lack of precision is exacerbated if the number of finite volumes is low.
By contrast, a MB model is able to track the exact points where phase transitions occur along the exchanger length. As a result, the best suited correlation is always exploited to compute α_{wf}, and the accuracy of a MB model can be very good even with only three zones used for the exchanger discretization. But this aspect is obviously not the only parameter acting on the model precision.

The empirical correlations used to compute α_{wf} involve the dimensionless Nusselt number (Nu):

$$Nu = \frac{\alpha_{wf} \cdot L_c}{k} \tag{3.32}$$

where L_c is a characteristic length (often corresponding to the hydraulic diameter) and k is the thermal conductivity of the fluid. The Nusselt number represents thus the ratio between convective and conductive heat transfers. Empirical correlations to compute Nu take the general form [39]:

$$Nu = C \cdot Re^m \cdot Pr^n \tag{3.33}$$

where Re and Pr are dimensionless quantities, respectively the Reynolds and Prandtl number, defined as:

$$Re = \frac{L_c \cdot \dot{m}_{wf}}{A_{flow} \cdot \mu} \tag{3.34}$$

$$Pr = \frac{cp \cdot \mu}{k} \tag{3.35}$$

The quantity cp is the specific heat capacity of WF, μ its dynamic viscosity, and A_{flow} depicts the flow section area. Combining Eqs. (3.33) to (3.35) gives:

$$Nu = C \cdot \left(\frac{L_c \cdot \dot{m}_{wf}}{A_{flow} \cdot \mu}\right)^m \cdot \left(\frac{cp \cdot \mu}{k}\right)^n \tag{3.36}$$

In the liquid and vapor zones, the WF properties are assumed to be constant so that the Nusselt number expressed by Eq. (3.36) becomes a function of $\dot{m}_{wf}$ only, and the HTC in these zones can take the general forms:

$$\alpha_{wf,liq} = \left(\frac{\dot{m}_{wf}}{\dot{m}_{nom}}\right)^{a_{liq}} \cdot \alpha_{liq,nom} \tag{3.37}$$

$$\alpha_{wf,vap} = \left(\frac{\dot{m}_{wf}}{\dot{m}_{nom}}\right)^{a_{vap}} \cdot \alpha_{vap,nom} \tag{3.38}$$

As a result, single-phase HTC are only functions of the WF mass flow through the condenser, depending on nominal heat transfer coefficients identified experimentally: $\alpha_{liq,nom} = 150$ W/m^{2}K and $\alpha_{vap,nom} = 75$ W/m^{2}K, with $\dot{m}_{nom} = 0.0156$ kg/s. The identified exponents are $a_{liq} = 0.86$ and $a_{vap} = 0.96$. Eqs. (3.37) and (3.38) are thus exploited respectively in the liquid and vapor zones of the MB condenser model to compute the HTC and the total heat flux $\dot{Q}_{wf,tot}$.
In the case of the two-phase zone, the biphasic HTC is equal to $\alpha_{wf,liq}$ multiplied by a correction factor:

$$\alpha_{wf,TwoPhase} = \alpha_{wf,liq} \cdot \Big(X + Y\Big)^{-1/2} \tag{3.39}$$

With:

$$X = \left[\left(\left(\frac{\rho_{wf,sat,liq}}{\rho_{wf,sat,vap}}\right)^{0.37} \cdot (1.2 \cdot x_{wf,avg})^{0.4}\right) + (1 - x_{wf,avg})\right]^{-2.2} \cdot (1 - x_{wf,avg})^{0.01} \tag{3.40}$$

$$Y = \left(\frac{\alpha_{vap}}{\alpha_{liq}}\right)^{-2} \cdot \left[1 + \left(8 \cdot \left(\frac{\rho_{wf,sat,liq}}{\rho_{wf,sat,vap}}\right)^{0.67} \cdot (1 - x_{wf,avg})^{0.7}\right)\right]^{-2} \cdot x_{wf,avg}^{0.01} \tag{3.41}$$

This method used in the previous model developed by *Volvo Trucks* is presented by *Grelet et al.* in [17], and comes originally from the work of *Horst et al.* [36]. In the previous FV model, the mean fluid quality $x_{wf,avg}$ appearing in Eqs. (3.40) and (3.41) is simply assumed to be equal to the working fluid quality $x_{wf,out}$ at the outlet of the considered control volume:

$$x_{wf,out} = \frac{h_{wf,out} - h_{wf,sat,liq}}{h_{wf,sat,vap} - h_{wf,sat,liq}} \tag{3.42}$$

In the case of the two-phase zone of the moving boundary model, this assumption is meaningless. One could argue that by definition of the MB condenser model, $x_{wf,in} = 1$ and $x_{wf,out} = 0$ is always true for the biphasic zone in normal operating conditions, and fixing the arithmetic mean $x_{wf,avg} = 0.5$ could be a good simplification. However, this assumption is not often exploited in the literature since it induces possibly large errors on the HTC value. Another method is thus required for the new MB model.
Two solutions are commonly preferred in the literature to compute a mean value for $\alpha_{wf,TwoPhase}$. The first one would consist in the integration of Eqs. (3.39) to (3.41) between $x_{wf,in}$ and $x_{wf,out}$ (*Cuevas et al.* [31]), but it could be costly from a computational point of view. The second one is the application of a slip model to compute averaged properties in the biphasic zone, instead of arithmetically averaged quantities. In this study, this second solution is chosen, similarly to the work of *Horst et al.* [36].

The slip flow model initially proposed by *Zivi* [40] is chosen for its simplicity. Firstly, the slip value S is introduced:

$$S = \sqrt[3]{\frac{1}{\theta}} \tag{3.43}$$

With the ratio between saturated vapor and liquid densities:

$$\theta = \frac{\rho_{wf,sat,vap}}{\rho_{wf,sat,liq}} \tag{3.44}$$

The average void fraction γ_{avg} is computed with the equation proposed by *Jensen* in [41]:

$$\gamma_{avg} = \frac{(x_{wf,out} - x_{wf,in}) \cdot (1 - S \cdot \theta) + \theta \cdot \Big(x_{wf,in} \cdot (S-1) + 1\Big) \cdot \Big(x_{wf,out} \cdot (S-1) + 1\Big) \cdot \varepsilon}{(x_{wf,out} - x_{wf,in}) \cdot (1 - S \cdot \theta)^2} \tag{3.45}$$

With:

$$\varepsilon = ln\ \frac{\left(x_{wf,out}\cdot(S-1)+1\right)\cdot\left(x_{wf,in}\cdot(1-\theta)+\theta\right)}{\left(x_{wf,in}\cdot(S-1)+1\right)\cdot\left(x_{wf,out}\cdot(1-\theta)+\theta\right)} \tag{3.46}$$

Assuming that $x_{wf,in}=1$ and $x_{wf,out}=0$ in the biphasic zone of the condenser, Eq. (3.45) is simplified and becomes:

$$\gamma_{avg} = \frac{1-S\cdot\theta-S\cdot\theta\cdot ln\left(\frac{1}{S\cdot\theta}\right)}{(1-S\cdot\theta)^2} \tag{3.47}$$

This hypothesis concerning inlet and outlet qualities is only true if the model considers three zones on the WF side, i.e. if the fluid enters the condenser in the vapor state and leaves it in the liquid state. It corresponds to normal operating conditions of the Rankine box, for which the MB model has to be as accurate as possible. By contrast, a small lack of precision is admissible if only two zones are present, so that this simplification can be accepted.

Finally, the average fluid density and enthalpy in the biphasic zone are computed according to *Kaern et al.* [42]:

$$\rho_{wf,avg} = \rho_{wf,sat,liq}\cdot(1-\gamma_{avg}) + \rho_{wf,sat,vap}\cdot\gamma_{avg} \tag{3.48}$$

$$h_{wf,avg} = \frac{\rho_{wf,sat,liq}\cdot h_{wf,sat,liq}\cdot(1-\gamma_{avg}) + \rho_{wf,sat,vap}\cdot h_{wf,sat,vap}\cdot\gamma_{avg}}{\rho_{wf,avg}} \tag{3.49}$$

And from the value of $h_{wf,avg}$, the average working fluid quality is calculated by:

$$x_{wf,avg} = \frac{h_{wf,avg}-h_{wf,sat,liq}}{h_{wf,sat,vap}-h_{wf,sat,liq}} \tag{3.50}$$

One can highlight that Eqs. (3.43) to (3.50) are only dependent on the WF saturation properties. As a result, $x_{wf,avg}$ is a function of the condensation pressure only. This averaged quality is finally introduced in Eqs. (3.40) and (3.41) to compute $\alpha_{wf,TwoPhase}$ for the second zone of the MB condenser model. But one can highlight that simulations performed with the new MB model have shown that fixing simply $x_{wf,avg}=0.5$ in the two-phase zone or using the slip model presented above to compute $x_{wf,avg}$ does not lead to significant differences. For the sake of simplicity, choosing $x_{wf,avg}=0.5$ is thus acceptable, only in the case of the condenser. In fact, with the boiler model, simulations have shown that this simplification results in too fast time constants in the two-phase zone. As a result, the slip model needs to be exploited in this zone, as shown later in the text in the section dedicated to the MB boiler model.

3.2.4 Modelling of the exchanger wall

As shown in Fig. 3.7, one wall element corresponds to each volume defined on the working fluid side of the condenser. For a given WF zone, the corresponding wall temperature T_{wall} has to be known to compute the total heat flux $\dot{Q}_{wf,tot}$ (Eq. 3.14). As said before, this heat flux is computed from the temperature gradient between wall and WF at the *previous* time step. In other words, the energy conservation equation applied to a wall element at time t aims to compute the wall temperature that will be used at the

following time step to calculate the heat flow between the working fluid and the wall, but also between the wall and the air flow.

As a reminder, an average wall temperature T_{wall} is considered for each of the three wall elements. This MB model neglects temperature gradients across the wall thickness and along the longitudinal wall direction, similarly to the previous finite volume model. However, it does not mean that the same wall element can be used for a MB or a FV model. In fact, with a FV model the mass of each wall element is simply the total exchanger mass $m_{wall,tot}$ (mass of the tubes, fins, etc.) divided by the number of finite volumes. By contrast, in a MB model the mass of each of the three wall elements is dependent on its corresponding zone length fraction:

$$m_{wall,i} = F_i \cdot m_{wall,tot} \quad (i = 1,2,3) \tag{3.51}$$

This variable mass inside a given wall element complicates the formulation of the energy conservation equation, which is written for the element i as:

$$cp_{wall} \cdot \frac{m_{wall,i}(t) \cdot T_{wall,i}(t) - m_{wall,i}(t-1) \cdot T_{wall,i}(t-1)}{\Delta t} = \dot{Q}_{wf,i} - \dot{Q}_{air,i} + \dot{Q}_{left} + \dot{Q}_{right} \tag{3.52}$$

In this equation, cp_{wall} is the specific heat capacity of the metal, $\dot{Q}_{wf,i}$ is the heat flux from WF to the wall in zone i of the condenser, and $\dot{Q}_{air,i}$ is the heat exchange between the wall and the air flow. These two heat fluxes are defined as positive in normal operating conditions of the condenser (condensation and cooling of the working fluid; heating-up of the air flow), so it explains the positive and negative signs before $\dot{Q}_{wf,i}$ and $\dot{Q}_{air,i}$ respectively.

The linear movement of zone boundaries along the exchanger longitudinal direction induces mass transfers between adjacent wall elements, but also energy transfers: a small fraction of the wall mass that is included in a given zone at time t-1 and goes to an adjacent zone at time t carries out a certain amount of thermal energy. These energy transfers are represented by $\dot{Q}_{left}$ and $\dot{Q}_{right}$ in Eq. (3.52), and are illustrated in Fig. 3.9. On this schema, the second wall element (corresponding to the two-phase WF zone) is represented. The boundaries B_{1-2} (between zones 1 and 2, Eq. 3.6) and B_{2-3} (between zones 2 and 3, Eq. 3.7) are moving, so that the zone fraction goes from $F_2(t\text{-}1)$ to $F_2(t)$.

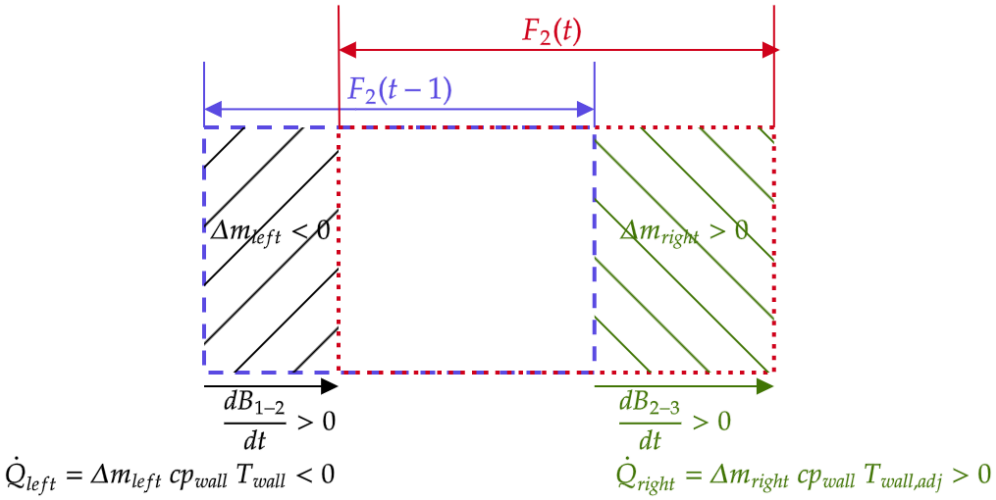

Figure 3.9: Working principle of the wall element (example of zone 2).

Since B_{1-2} is moving to the right, a small portion of the wall leaves the second zone on the left-hand side of the zone (hatched black lines in Fig. 3.9). The corresponding variation of mass Δm_{left} that leaves the zone on this side is negative, and is expressed as:

$$\Delta m_{left} = -\frac{dB_{1-2}}{dt} \cdot m_{wall,tot} \tag{3.53}$$

The corresponding energy that leaves the second wall control volume during the time step Δt is also negative, and is computed as:

$$\dot{Q}_{left} = \frac{\Delta m_{left} \cdot cp_{wall} \cdot T_{wall}(t-1)}{\Delta t} \tag{3.54}$$

Obviously, this heat flux becomes an energy gain for the first zone. On the other side of the zone, B_{2-3} increases and the zone expands. The corresponding variation of mass Δm_{right} is thus positive (hatched green lines in Fig. 3.9):

$$\Delta m_{right} = \frac{dB_{2-3}}{dt} \cdot m_{wall,tot} \tag{3.55}$$

The resulting energy transfer from the third to the second zone is positive for the second wall control volume, and is expressed as:

$$\dot{Q}_{right} = \frac{\Delta m_{right} \cdot cp_{wall} \cdot T_{wall,adj}(t-1)}{\Delta t} \tag{3.56}$$

It is important to highlight that for a given moving boundary, if the motion results in an increase of the wall mass, the energy transferred due to this movement is computed from the average temperature of the *adjacent* wall element at the previous time step, from where this energy comes from. It is the case for the heat flux $\dot{Q}_{right}$ in the example above (Eq. 3.56).
By contrast, a boundary motion resulting in a decrease of the wall mass is associated to an energy loss computed with the average temperature of the wall element itself, as shown by Eq. (3.54) to calculate $\dot{Q}_{left}$ in the proposed example. One should highlight that for the first zone, $\dot{Q}_{left}$ is always zero since the left-hand side of this volume is fixed and corresponds to the exchanger inlet. Similarly, $\dot{Q}_{right} = 0$ in the case of the third zone.

In [36], *Horst et al.* state that these energy transfers between adjacent zones are of primary importance to model correctly the wall temperature dynamics. For this purpose, several methods are presented in the literature and this one corresponds to a good trade-off between accuracy and computational complexity.

From boundaries movements imposed by the WF side of the MB condenser model, the evolution of each wall mass element from $m_{wall,i}(t\text{-}1)$ to $m_{wall,i}(t)$ is known, as well as energy transfers between adjacent volumes. Therefore, Eq. (3.52) can be solved with the value of $\dot{Q}_{wf,i}$ and $\dot{Q}_{air,i}$ at time t to compute the average wall temperature:

$$T_{wall,i}(t) = \frac{\left[\dot{Q}_{wf,i} - \dot{Q}_{air,i} + \dot{Q}_{left} + \dot{Q}_{right}\right] \cdot \frac{\Delta t}{cp_{wall}} + m_{wall,i}(t-1) \cdot T_{wall,i}(t-1)}{m_{wall,i}(t)} \tag{3.57}$$

And this wall temperature will be used at the following time step to calculate the heat flux on both sides of the exchanger.

3.2.5 Air side of the condenser

As introduced by the block diagram in Fig. 3.7, the fact that the condenser is a cross-flow exchanger means that the total entering air flow $\dot{m}_{air,in}$ at temperature $T_{air,in}$ is divided between the three zones of the MB model as a function of zones fractions F_i (assuming a perfect distribution on the condenser surface):

$$\dot{m}_{air,in,i} = F_i \cdot \dot{m}_{air,in} \quad (i = 1,2,3) \tag{3.58}$$

The value of interest for each air element i is the heat flux transferred from the wall to the corresponding air control volume, which is needed to compute averaged wall temperatures at the following time step:

$$\dot{Q}_{air,i} = F_i \cdot A_{air,tot} \cdot \alpha_{air} \cdot (T_{wall,i} - T_{air,i}) \tag{3.59}$$

In this equation, $A_{air,tot}$ is the total exchange area on the air side of the condenser, and α_{air} is the convective heat transfer coefficient between the air flow and the wall. In the previous FV model, this HTC is fixed to a constant value: $\alpha_{air} = 80\ W/m^2K$ for each zone to fit empirical results. The same value is thus chosen for the new MB model. Similarly to the equations presented in the previous sections, the heat flux $\dot{Q}_{air,i}$ is defined as positive in normal operating conditions of the condenser, when the heat transfer goes from the wall to the air flow. The air temperature appearing in Eq. (3.59) is not the mean air temperature inside zone i. In fact, due to the cross-flow configuration of this heat exchanger, it was chosen to compute $\dot{Q}_{air,i}$ using the outlet air temperature, similarly to the previous FV model:

$$T_{air,i} = T_{air,out,i} \tag{3.60}$$

Control volumes on the air side are very similar to wall elements and could also consider energy and mass transfers between neighboring zones. However, simulations have shown that these transfers are not significant in the case of the condenser air side. In fact, the air mass transferred from one zone to a neighbor during a time step Δt is negligible in comparison with the total air mass flow going through the condenser. The energy transfers between adjacent air volumes due to the moving boundaries are thus negligible, since advection terms are clearly dominating the dynamic of the energy transfer.

The mass contained in each control volume i on the air side is expressed at time t as:

$$m_{air,i}(t) = F_i \cdot V_{air,hex} \cdot \rho_{air,in} \tag{3.61}$$

where $V_{air,hex}$ is the total volume on the air side of the condenser. The density $\rho_{air,in}$ is computed assuming that the air is an ideal gas. The inlet density is chosen to compute $m_{air,i}(t)$ to simplify the model. This hypothesis is motivated by the fact that pressure drops are neglected by the model, and it is assumed that the air density does not vary significantly due to the increase in air temperature through the exchanger.

Once the heat flux $\dot{Q}_{air,i}$ and the mass $m_{air,i}(t)$ are known, the energy conservation equation can be applied to the air control volume of interest with a backward time derivative, using Eq. (3.60):

$$\begin{aligned} \dot{Q}_{air,i} + \dot{Q}_{left} + \dot{Q}_{right} = {} & \dot{m}_{air,out,i} \cdot cp_{air} \cdot T_{air,out,i}(t) - \dot{m}_{air,in,i} \cdot cp_{air} \cdot T_{air,in} \\ & + \frac{m_{air,i}(t) \cdot cp_{air} \cdot T_{air,out,i}(t) - m_{air,i}(t-1) \cdot cp_{air} \cdot T_{air,out,i}(t-1)}{\Delta t} \end{aligned} \tag{3.62}$$

where cp_{air} is the specific heat capacity of air. In this equation, the unknown is the outlet temperature $T_{air,out,i}(t)$. The fluxes $\dot{Q}_{left}$ and $\dot{Q}_{right}$ corresponds to the energy transfers between adjacent zones, when boundaries imposed by the WF side are moving, similarly to the working principle of the wall presented above. Solving Eq. (3.62) for $T_{air,out,i}(t)$ gives:

$$T_{air,out,i}(t) = \frac{\frac{\dot{Q}_{air,i} + \dot{Q}_{left} + \dot{Q}_{right}}{cp_{air}} + \dot{m}_{air,in,i} \cdot T_{air,in} + \frac{m_{air,i}(t-1)}{\Delta t} \cdot T_{air,out,i}(t-1)}{\dot{m}_{air,out,i} + \frac{m_{air,i}(t)}{\Delta t}} \tag{3.63}$$

Finally, the mean air temperature at the outlet of this cross-flow condenser is computed using a weighted average between the outlet temperature of the three zones:

$$T_{air,out} = \sum_{i=1}^{3} F_i \cdot T_{air,out,i} \tag{3.64}$$

Similarly to the computation of the heat flux on the WF side, it is the temperature gradient at the *previous* time step that is used in Eq. (3.59). As a reminder, in *Matlab-Simulink* the output of a given block cannot be itself an input of the same block. Since $\dot{Q}_{air,i}$ and $T_{air,out,i}$ are outputs of one air element, $\dot{Q}_{air,i}$ cannot be computed at time t using the temperature $T_{air,out,i}$ at the same time step. As a result, a *memory block* is necessary to store the previous value of the outlet temperature.

3.3 Particularities of the MB boiler model

In the previous section, the moving boundary model developed in the scope of this master thesis was presented in detail, and illustrated with the example of the air condenser. However, one has to keep in mind that the Rankine box is equipped with another heat exchanger, the exhaust boiler, whose previous FV representation is also replaced by the MB model. The working principle of this new boiler model is almost identical to the condenser. In this section, the particularities of the boiler model are firstly highlighted. Empirical correlations used to compute the heat transfer coefficient on the WF side of this exchanger are presented thereafter.

The exhaust boiler is a plate-fin heat exchanger (Fig. 3.10). In waste heat recovery systems, this type of heat exchanger is widely used due to its high heat transfer surface area to volume ratio. Plates and fins are disposed to obtain a counter-flow configuration. Similarly to the condenser model, this boiler is characterized by the volume, the flow section and the exchange area on both exchanger sides (WF and exhaust gases) as well as the mass of the separation wall.

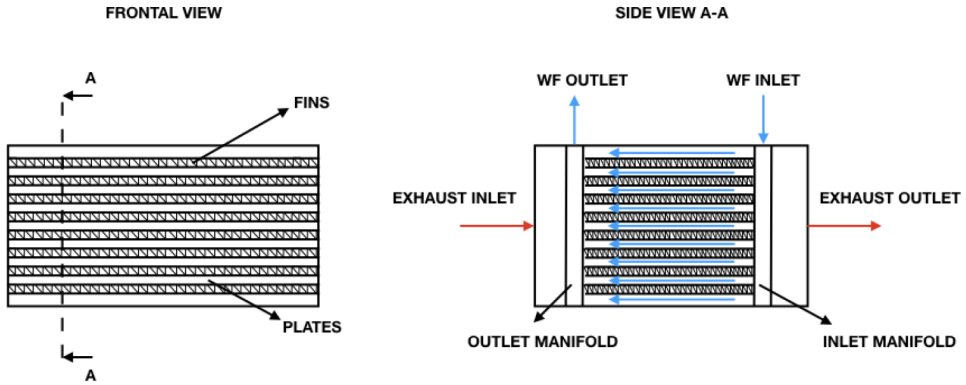

Figure 3.10: Schematic representation of the exhaust boiler (plate-fin exchanger).

3.3.1 Similarities and differences with the condenser model

The major assumptions associated to the boiler are the same than the ones of the condenser model. Pressure drops and thermal losses to the ambient are not taken into account. Contrary to the condenser, the exhaust boiler is a *counter-flow* heat exchanger (Fig. 3.11), modelled as a straight pipe of uniform cross-section in the flow direction (1-D model).

The working principle on the WF side of the exchanger remains exactly the same to compute the length fraction of each zone; maximum and minimum length fractions F_{max} and F_{min} are also used to avoid singularities caused by a disappearing zone.
In normal operating conditions, working fluid enters the exhaust boiler in the liquid state and is heated up to the liquid saturation point (zone 1). The corresponding desired outlet enthalpy is thus: $h_{out,des} = h_{sat,liq}(P_{ev})$. After that, the WF evaporation occurs in zone 2, until the vapor saturation point is reached: $h_{out,des} = h_{sat,vap}(P_{ev})$. Finally, the remaining length of the exchanger enables a super-heating of the WF flow above the saturation temperature of cyclopentane (zone 3). Apart from these standard conditions, situations with only two or one zone(s) are also possible, resulting in 6 possible configurations depending on the presence/absence of each zone, similarly to the condenser model.

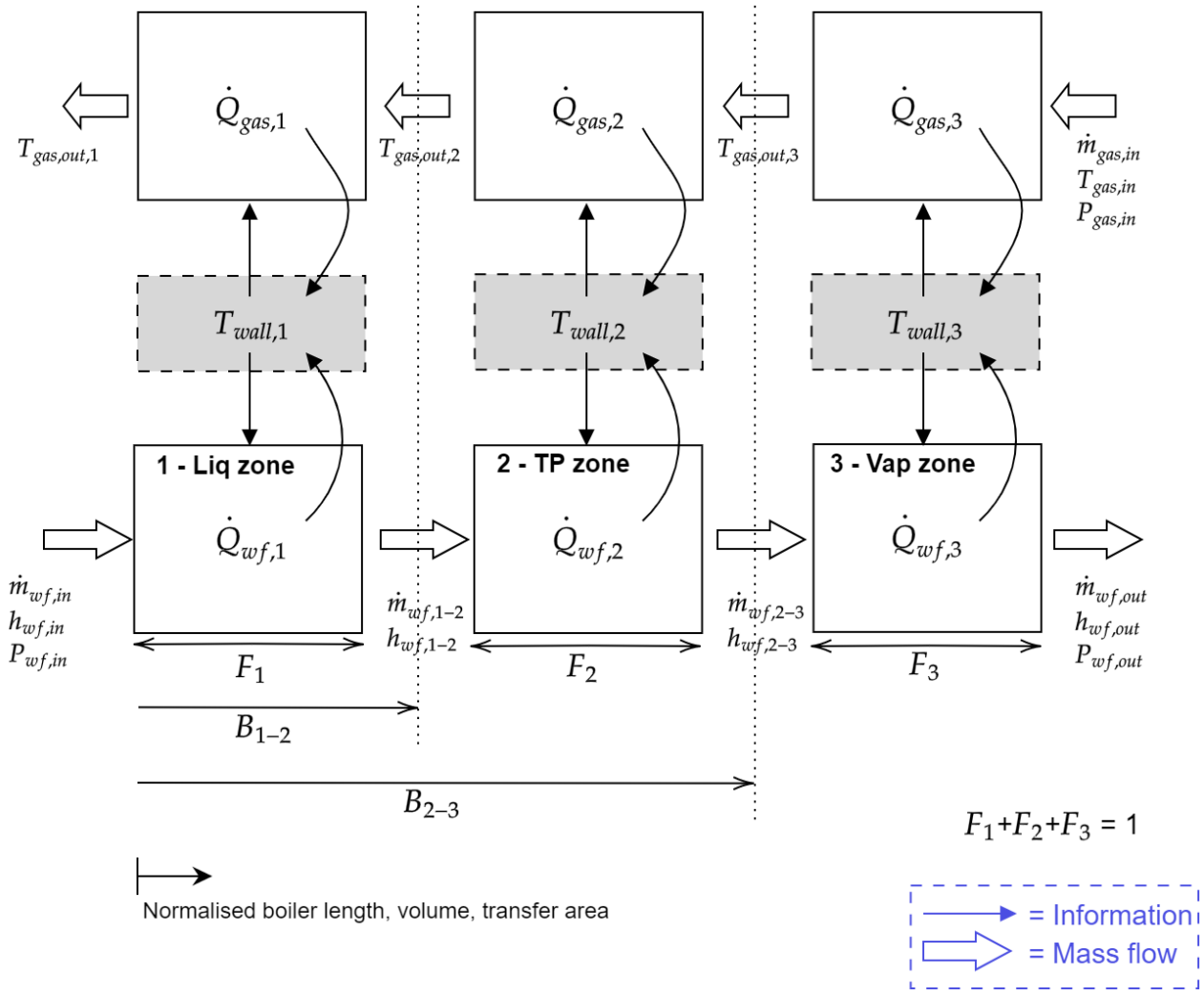

Figure 3.11: Block diagram of the moving boundaries boiler model.

Averaged properties between the inlet and the outlet of a given zone are also employed. Mass and energy conservation equations presented by Eqs. (3.9) to (3.31) remain valid to compute outlet properties and length fraction for each moving control volume. Due to the fact that heat transfer goes *from* exhaust gases *to* the working fluid in the exhaust boiler, some adjustments concerning sign convention are operated with respect to the condenser model, where the thermal energy is transferred *from* WF *to* the ambient air. The major difference on the WF side is that empirical correlations used to compute the HTC are not the same for the boiler and the condenser, as explained in the following section.

Wall elements of the condenser model described by Eqs. (3.51) to (3.57) are exactly the same for the exhaust boiler. In comparison with the cross-flow condenser model, the main differences are visible on the air side of the boiler (Fig. 3.11): the counter-flow configuration means that the whole gas mass flow goes through each control volume on the gas side, and the outlet properties of one block become the inlet conditions of the next one. Gas elements are thus similar to air elements forming the condenser air side, but they are connected differently (in series and not in parallel). However, contrary to the condenser model where the outlet air temperature is chosen to compute the temperature gradient between the air flow and the wall, the heat flux in each gas element:

$$\dot{Q}_{gas,i} = F_i \cdot A_{gas,tot} \cdot \alpha_{gas} \cdot (T_{gas,avg,i} - T_{wall,i}) \tag{3.65}$$

is computed with the arithmetically average gas temperature:

$$T_{gas,avg,i} = \frac{T_{gas,in,i} + T_{gas,out,i}}{2} \tag{3.66}$$

A constant heat transfer coefficient $\alpha_{gas} = 70\ W/m^2K$ is chosen, similarly to the previous FV boiler model developed by *Volvo Trucks*, where this constant HTC was fixed to fit empirical data.
The energy conservation in each gas element writes as a function of the average gas temperature, taking into account energy transfers between adjacent zones ($\dot{Q}_{left}$ and $\dot{Q}_{right}$):

$$\begin{aligned}\dot{Q}_{gas,i} + \dot{Q}_{left} + \dot{Q}_{right} = {} & \dot{m}_{gas,in,i} \cdot cp_{gas} \cdot T_{gas,in,i} - \dot{m}_{gas,out,i} \cdot cp_{gas} \cdot T_{gas,out,i} \\ & - \frac{m_{gas,i}(t) \cdot cp_{gas} \cdot T_{gas,avg,i}(t) - m_{gas,i}(t-1) \cdot cp_{gas} \cdot T_{gas,avg,i}(t-1)}{\Delta t}\end{aligned} \tag{3.67}$$

Inserting Eq. (3.66) into Eq. (3.67) to express $T_{gas,avg,i}(t)$ and solving for $T_{gas,out,i}$ gives:

$$T_{gas,out,i} = \frac{\frac{-\dot{Q}_{gas,i} - \dot{Q}_{left} - \dot{Q}_{right}}{cp_{gas}} + \dot{m}_{gas,in,i} \cdot T_{gas,in,i} - \frac{m_{gas,i}(t)}{2 \cdot \Delta t} \cdot T_{gas,in,i} + \frac{m_{gas,i}(t-1)}{\Delta t} \cdot T_{gas,avg,i}(t-1)}{\dot{m}_{gas,out,i} + \frac{m_{gas,i}(t)}{2 \cdot \Delta t}} \tag{3.68}$$

This equation is the alter ego of Eq. (3.63) presented in the section devoted to the condenser. After the computation of the heat flux with Eq. (3.65), the outlet gas temperature is calculated with Eq. (3.68). This outlet temperature is thus the inlet temperature of the following gas element. Finally, the temperature of the exhaust gases leaving the Rankine box is simply equal to the outlet temperature of the last control volume.

3.3.2 Computation of the heat transfer coefficient

In the liquid and vapor zones on the WF side of the exhaust boiler, the heat transfer coefficient between the wall and the single phase fluid flow is calculated with the Dittus-Boelter equation [39]:

$$\alpha_{wf,liq/vap} = \frac{Nu \cdot k}{L_c} = \left[0.023 \cdot Re^{0.8} \cdot Pr^{0.4}\right] \frac{k}{L_c} \tag{3.69}$$

where Nu, Re and Pr are respectively the Nusselt, Reynolds and Prandtl numbers. This equation is chosen because it is already used in the previous FV model of the exhaust boiler.
In the second zone on the WF side, where the fluid is in two-phase state, a modified version of the Shah correlation [43] is used:

$$\alpha_{wf,TwoPhase} = \alpha_{wf,liq} \cdot \left[1 + \left(\frac{3.8}{P_{red}^{0.38}} \cdot \left(\frac{x_{wf,avg}}{1 - x_{wf,avg}}\right)^{0.76}\right)\right] \tag{3.70}$$

where P_{red} is the reduced pressure (ratio between the evaporation pressure and the WF critical pressure). To calculate the average fluid quality $x_{wf,avg}$ in the second zone, the slip model presented in the section dedicated to the condenser is employed. The application of this slip model is an evolution with respect to the previous FV boiler model, where the fluid quality appearing in Eq. (3.70) is simply equal to the outlet quality of the considered control volume.
The particularity of the boiler is that, for the second zone, it is always assumed that $x_{wf,in} = 0$ and $x_{wf,out} = 1$, so that the slip model developed by *Jensen* [41] (Eq. 3.45) becomes:

$$\gamma_{avg} = \frac{1 - S \cdot \theta + S \cdot \theta \cdot ln\left(S \cdot \theta\right)}{(1 - S \cdot \theta)^2} \tag{3.71}$$

where S and θ are defined respectively by Eqs. (3.43) and (3.44). From the value of the average void fraction γ_{avg}, the mean fluid quality $x_{wf,avg}$ is computed with Eqs. (3.48) to (3.50).

3.4 Recuperator 0D model

The counter-flow recuperator (also called regenerator) integrated into the Rankine box (see Fig. 2.13) aims to improve the system efficiency, by transferring thermal power from the WF at the expander outlet to the WF leaving the feed pump. Indeed, the working fluid at the expander outlet (low-pressure level) is still hot enough to transfer thermal energy before being condensed. On the other hand, it is interesting to pre-heat the WF at the pump outlet (high-pressure level) before entering the exhaust boiler.

Contrary to the exhaust boiler and the condenser, the recuperator is not represented by a 1-D model in the Rankine box simulation tool developed up to now by *Volvo Trucks*. In fact, this new component is not yet completely characterized (exchange area and volume on each side of the exchanger, evaluation of heat transfer coefficients, etc.). This lack of data made impossible to build a precise 1-D finite volumes model for the recuperator. As a result, a 0-D approach is employed to include this new component in the Rankine box model.
In this simplified method, it is assumed that on the recuperator hot side (WF at the expander outlet), the fluid is cooled down until the vapor saturation point. From the knowledge of the inlet fluid enthalpy, the retrieved thermal power writes:

$$\dot{Q}_{recup} = \dot{m}_{wf} \cdot \left(h_{wf,exp,out} - h_{sat,vap}(P_{cd})\right) \tag{3.72}$$

In other words, the hot fluid is assumed to be de-superheated in this exchanger, without being partially condensed. And the 0-D model considers that the heat flux $\dot{Q}_{recup}$ is transferred (with an efficiency equal to 0.7) to WF at the pump outlet (recuperator cold side). However, if $h_{wf,exp,out} < h_{sat,vap}(P_{cd})$, the model sets logically $\dot{Q}_{recup}$ to zero.
This working principle is illustrated in Fig. 3.12. Due to the form of the T-s diagram determining temperature gradient between hot and cold sides in the recuperator, it is impossible for $\dot{Q}_{recup}$ defined by Eq. (3.72) to be sufficient to heat-up the fluid leaving the pump until the liquid saturation point, $h_{sat,liq}(P_{ev})$.

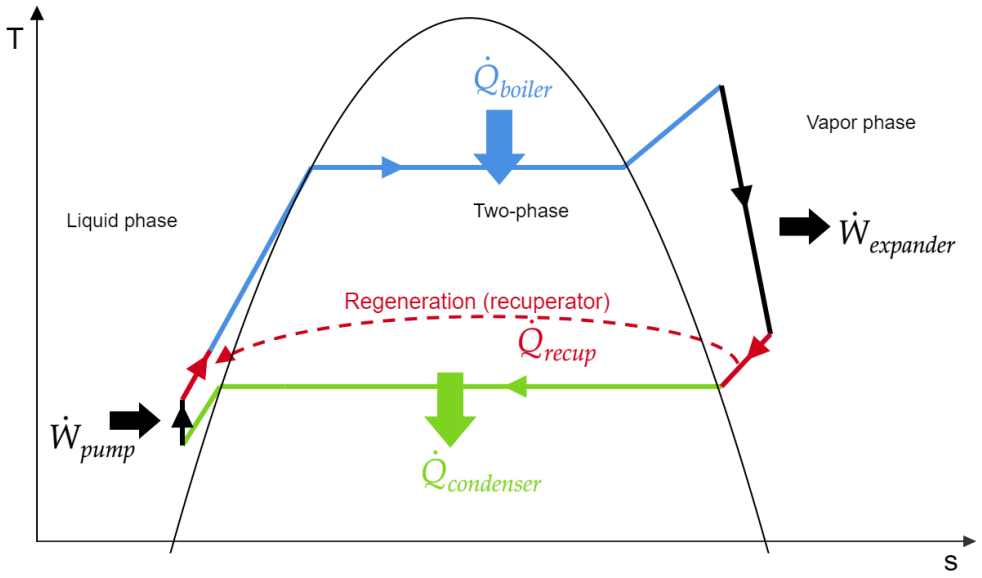

Figure 3.12: Thermal power exchanged in the recuperator (assumption of the 0D model).

In the new Rankine box where moving boundary models are used for the exhaust boiler and the condenser, the recuperator model is not modified and this 0-D approach is still preferred. Modelling this additional heat exchanger with the MB method is left as perspective for further work, when all its characteristics will be known.
However, one can already anticipate some particularities of such a model. In fact, on the recuperator hot side, at most two zones would be necessary: a first zone where WF is in the vapor state, and another containing two-phase WF. Indeed the existence of a liquid zone on this side is improbable, it would mean that the fluid is totally condensed in the recuperator before entering the air condenser. In any case, zone boundaries would be defined on the recuperator hot side: it is on this side that working fluid is likely to change phase. In addition, WF would be always in the liquid state on the cold side.

In conclusion, an MB model of the recuperator is not developed in the scope of this master thesis, and the simplified 0-D model described in this section is still employed. However, such a moving boundary model with at most two zones defined on the hod side would be a particular case of MB models, traditionally used for boilers and condensers where 3 zones are identified. Hence, it can be considered that the MB approach is not suitable to model this exchanger where complete phase transition does not occur.

3.5 Modification of the Rankine box controller

In this section, the working principle of the controller developed by *Volvo Trucks* to control the Rankine box model is briefly described. After that, adjustments made to adapt this controller to the new moving boundaries heat exchanger models are discussed in detail.

3.5.1 Working principle of the controller

The controller of the Rankine box is composed of five simple PID controllers, each operating on a controllable input of the complete system, in order to track set-point values for different physical quantities that are important to control:

1. The feed pump rotation speed is controlled to vary the WF mass flow rate, in order to track a super-heating set-point at the outlet of the exhaust boiler, before entering the piston expander. Indeed, a superheat above the WF saturation temperature is required to ensure a safe functioning of the expander (no liquid mass flow through this component). The set-point was determined from previous work and is fixed to 30 K.

2. The controller acts on the exhaust bypass valve position to regulate the exhaust mass flow which goes effectively through the exhaust boiler (see Fig. 2.13). This position is fixed to guarantee that the WF temperature at the boiler outlet does not exceed 230°C, according to technical requirements of the piston expander. If a part of the exhaust mass flow is not sent to the boiler, it represents a waste of thermal energy but it is necessary to ensure safe system operations.

3. To make sure that working fluid entering the feed pump is totally in the liquid state, a sub-cooling set-point is fixed at the outlet of the air condenser. This value, generally fixed to 20 K with cyclopentane, is achieved by acting on the cooling fan speed to control the air mass flow rate in the condenser.

4. However, the fan rotation speed is limited to 4700 rpm. Under certain conditions, the sub-cooling set-point cannot be satisfied even if this maximum speed is reached. In this case, the controller varies the WF tank pressurization in order to increase the condensation pressure. In other words, the controller acts on two parameters (fan speed and low-pressure level) to track the sub-cooling at the condenser outlet.

5. The set-point value of the high-pressure level (evaporation pressure) is fixed proportionally to the WF mass flow rate. However, this pressure is limited to 35 bars even with a very large flow rate. Afterwards, the expander rotation speed is controlled to track this set-point value. Indeed, the piston expander model computes the inlet pressure as a function of its rotation speed and the WF mass flow rate, knowing that the outlet pressure is imposed by the WF tank pressurization.

As a reminder, a PID controller computes the value of a controllable input $u(t)$ as:

$$u(t) = \overbrace{K_p \cdot e(t)}^{\text{proportional term}} + \underbrace{K_i \int_0^t e(\tau)\, d\tau}_{\text{integral term}} + \overbrace{K_d \frac{de(t)}{dt}}^{\text{derivative term}} \tag{3.73}$$

where $e(t)$ is the error between the output value that is necessary to control (the sub-cooling at the condenser outlet for example) and its corresponding set-point (reference value). Parameters K_p, K_i and K_d are respectively called proportional, integral and derivative gains.
For each of the five PID controllers introduced above, these gains were adjusted to track as accurately as possible the set-point values during transient simulations of the Rankine box along different road cycles. More precisely, the derivative gain is always fixed to zero, since this derivative action was considered to be useless according to previous work[2]. Proportional and integral gains were fixed in order to find a trade-off between controller rapidity and stability, while minimizing oscillatory behaviors and steady-state errors.

[2]In this case, these controllers would be called *PI* and not *PID* controllers.

3.5.2 Step responses campaign

After some steady simulations to verify the accuracy of new boiler and condenser MB models (see later in the text), they are integrated to the complete Rankine box model on *Simulink*. However, first simulations have shown that the controller described above, adjusted to deal with the previous FV model of heat exchangers, is not totally able to operate with new MB models. For example, set-point value of the super-heating is far from being satisfied during transient simulations, and steady-state errors are also observed . In other words, the controller has to be modified to control well the new box model.

This situation could have been anticipated, since heat exchangers are responsible for the main transient characteristics of ORC power systems. This finding is even more true for the Rankine box model developed by *Volvo trucks*, where expander and pump models are relatively simple and do not take into account for example thermal losses and components inertia[3]. Moreover, heat exchangers are components that undergo directly varying external conditions during transients: the exhaust mass flow rate and temperature in the case of the exhaust boiler, and the ambient air temperature with the condenser.
In addition, FV and MB models are based on two completely different approaches. Even if they share several aspects (correlations to compute HTC for example), it is normal that they do not present the same transient behaviors. Furthermore, the number of finite volumes is equal to 10 with the FV model, while the MB method considers only 3 control volumes at most. This simple observation also explains why perturbations imposed to these models do not lead exactly to the same variable outputs. As a result, the need to adapt the controller to the new Rankine box model is easily understood.

Among the five PI controllers presented above, this study has shown that *only* the controller acting on the pump rotation speed (to track the super-heating set-point at the exhaust boiler outlet) needs to be modified. Other controllers will not be revised in the scope of this master thesis, because it was demonstrated that they are still able to operate well in parallel with the new Rankine box model.
Indeed, during a road cycle, exhaust conditions are changing very rapidly so that the thermal power transferred from exhaust gases to WF varies significantly in time. As a result, the super-heating above the saturation temperature can fluctuate greatly, which is challenging for the corresponding controller. Because the new MB boiler model has its own transient responses, the gains of the PID controller acting on the pump rotation speed are modified, as explained below.

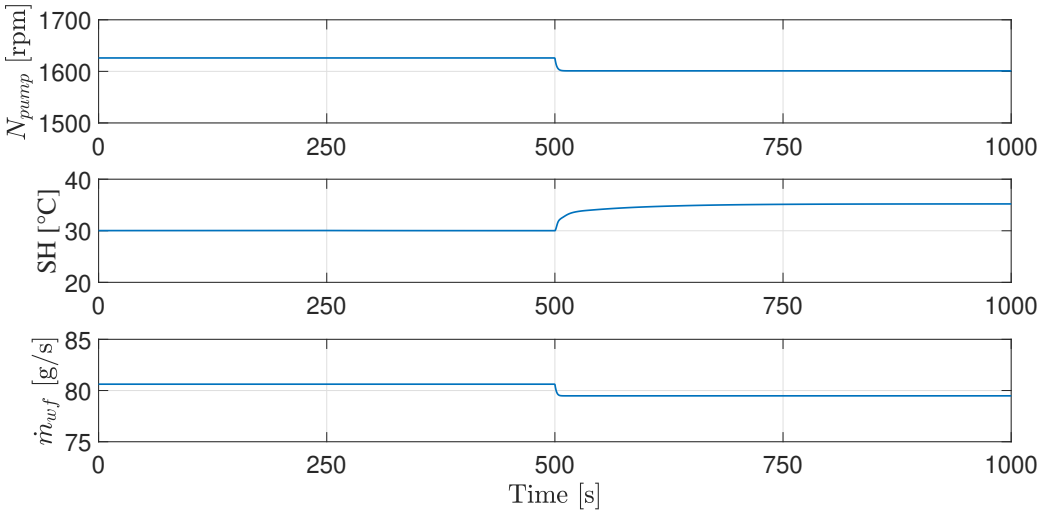

Figure 3.13: Example of step response obtained for the super-heating (SH) at the expander inlet and the WF mass flow rate, by imposing a sudden decrease in pump rotation speed (-25 rpm at $t = 500$ s).

[3]The piston expander and pump models are presented in detail in the next chapter, where all the components are reviewed to model the impact of lubricant on ORC performances.

To tune this controller, a multitude of simulations are performed to evaluate the step response of the Rankine box model when a sudden change in pump rotation speed is applied. One of these simulations is illustrated in Fig. 3.13. It can be observed that the imposed step is a decrease equal to -25 rpm (at $t = 500$ s) in pump rotation speed, which is the controllable variable of interest. This sudden variation induces a decrease in WF mass flow rate,which in turn causes an increase in super-heating at the boiler outlet.
All the step responses are evaluated after having obtained steady conditions beforehand, with different values of exhaust mass flow and exhaust gases temperature. In each case, the static gain (relative change in SH with respect to the decrease in pump speed), the time constant (time required to reach 63% of the steady-state response) and the response time delay are computed. Finally, an averaged value for each of these parameters is extracted. The mean static gain is noted G_{eq}, the averaged time constant writes τ_{eq} and θ_{eq} is the mean time delay.
After that, the SIMC method (proposed by *Skogestad et al.* in [44]) is used to compute the proportional and integral gains of the controller:

$$\begin{cases} K_p = \dfrac{1}{G_{eq}} \dfrac{\tau_{eq}}{\tau_c \cdot \theta_{eq}} \\ T_I = min\left(\tau_{eq}\ ;\ 4 \cdot (\tau_c + \theta_{eq})\right) \quad \text{with :} \quad K_i = \dfrac{K_p}{T_i} \end{cases} \tag{3.74}$$

τ_c is a parameter that can be tuned to obtain a good trade-off between rapidity and stability. In this case, it is fixed to: $\tau_c = 2\ \tau_{eq}$. Controller gains obtained with this method for the new MB model are compared in the table below to the values corresponding to the FV approach.

	$\mathbf{K_p}$	$\mathbf{K_i}$	$\mathbf{K_d}$
Previous FV model	-14	-1	0
New MB model	-2.5	-2	-120

Table 3.2: Comparison between the gains of the PID controller acting on the pump rotation speed, computed for the previous FV approach and the new MB model.

One can highlight that the derivative gain is non-zero with the controller of the MB model, contrary to the previous controller. Indeed, simulations have shown an interest to fix a relatively large derivative gain to ensure a good stability, while the SIMC method does not provide a method to compute K_d. Its exact value was chosen by trial and error, in the same way than τ_c.
In the new Rankine box model, these gains are thus used for the PID controller acting on the pump rotation speed, to track the super-heating set-point at the expander inlet. The quality of this controller will be discussed later in the text, in the section devoted to transient simulations along a road cycle.

3.6 Comparison between FV and MB models

In this section, simulation results obtained with the new MB model are presented, and compared to those computed with the previous FV approach. At first, the MB model is simulated alone to illustrate its working principle and to validate it with respect to the FV model. Once the quality of the MB method is demonstrated, new boiler and condenser models are integrated to the complete Rankine box on *Matlab-Simulink*, with the modified controller presented in the previous section. Finally, this complete model is used to perform transient simulations along a road cycle.

Unfortunately, it is only possible to compare simulations results between them, obtained with MB or FV models. In other words, the quality of the model developed in this study can only be assessed by comparison with the previous model, since empirical results are not yet available. In fact, the prototype of the Rankine system developed by *Volvo Trucks* should have been tested during the period of this internship. But the post-processing of empirical measurements was postponed due to the Covid-19 pandemic, so that these results are not exploitable in the scope of this master thesis.

3.6.1 Validation of the moving boundary model

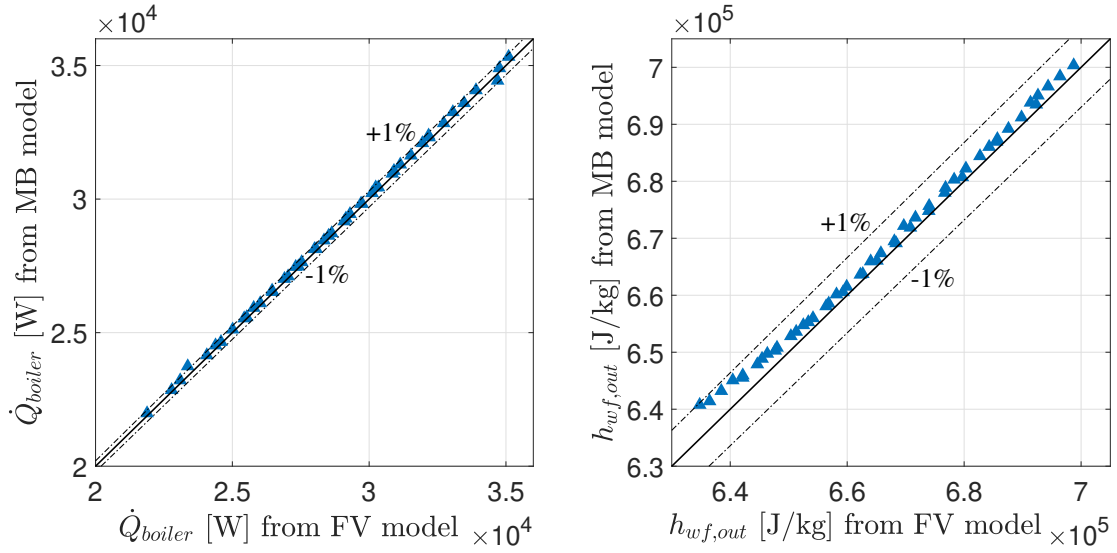

Figure 3.14: Parity plots of the heat flow rate transferred to the WF in the boiler and the WF outlet enthalpy, computed with FV and MB models for different WF inlet steady conditions ($\dot{m}_{wf} = 0.06$ kg/s). Exhaust conditions are the same for each simulation: $T_{exh} = 600$ K and $\dot{m}_{exh} = 0.15$ kg/s.

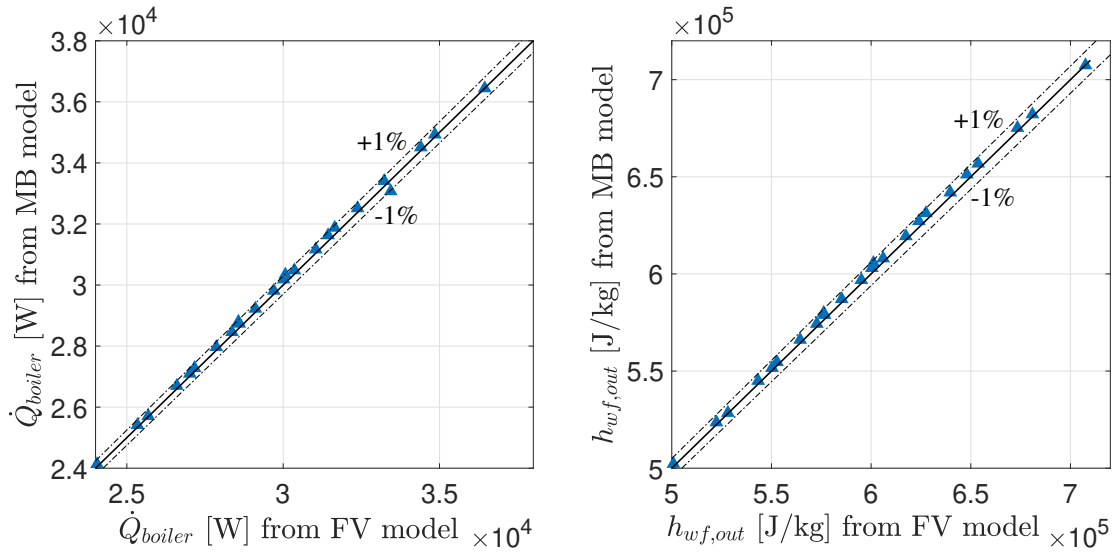

Figure 3.15: Parity plots of the heat flow rate transferred to the WF in the boiler and the WF outlet enthalpy, computed with FV and MB models for different exhaust conditions: $T_{exh} \in [300; 350]$ °C, $\dot{m}_{exh} \in [0.12; 0.15]$ kg/s. WF inlet conditions are the same for each simulation: $P_{ev} = 20$ bars and $h_{wf,in} = 10^5$ J/kg ($\dot{m}_{wf} = 0.06$ kg/s).

In the first instance, steady simulations involving only MB heat exchanger models are performed, and compared to the outputs of the previous FV method. For the sake of brevity, the results presented in this section concern the exhaust boiler only, but the air condenser model was also validated with additional simulations.
Figs. 3.14 and 3.15 present parity plots which compare steady results obtained with the exhaust boiler MB or FV models. Each point on these plots represents a steady simulation; the outputs of interest are the heat flow rate transferred to the WF in the exhaust boiler, and the WF outlet enthalpy. In Fig. 3.14, all the results are obtained with the same exhaust conditions while WF properties at the boiler inlet differ between each simulation. By contrast, it is the exhaust conditions that are varied between simulations shown in Fig. 3.15. One can observe on these four parity plots that all the points are near the bisector, in the interval +/- 1%. It means that for a chosen set of inputs (WF inlet properties, WF mass flow rate, exhaust temperature and exhaust mass flow rate), FV and MB boiler models give nearly the same output values (WF outlet enthalpy and heat flow rate).
In conclusion, the precision of the new exchanger model developed in the scope of this master thesis is demonstrated in steady-state conditions regarding simulation results obtained with the FV model. And it is important to highlight that the accuracy of this previous model was validated earlier by *Volvo Trucks*, from empirical results obtained by a subcontractor involved in the *Rankine Generation 3* project.

In order to illustrate the working principle of boundaries between zones defined in the boiler MB model, a set of steady-state simulations is presented in Fig. 3.16. To obtain these results, each input of the boiler model remains the same except the value of the exhaust mass flow rate. As a result, the heat input provided by the exhaust gases varies between each simulation.

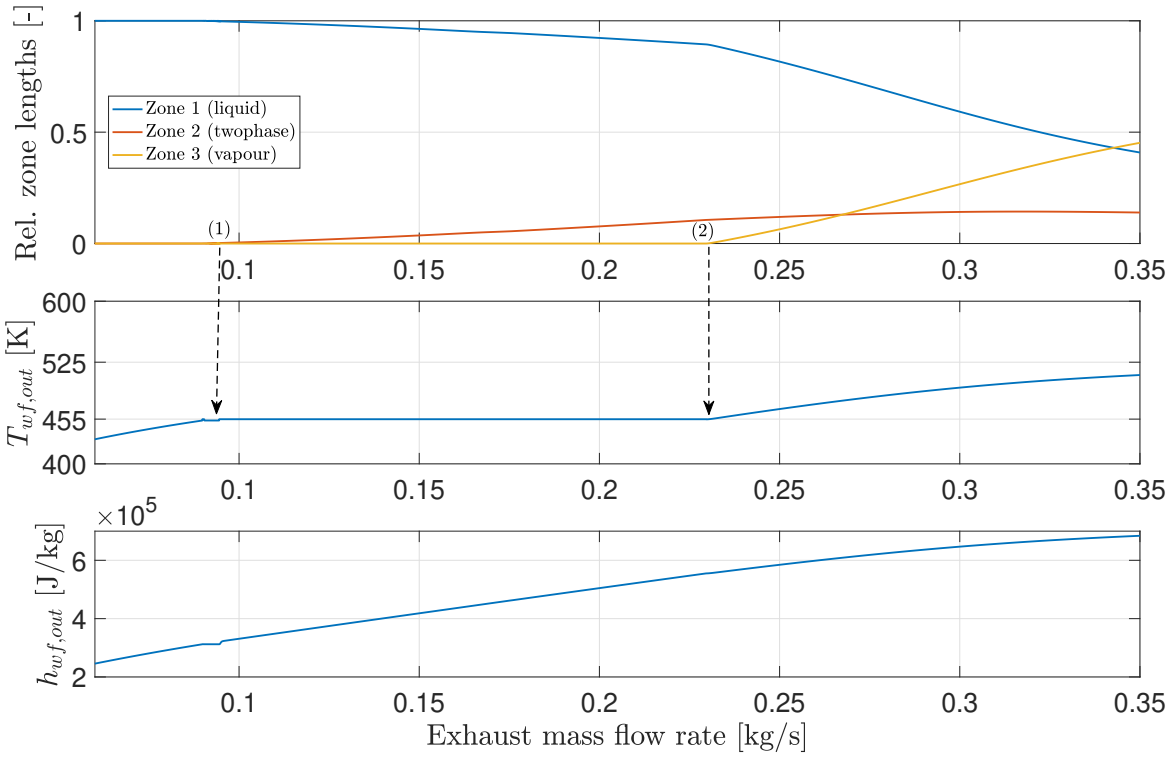

Figure 3.16: Evolution of relative zone lengths in the MB boiler model, WF outlet temperature and WF outlet enthalpy as a function of the exhaust mass flow rate, with fixed inputs: $T_{exh} = 550$ K, $\dot{m}_{wf} = 0.08$ kg/s, $P_{ev} = 20$ bars and $h_{wf,in} = 0.5 \cdot 10^5$ J/kg.

It can be observed that, with a very low exhaust mass flow, the relative length of the liquid zone (with respect to the total boiler length) is equal to 1, which means that this zone takes the entire place in the exchanger. In this case, WF is still below the liquid saturation point at the boiler outlet: $T_{wf,out}$ is lower than the saturation temperature of cyclopentane (455 K at $P_{ev} = 20$ bars).
When the heat input increases, the WF outlet enthalpy increases until the liquid saturation enthalpy (point 1 in Fig. 3.16). From this point, the second (two-phase) zone in the boiler becomes non-zero, since WF is partially vaporized. Then WF outlet enthalpy continues to increase with the exhaust mass flow rate, while WF temperature remains logically equal to the saturation temperature.
At point 2, the heat input is sufficient to reach the vapor saturation point at the boiler outlet, meaning that WF is totally vaporized. If the exhaust mass flow is further increases, one can observe that the vapor zone (zone 3) appears and grows, so that a super-heating above the saturation temperature is achieved. From point 2, the relative length of zone 1 decreases significantly, and by definition the sum of the three zones remains always equal to 1.

This example is interesting to illustrate the basic functioning of the model, but it also highlights different aspects that will be observed during transient simulations. In fact, the chosen WF conditions at the boiler inlet are similar to those observed while simulating the Rankine box along a driving cycle.
At first, one can see in Fig. 3.16 that the relative length of zone 1 is always greater than the others: WF flowing through the boiler is most of the time in the liquid state. However, the second zone (two-phase) rarely exceeds 10% of the exchanger length. This zone is relatively small due to the high HTC observed when WF is biphasic. In addition, the saturation curve of cyclopentane is not very large, meaning that the difference between liquid and vapor saturation enthalpies is restrained.
In addition, Fig. 3.16 shows that the super-heating at the boiler outlet increases rapidly with the length of the last zone. Indeed, even if the vapor HTC is quite small, the counter-flow layout of the boiler implies that the exhaust gases temperature is maximum near the fluid outlet. As a result, the temperature gradient between WF and exhaust gases is very high in the third zone, so that the heat transfer is very efficient.

The second simulation that is chosen here to illustrate the working principle of the exhaust boiler model is presented in Figs. 3.17 and 3.18. In this case, a transient simulation is performed to assess the model's dynamic behavior, by imposing a variable exhaust mass flow rate. This one evolves sinusoidally over time, with a superimposed growing trend (Fig. 3.17). It is the only perturbation since all the other input values are constant.

One can see in Fig. 3.18 the resulting evolution of zone boundaries. As expected, these boundaries vary sinusoidally. It is particularly the case for the first zone, but one can observe that this transient response is not a perfect sinusoid. When the exhaust mass flow rate is low, the third (vapor) zone disappears, meaning that the fluid is not totally vaporized at the boiler outlet. In fact, as soon as this zone length is zero, the WF outlet temperature remains constant and equal to the saturation temperature.
The growing trend of the exhaust mass flow rate also has an impact on zone boundaries. At first, the minimum reached by the first zone length at each sinusoid tends to decrease. At the same time, the vapor zone tends to become larger, which explains logically the evolution of the outlet WF temperature.

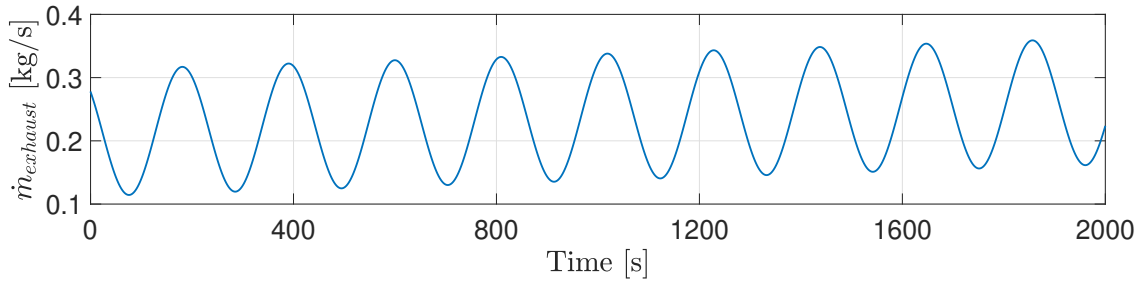

Figure 3.17: Evolution of the imposed exhaust mass flow rate during the transient simulation whose results are shown in 3.18.

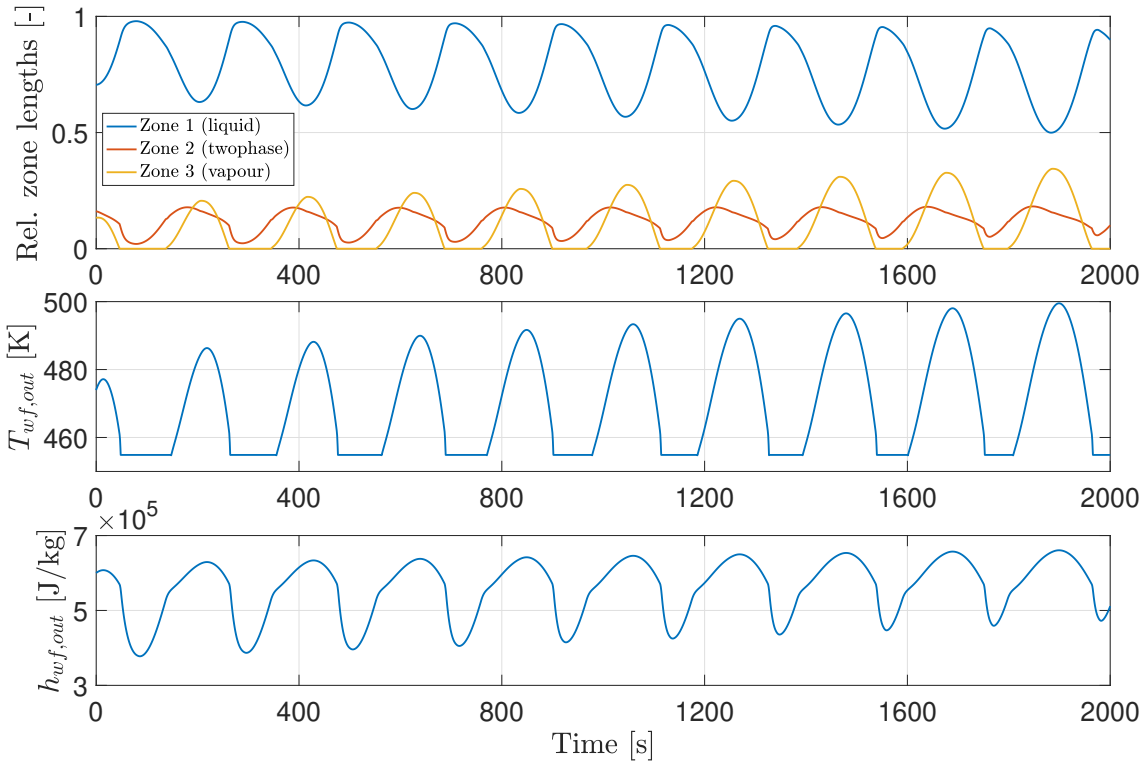

Figure 3.18: Evolution of the outputs of the MB boiler model during the transient simulation characterized by the exhaust mass flow rate shown in Fig. 3.17, while other inputs are constant: $T_{exh} = 550$ K, $\dot{m}_{wf} = 0.08$ kg/s, $P_{ev} = 20$ bars and $h_{wf,in} = 10^5$ J/kg.

3.6.2 Transient simulations along a driving cycle (FK)

The road cycle that is simulated in this study is the Frankfurt-Koblenz (FK) driving cycle. It corresponds to a German highway itinerary (almost 150 minutes long) that includes some rising sections. Large engine loads are thus observed during this cycle, which means that the exhaust thermal energy (proportional to exhaust gases temperature and exhaust mass flow) that is possible to recover with the Rankine system is relatively large (mean thermal power: 49 kW).
The engine map corresponding to the FK road cycle is shown in Fig. 3.19. However, quantities of interest from the point of view of the waste heat recovery system is the exhaust mass flow rate and the exhaust temperature (Fig. 3.20). These inputs of the Rankine box model are computed thanks to the global simulation platform developed by *Volvo Trucks*, which simulates the engine block and other components of

interest.
It can be observed that the exhaust mass flow fluctuates significantly, coming from highly transient power and torque demands during the cycle. By contrast, the exhaust temperature varies more slowly: it is partially due to the exhaust after treatment system (EATS) which constitutes an important thermal inertia. This variable exhaust thermal power along FK cycle is a disturbance for the Rankine box, whose controller is in charge of tracking set-point values for several physical quantities (as explained previously in the section devoted to the controller).

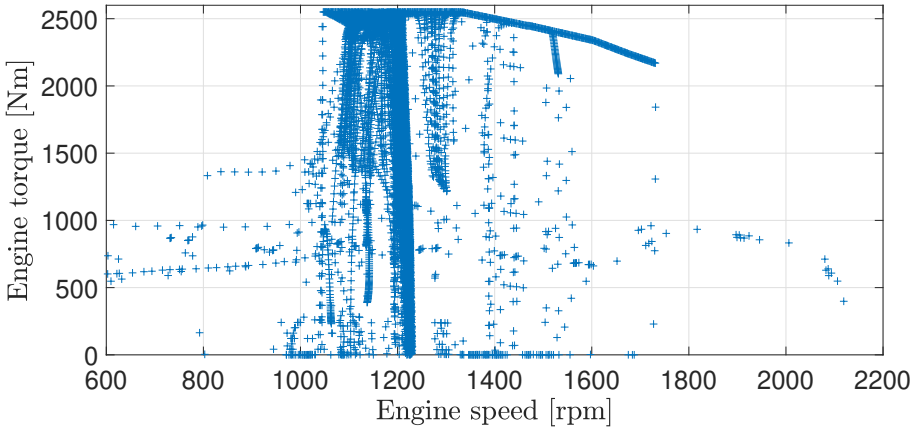

Figure 3.19: Engine map representing the operating points encountered during FK road cycle.

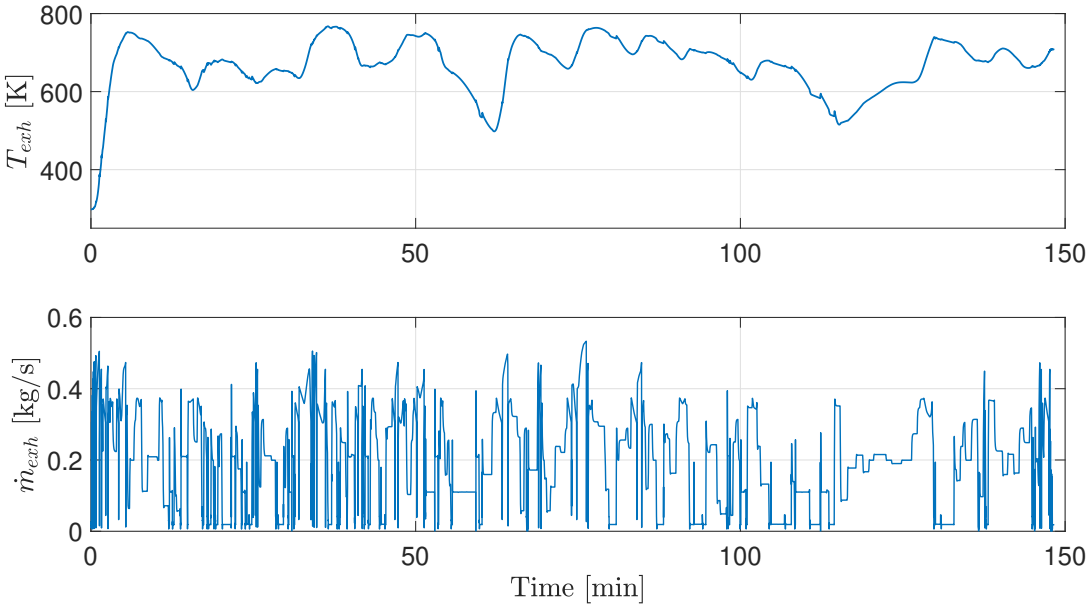

Figure 3.20: Evolution of the exhaust gases temperature and exhaust mass flow rate during FK road cycle.

New MB heat exchangers model (boiler and condenser) are integrated to the complete Rankine box model, in order to perform this transient simulation. The uncontrollable inputs of the whole system are simply the exhaust mass flow rate and temperature imposed by the cycle, as well as the air temperature. The controllable inputs (e.g. the expander and pump rotation speeds) are managed by the controller. An overview of the box model on *Matlab-Simulink* is presented in Fig. 3.21. Simulations are performed with a constant time step equal to 0.01 s, and the selected solver is *Ode1 - Euler* (backward scheme).

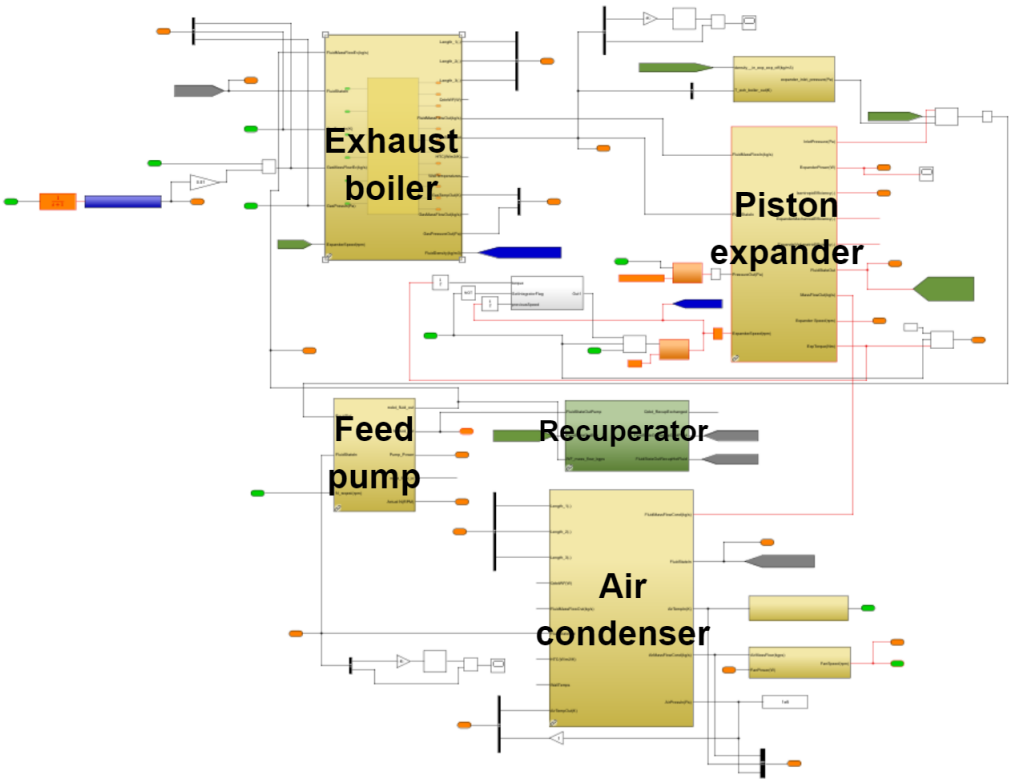

Figure 3.21: Complete Rankine box model on *Matlab-Simulink*.

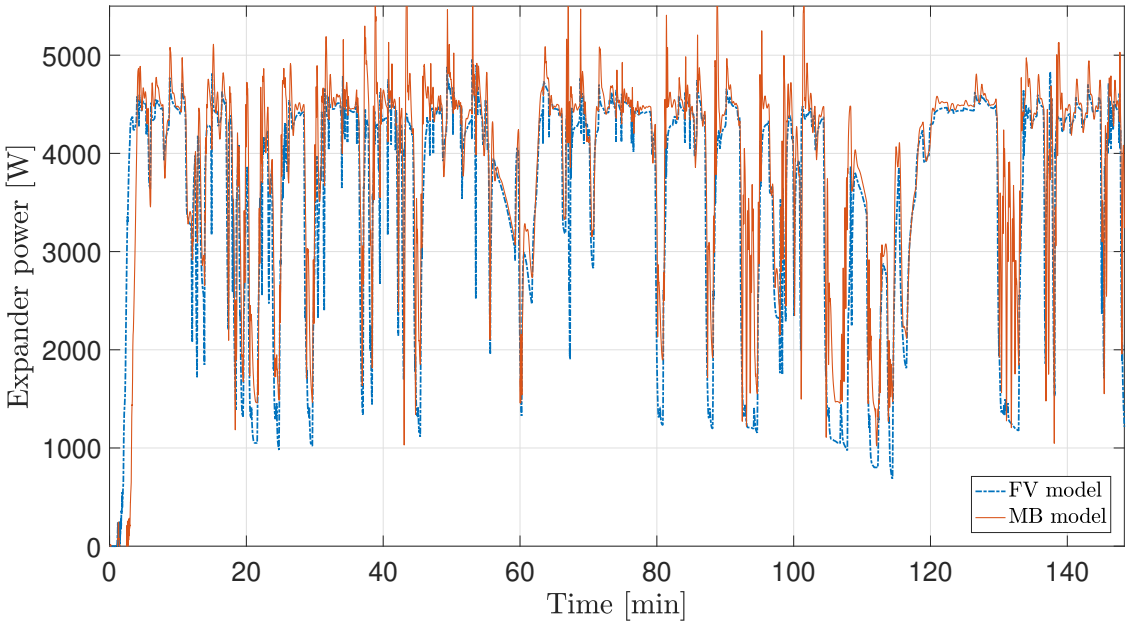

Figure 3.22: Comparison of the expander power computed by FV and MB models during the FK cycle.

In this section, simulation results during the FK cycle obtained with the new MB heat exchanger model are compared to those computed with the previous Rankine box model (FV approach). Fig. 3.22 shows the evolution of the expander gross power during the cycle, computed with these two models. The power consumptions of the feed pump and the fan (air condenser) are presented in Fig. 3.23.
It can be observed that the results computed with the MB or the FV approach are comparable, and follow the same trends during this cycle. However, the peak values of expander power differ slightly and some oscillations are identified in the case of the MB model, for the pump and expander powers. In Fig. 3.23,

one can also highlight that the fan power is often equal to a limit value, corresponding to the maximum fan speed. When the air mass flow in the condenser is already maximized, it is required to increase the condensation pressure to reach the WF sub-cooling set-point at the condenser outlet. This working principle of the controller was already discussed in Section 3.5.1.
The evolution of the evaporation and condensation pressures is shown for the two models in Fig. 3.24. Once again, the MB model gives nearly the same results than the previous FV model, but some oscillations are observed especially for the high-pressure level.

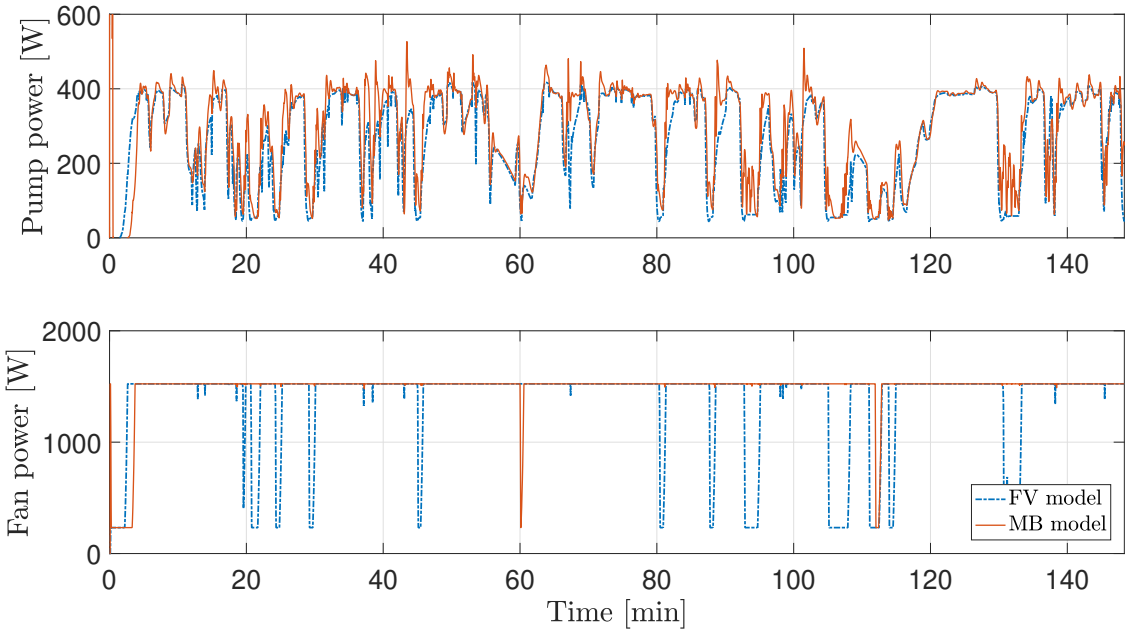

Figure 3.23: Comparison of pump and fan powers computed by FV and MB models during the FK cycle.

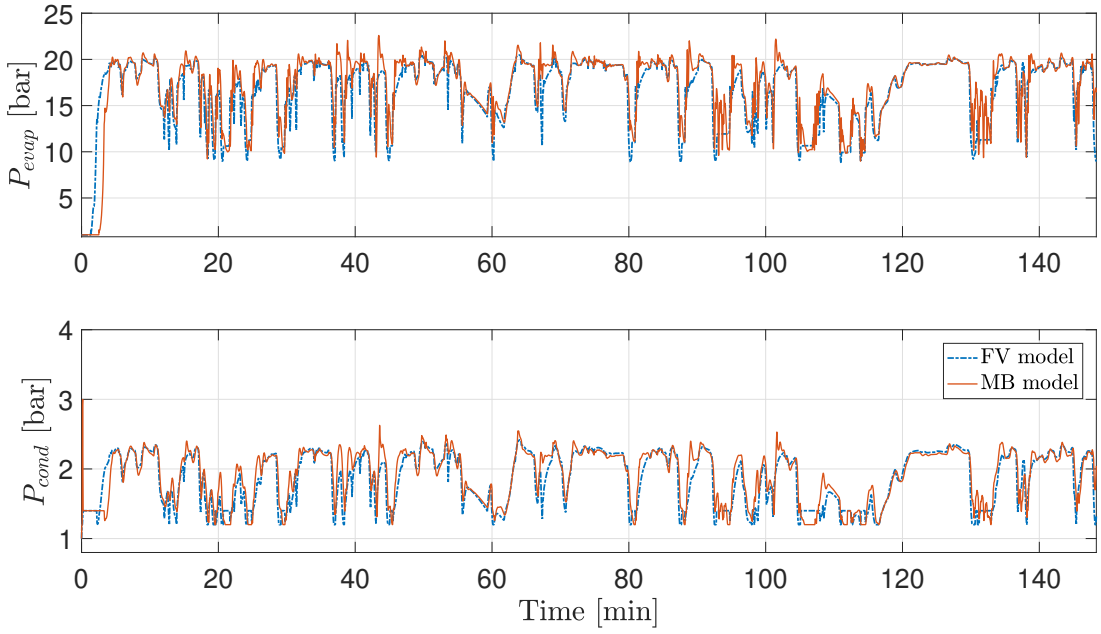

Figure 3.24: Comparison of the evaporation and condensation pressures during the FK cycle, simulated with FV and MB models.

The two models give nearly the same results, but one can suggest that differences observed at some points of the cycle are considerable. The averaged relative difference during the whole cycle between the

expander power computed with the MB or FV model (Fig. 3.22) is equal to 7.3%, which is not negligible. Indeed, MB models of heat exchangers were validated in steady-state (see previous section) and it was concluded that they give the same results within 1% compared to the previous model. By contrast, during transient simulations of the complete Rankine box, the results also depend on the controller actions. For example, the condensation pressure is a controllable input of the box model and one can observe in Fig. 3.24 that this input is not the same for the two simulations.

In the same way, Fig. 3.25 shows the evolution of the WF mass flow rate during the cycle, which mostly depends on the pump rotation speed that is imposed by the controller. Once again, some differences are identified and oscillations are observed with the MB model (near $t = 130$ min for example). Furthermore, oscillations at this point are also observable for all the other simulation results presented above (except the fan power). As a result, it is not surprising that the expander and pump powers computed with the two models are not exactly the same, since controllable inputs of the Rankine box are not always equal during transients for both simulations. In conclusion, the fact that the new box model does not give exactly the same results than the previous model is mainly due to the controller actions than the new model itself.

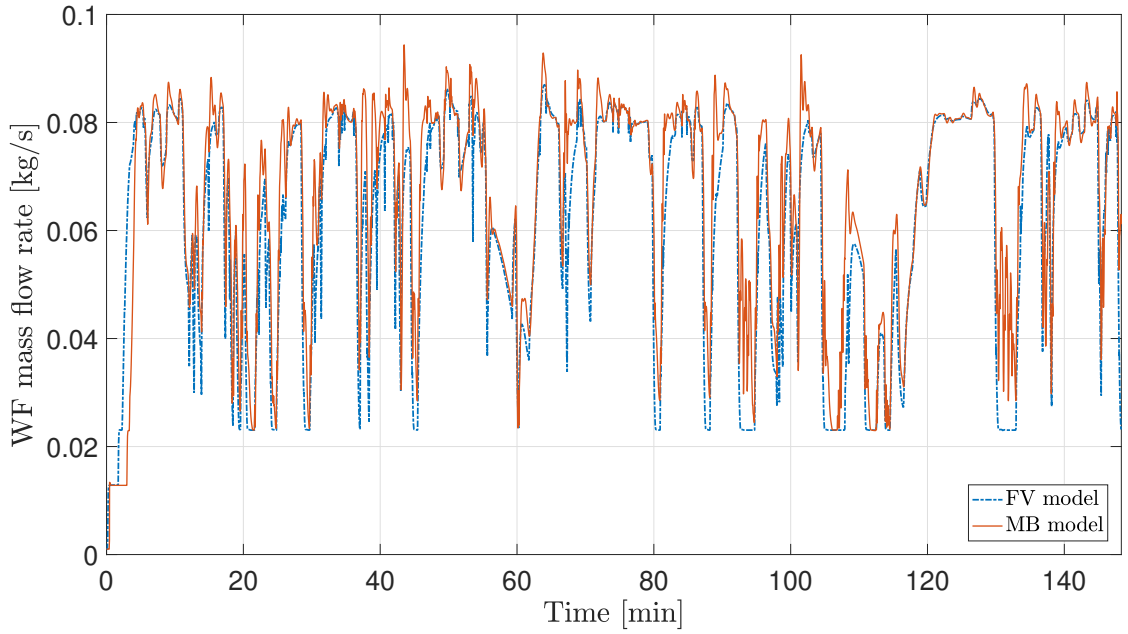

Figure 3.25: Comparison of the WF mass flow rate during the FK cycle, simulated with FV and MB models.

The pump rotation speed, which is mainly responsible for the evolution of the WF mass flow rate, is varied to track the super-heating set-point (30 K) at the exhaust boiler outlet. As discussed earlier, the corresponding PID controller was the only controller that needed to be adapted to the new MB boiler model (modified gains). The quality of this controller can be verified by the analysis of the super-heating during the FK cycle, as shown in Fig. 3.26. With the new MB model, it can be observed that the super-heating deviates least from the set-point value than in the case of the previous FV model. In fact, the new controller seems to act faster, but the price to pay is the oscillations that can be viewed on the second plot in Fig. 3.26.
In other words, the PID controller associated to the MB model acts more rapidly when the super-heating is far from its set-point. As a result, the pump speed and the WF mass flow rate are adjusted faster than in the case of the previous model. Furthermore, oscillations observed on the evolution of the WF mass flow (Fig. 3.25) have an impact on all the other quantities, especially the pump power and the expander gross power.

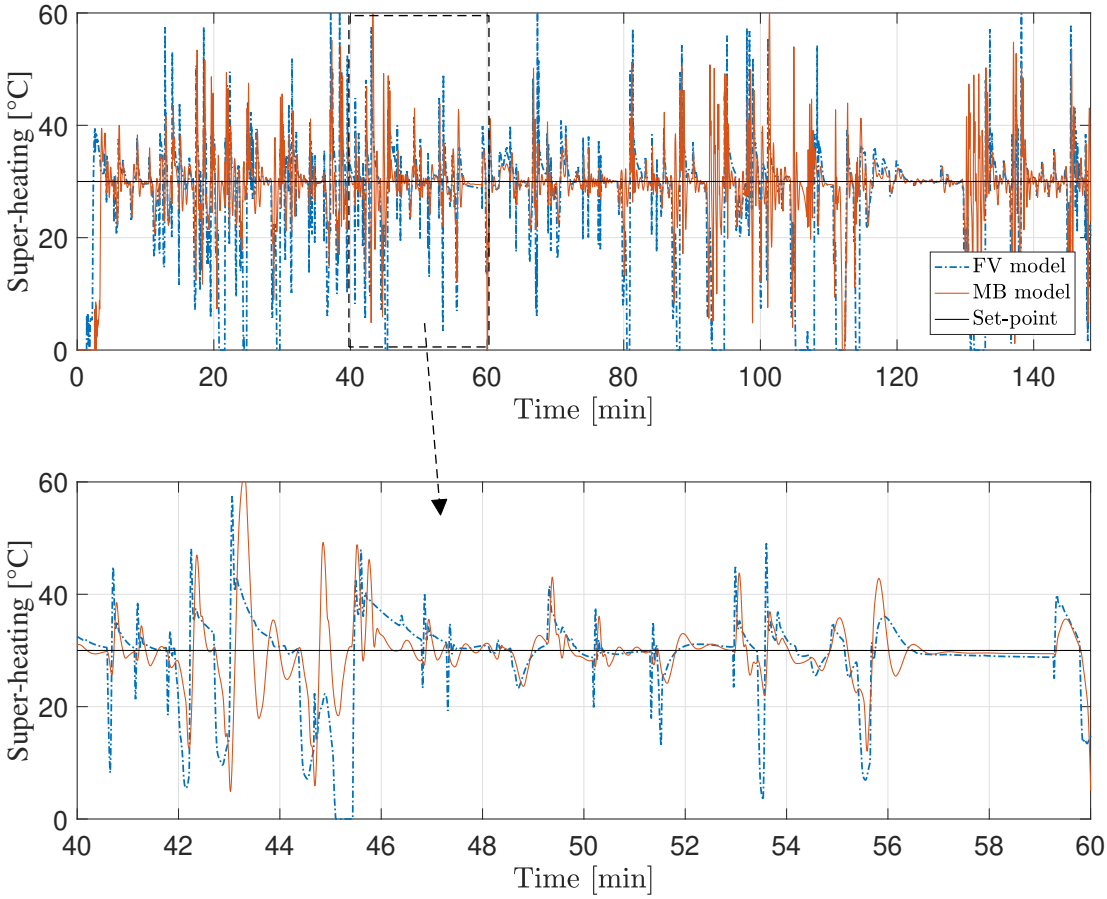

Figure 3.26: Comparison of the super-heating at the expander inlet during the FK cycle, simulated with FV and MB models.

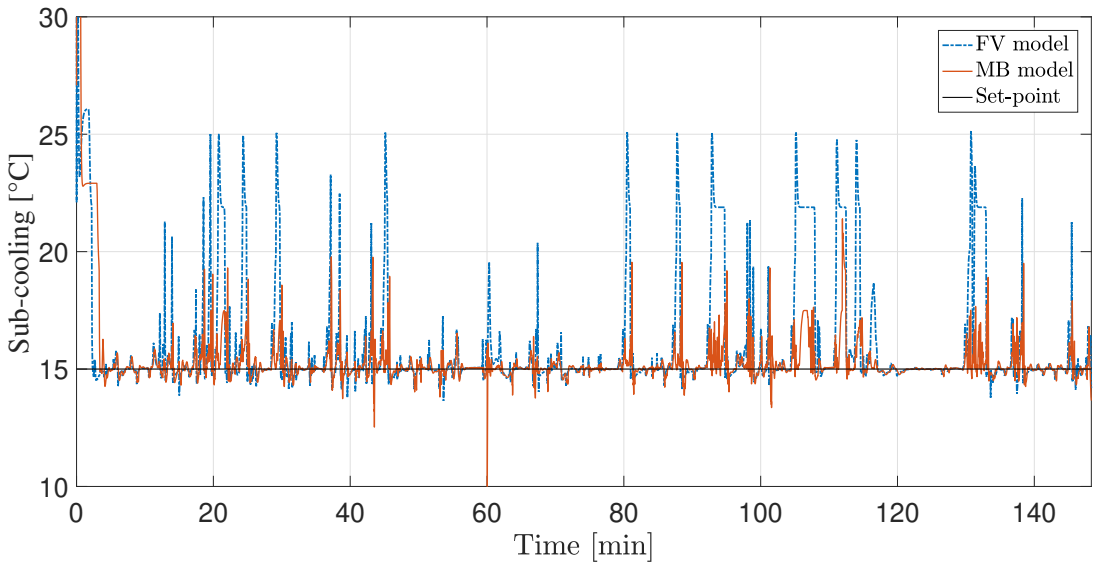

Figure 3.27: Comparison of the sub-cooling at the condenser outlet during the FK cycle, simulated with FV and MB models.

The evolution of the sub-cooling at the condenser outlet is shown in Fig. 3.27. One can observe that the set-point value (15 K) is tracked more precisely with the MB model than the FV model. However, it is important to remind that the two PID controllers responsible for the sub-cooling are *not* modified before being used in parallel with the new MB model. This sub-cooling is managed by acting on the fan speed and the condensation pressure; it is thus coherent that fast changes in condensation pressure (Fig. 3.24) can be correlated to the better tracking of the sub-cooling set-point. However, some oscillations are also observed in this case.
This example of the sub-cooling, which is an important physical quantity to control, also illustrates that simulation results depend strongly on the interaction between the Rankine box controller and the component models. In fact, the same controller used here for the sub-cooling management gives clearly not the same transient behavior if it is associated to the MB or FV heat exchanger models.

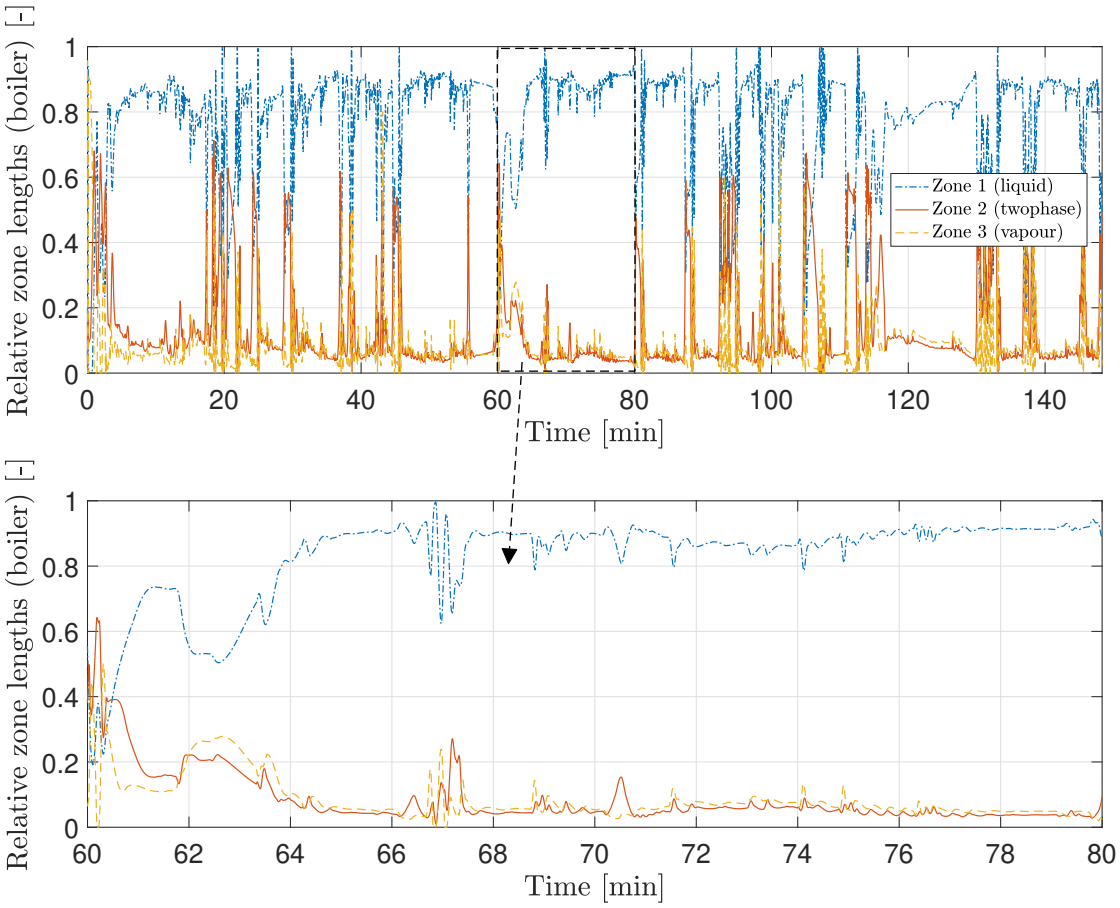

Figure 3.28: Evolution of relative zone lengths of the moving boundaries boiler model during the FK cycle.

The evolution of the relative zone lengths in the boiler MB model during the FK cycle is shown in Fig. 3.28. A zoom corresponding to 20 minutes of the cycle is proposed on the second plot. As already shown in the previous section, the larger zone in the model is always the first one, where working fluid is in the liquid state. It means that a large part of the exchanger is required to heat-up the WF until the liquid saturation point. In addition, two-phase and vapor zones present comparable lengths, which are most of the time lower than 20% of the exchanger length. The heat transfer during the vaporization process (until the vapor saturation point) is thus very efficient. Moreover, a small remaining length available for the last zone is sufficient to ensure a super-heating varying around 30°C. These observations are mainly due to the cross-flow layout of the exhaust boiler.

In addition, it is interesting to show that these relative zone lengths evolve very rapidly during the cycle. It is thus easily understood that stability problems could occur with this type of heat exchanger modelling.

These boundaries between zones that are computed with the new MB model is not a result that is possible to compute with the previous FV approach. It is indeed one of the principal interests of the moving boundaries method. It highlights also the fact that this model is intrinsically well suitable for the control: the evolution of the vapor zone length can be directly correlated with the super-heating at the boiler outlet.

In Fig. 3.29, the evolution of zone boundaries in the MB condenser model is presented. Due to the 0-D model of the recuperator (Section 3.4), the length of the vapor zone in the condenser is always zero. More precisely, this zone is fixed to the minimum zone length fixed in the model to avoid singularities. Indeed, the simplified recuperator model assumes that working fluid leaving the expander is cooled down in this additional heat exchanger until the vapor saturation point. As a result, the fluid entering the air condenser is not superheated, and the first (vapor) zone is unnecessary.
Contrary to the boiler model, it is important to highlight that the relative length of the two-phase zone is the most important. It means that the major part of the exchanger is used to condense the WF. Finally, the liquid zone ensures a sub-cooling below the saturation temperature.

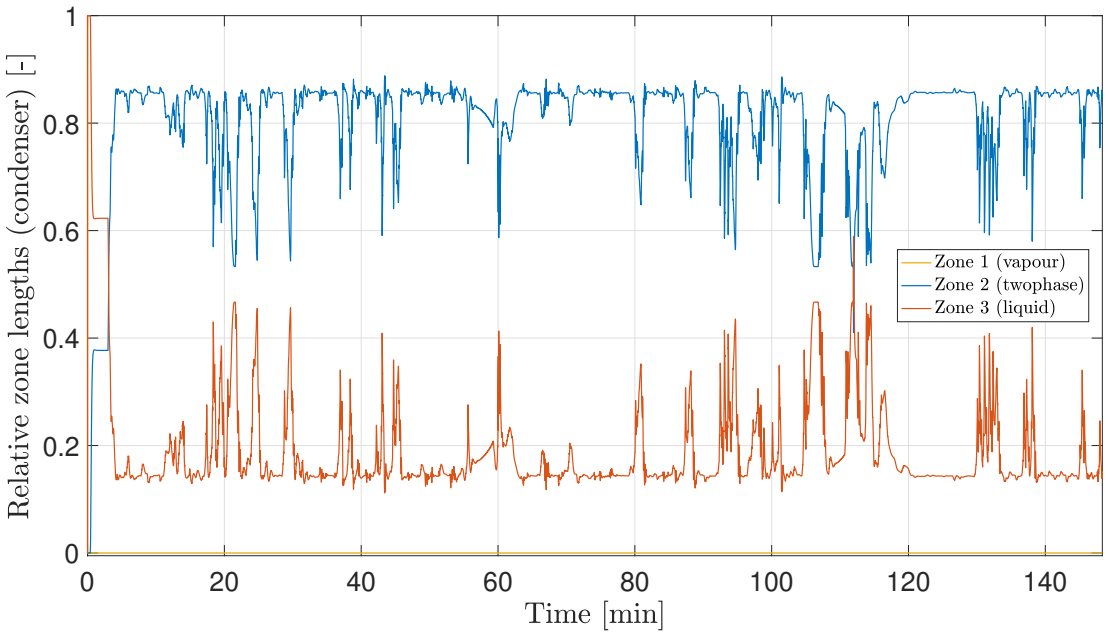

Figure 3.29: Evolution of relative zone lengths of the moving boundaries condenser model during the FK cycle.

The WF temperature at the boiler outlet is also a physical quantity that is controlled. For this purpose, the same PID controller is used than in the case of the previous FV model. The evolution of this temperature is shown in Fig. 3.30. The corresponding set-point is equal to 210°C, in order to ensure that this temperature is never greater than 230°C (maximum temperature admissible for the piston expander). It can be observed that this set-point is tracked similarly with the MB model or the FV model. However, some minima observed with the FV approach are not identified in the case of the MB model.
The input that is controlled to manage this temperature is the exhaust by-pass valve position, whose evolution is shown in Fig 3.31 during a part of the FK cycle. Here again some oscillations are observed in the case of the MB model, while the controller is the same for the two simulations.

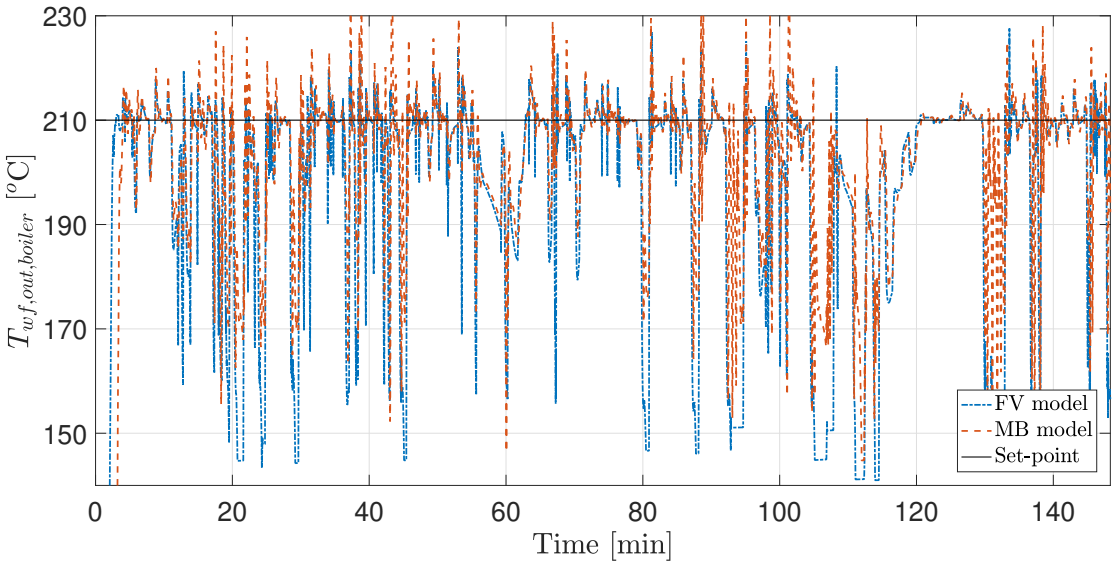

Figure 3.30: Comparison of the WF temperature at the boiler outlet during the FK cycle, simulated with FV and MB models.

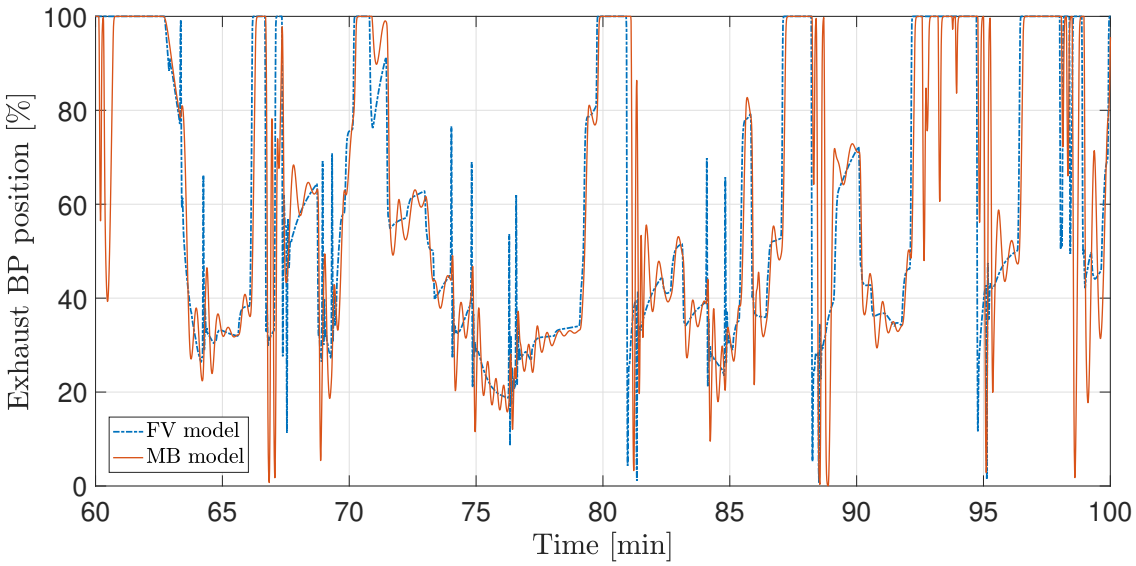

Figure 3.31: Comparison of the exhaust by-pass valve position during a part of the FK cycle, simulated with FV and MB models (position = 100% means that the exhaust mass flow is entirely sent to the boiler).

3.7 Conclusion

In the first part of this master thesis, a new moving boundary model is developed to replace the previous one used by *Volvo Trucks*, based on a finite volumes approach. At first, a brief literature review is proposed. The interests of this new model are presented, and these two modelling approaches are compared. To construct a 1-D model of a heat exchanger, the FV method is based on a spatial discretization into different control volumes. This method exhibits a high stability and a good accuracy, but it requires a relatively long CPU time. On the other hand, the new MB model implies only three zones, that are defined according to the fluid state on the WF side of the heat exchanger (liquid, two-phase or vapor). This method is generally faster, but also less accurate and presents a reduced stability.

After that, the new MB model is presented in detail. The example of the air condenser model (cross-flow heat exchanger) is chosen to illustrate the working principle of the moving boundaries between zones. The modelling of the air side as well as the separation wall are also presented. This model is based on the mass and energy conservation equations applied in each control volume. The main particularity is that moving boundaries imply mass and energy transfers between adjacent zones, that are precisely taken into account in this new model. Finally, the particularities of the MB exhaust boiler (counter-flow heat exchanger) are discussed.

All the empirical correlations that were chosen for the previous FV model are also used in the new MB model to compute convective heat transfer coefficients. Different correlations are employed depending on the WF state. The principal interest related to the transfer coefficient is that, in an MB model, the exact points where phase transitions occur are exactly tracked by the model. As a result, the good empirical correlation is employed all along the exchanger length. By contrast, in each fixed control volume, the FV model is forced to select the correlation for HTC depending on the WF state at the outlet of this volume. This approach is thus inaccurate if the WF state is not the same between the inlet and outlet of a volume. The new model shares also with the previous FV approach some hypotheses and simplifications. For example, pressure losses are neglected as well as the temperature gradients across the wall thickness and along the exchanger length.

After that, steady-state simulations are presented to validate this new heat exchanger model, by comparison with the FV model. The conclusion is that, for a given set of input values, these two models give similar steady results, with a relative difference lower than 1%. Unfortunately, it is impossible to validate this model regarding empirical results: the Covid-19 pandemic made impossible to exploit in the scope of this master thesis the empirical measurements conducted by *Volvo Trucks*. This comparison is left as a perspective for further work. However, the previous FV model was validated with empirical results earlier during the *Rankine Generation 3* project. As a result, it can be considered that the MB model is also validated.

Since most of the transient characteristics of the complete Rankine box model are contained in the heat exchanger models, this study has shown that the controller developed previously to be used with FV models is not totally adapted to the new MB approach. More precisely, the PID controller acting on the WF pump speed to track the super-heating set-point at the boiler outlet needs to be adapted to the new Rankine box model, where the MB boiler and condenser are integrated. This controller is tuned thanks to a step responses campaign, using the SIMC method to compute the PID gains from the averaged static gain, time constant and time delay.

Transient simulations of the complete Rankine box model are then performed along the FK road cycle, to compare results obtained with the new MB model or with the FV method. It is concluded that the precision of the MB model is very good, since it gives nearly the same results than the previous model. The stability of the model is satisfying, and the super-heating set-point at the outlet of the exhaust boiler is tracked accurately during the FK cycle. Furthermore, it is important to highlight that differences between simulation results computed with these two methods come also from the interaction with the controller, and not only from the new model itself.

Finally, it is important to remind that one of the principal interests of the moving boundaries approach is its high computational efficiency. And one can conclude that the new MB model developed in the scope of this master thesis is much faster than the previous FV model. Indeed, with a time step equal to 0.01 s, the new Rankine box where MB models are integrated needs only 32 seconds to simulate the complete FK road cycle, which lasts about 150 minutes in the reality. By contrast, the previous box model where the FV approach is employed to model heat exchangers requires 116 seconds to simulate the FK cycle (with the same time step). It represents thus an outstanding decrease in CPU time equal to -72%. This high computational efficiency, associated to a good accuracy and stability, represents a major improvement of the Rankine box simulation tool developed by *Volvo Trucks* on *Matlab-Simulink*.

4 Impact of oil on working fluid properties and ORC performances

4.1 Literature review

The third part of this master thesis is dedicated to the evaluation of the Rankine box performances by taking into account the presence of oil in the working fluid. Until now, the ORC simulations are performed while considering a pure working fluid, composed only of cyclopentane. But in the reality, the small amount of oil that circulates through all the components of the Rankine cycle would have a major impact on the working fluid properties and its thermodynamic performances.

In an ORC system, some oil is needed to ensure the good and safe functioning of the expander. For the Rankine box developed by *Volvo Trucks*, a piston expander was chosen. To lubricate mechanical components, the oil creates a film between moving parts. In addition, it also ensures the sealing of the expander: not only the static sealing but also the dynamic sealing. The first one refers to the plugging of micro holes on pieces and assemblies. The second one depicts the fluid seal that is needed between pieces that are in relative motion and under different pressures (for example, the piston and the cylinder in the case of a piston expander). Unfortunately in the Rankine box, the oil is not injected at the expander inlet and then separated from the working fluid at the outlet: the oil goes through the whole cycle and all the other components (pump and heat exchangers). In fact, oil separators are not commonly employed for low-scale power units. Performances of each component of the Rankine box are thus impacted by the oil fraction added to cyclopentane.

Some authors, as *Dickes et al.* [45], highlight unexpected discrepancies between ORC performances measured experimentally with a WF/oil mixture and simulation results obtained while considering properties of pure working fluid. It is therefore essential to take into account the impact of lubricant to enhance the precision of ORC simulations tools. The work of *Popovic* [46] is dedicated to the lubricant effects on the performance of refrigeration systems. He concludes that the oil miscibility in the working fluid is of primary importance: the use of a miscible lubricant increases the system performance, since the evaporator efficiency is improved in comparison with a partially miscible lubricant. In addition, a low viscosity oil would also improve performance, but it could negatively impact the system reliability.
In the field of ORC power systems, *Yang et al.* state in [47] that in practice, the peak of cycle efficiency is reached for a certain oil circulation rate which is mainly dependent on expander characteristics.

The method developed in the scope of this master thesis to compute properties of the WF/oil mixture is presented in the following section. Models of Rankine box components, developed previously to take into account a pure working fluid, are also modified to deal with this mixture. These adjustments are introduced later in the text. The studies and articles used as references are directly cited in the model description. After that, the impact on Rankine box performances is evaluated as a function of the oil mass fraction added to cyclopentane.

4.2 Modelling of the Rankine box with the lubricant

In this section, the modifications that are proposed and implemented into the Rankine box model to take into account the impact of oil are presented. Firstly, a new method is developed to compute all the mixture properties from the knowledge of the pressure and the specific enthalpy of the fluid, starting from an existing empirical model. After that, each component of the Rankine box are modified as a consequence. Major improvements are proposed for the expander model, which is surely the most impacted component if the working fluid/oil mixture is precisely modelled. The heat exchanger models (exhaust boiler, air condenser and recuperator) are also adjusted, but to a lesser extent. Finally, the pump model remains basically the same since the mixture going through this component is in the liquid phase.

4.2.1 Pure cyclopentane properties and solubility model

In the Rankine box, the cyclopentane is chosen as working fluid, and is associated to a Polyalkylene Glycol Synthetic (PAG) Oil for the lubrication, whose properties of interest are presented in Tab. 4.1. Without any additional information, these properties are assumed to be constant and independent of the temperature.
The behavior of this mixture and the characterization of the interaction between this oil and the working fluid are of primary importance, but it is often an aspect that is neglected in the literature on low capacity ORC power plants. This assumption is credible if the oil mass fraction (i.e. the mass of oil per unit mass of WF/oil mixture) is relatively small. But in the case of the Rankine box developed by *Volvo Trucks*, this fraction can reach and even exceed 10% to ensure the lubrication of the expander. With such a great oil mass fraction, the need to model the real mixture and not only the working fluid is easily understood. Before describing the mixture model, the original method to compute pure cyclopentane properties is described in the following.

Specific heat capacity: cp_{oil}	2000 J/kg/K
Density: ρ_{oil}	1025 kg/m^3
Thermal conductivity: λ_{oil}	$\approx$ 0.15 W/m/K
Kinematic viscosity: ν_{oil}	145.8 mm^2/s (at 40°C)
ISO viscosity grade[1]	150

Table 4.1: Properties of the Polyalkylene Glycol Synthetic (PAG) Oil added to the cyclopentane in the Volvo Rankine box.

The Rankine box model is based on mass and energy conservation in each component of the cycle. To describe the pure working fluid state, the first thermodynamic variable that is chosen is obviously the pressure. The fluctuating characteristics of this system mainly depend on the heat exchangers, where the first law of thermodynamics is expressed under its transient form.
Due to the phase transitions occurring in the boiler and the condenser, it is impossible to use the fluid temperature as second variable to describe fluid states. As a result, the specific enthalpy is preferred, whose variations are assumed to be equal to the internal energy fluctuations (as explained previously in the chapter on heat exchanger modelling). Therefore, whenever other properties than pressure and

[1]The ISO viscosity classification used for industrial applications attributes a viscosity grade (VG) depending on the value of the kinematic viscosity evaluated at 40°C. The grade VG 150 corresponds to a kinematic viscosity between 135 and 165 mm^2/s at 40°C.

enthalpy of cyclopentane are needed, these two physical quantities are exploited to compute the density, the temperature as well as the fluid quality (Fig.4.1).

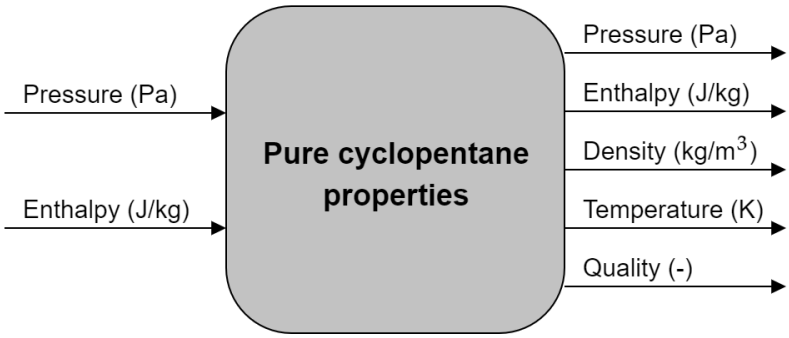

Figure 4.1: Simulink block system computing thermodynamic properties of pure cyclopentane from the knowledge of pressure and enthalpy.

Firstly, the density is computed from a 2-dimensional interpolation into a matrix of values obtained previously for different pairs of enthalpy and pressure with the *Refprop* thermodynamic database [48]. The liquid and vapor saturation enthalpies, only function of the pressure, are also calculated by interpolation between values computed with *Refprop*. After that, the pure working fluid quality is derived from the fluid enthalpy and pressure as:

$$x_{wf} = \frac{h_{wf} - h_{wf,sat,liq}(P)}{h_{wf,sat,vap}(P) - h_{wf,sat,liq}(P)} \tag{4.1}$$

One has to remind that if $h_{wf} < h_{wf,sat,liq}(P)$, the quality is set to $x_{wf} = 0$. Similarly, $x_{wf} = 1$ is chosen if $h_{wf} > h_{wf,sat,vap}(P)$. From the value of this quality, the working fluid state is easily determined:

$$\text{WF state} = \begin{cases} \text{liquid} & \text{if } x_{wf} = 0 \\ \text{two-phase} & \text{if } 0 < x_{wf} < 1 \\ \text{vapor} & \text{if } x_{wf} = 1 \end{cases} \tag{4.2}$$

Finally, the temperature of pure cyclopentane is calculated with mathematical descriptions as a function of pressure and enthalpy, depending on the fluid state:

$$T_{wf,liq} = \Big(a_1 \times P + a_2\Big) \times h_{wf}^2 + \Big(a_3 \times P + a_4\Big) \times h_{wf} + \Big(a_5 \times P + a_6\Big) \tag{4.3}$$

$$T_{wf,TwoPhase} = T_{wf,sat,liq}(P) + x_{wf} \times \Big(T_{wf,sat,vap}(P) - T_{wf,sat,liq}(P)\Big) \tag{4.4}$$

$$T_{wf,vap} = \Big(b_1 \times P + b_2\Big) \times h_{wf}^2 + \Big(b_3 \times P + b_4\Big) \times h_{wf} + \Big(b_5 \times P + b_6\Big) \tag{4.5}$$

where coefficients a_i and b_i are fixed to fit these mathematical descriptions with thermodynamic databases. Since cyclopentane is a pure working fluid, the evaporation and condensation processes occur at a constant temperature, so that Eq. (4.4) reduces to: $T_{wf,TwoPhase} = T_{wf,sat,vap}(P) = T_{wf,sat,liq}(P)$.
The aim of this work is the computation of the working fluid properties taking into account the oil mass fraction. However, the method has to remain basically the same to ensure a good incorporation of the

new block computing mixture properties in the complete Rankine box model: the pressure and the enthalpy remain the two physical quantities that are used to derive the other properties, similarly to Fig. 4.1.

In the literature, the physics of a mixture composed of a working fluid and a lubricant is traditionally represented as a liquid-vapor equilibrium, where the vapor phase is only composed of working fluid (*Youbi-Idrissi* [49], *Zhelezny et al.* [50]). In fact, the bubble point of the lubricant is much higher than the one of the pure working fluid, so that the oil is always considered in liquid form. As a result, the thermodynamic state of the mixture corresponds to one of the three following configurations:

1. *Liquid state mixture*: lubricant and cyclopentane are both in liquid state, forming a fluid whose properties vary with the oil mass fraction.
2. *Liquid-vapor equilibrium*: the lubricant remains totally in liquid form, but cyclopentane is partially vaporized. The working fluid quality represents the mass of cyclopentane in vapor state divided by the total cyclopentane mass.
3. *Liquid oil and vapor working fluid* (hypothetical case): the liquid phase of the mixture is made up of lubricant only, and the cyclopentane is totally in the vapor phase. This situation is hypothetical since a small WF fraction always remains in liquid state with the lubricant, as discussed later in the text.

In order to describe the flow composition, three physical quantities are used in this study. The *oil circulation rate*:

$$\kappa_{oil} = \frac{\dot{m}_{oil}}{\dot{m}_{wf,liq} + \dot{m}_{wf,vap} + \dot{m}_{oil}} \tag{4.6}$$

is defined as the ratio between the oil mass flow and the total mixture mass flow, with:

$$\dot{m}_{tot} = \dot{m}_{wf,tot} + \dot{m}_{oil} = \dot{m}_{wf,liq} + \dot{m}_{wf,vap} + \dot{m}_{oil} \tag{4.7}$$

Secondly, the *working fluid quality* is defined as usually:

$$x_{wf} = \frac{\dot{m}_{wf,vap}}{\dot{m}_{wf,liq} + \dot{m}_{wf,vap}} \tag{4.8}$$

Finally the *working fluid fraction in the liquid phase* is introduced:

$$\zeta_{wf} = \frac{\dot{m}_{wf,liq}}{\dot{m}_{wf,liq} + \dot{m}_{oil}} \tag{4.9}$$

This last quantity is useful to determine the composition of the liquid phase. If the mixture is totally in the liquid phase (case 1 mentioned above), one has $\dot{m}_{wf,tot} = \dot{m}_{wf,liq}$ and $\dot{m}_{wf,vap} = 0$. As a result, the working fluid fraction in the liquid phase is maximum and equal to:

$$\zeta_{wf,max} = 1 - \kappa_{oil} \tag{4.10}$$

The phase rule derived by Josiah Willard Gibbs is: $F = C - P + 2$ where F is the number of degrees of freedom, C the number of components and P the number of phases. For the WF/oil mixture, $C = P = 2$, so that $F = 2$ and one can highlight that the three quantities κ_{oil}, x_{wf} and ζ_{wf} are not independent. Therefore, the working fluid quality can be expressed as a function of the two other quantities, as derived by *Dickes* in [51]. The following demonstration comes from this reference.
Starting from a mass balance, the vapor mass flow is expressed as:

$$\dot{m}_{wf,vap} = \dot{m}_{tot} - \dot{m}_{wf,liq} - \dot{m}_{oil} \tag{4.11}$$

In addition, one has by definition:

$$\dot{m}_{oil} = \kappa_{oil} \cdot \dot{m}_{tot} \tag{4.12}$$

Combining this expression with Eq. (4.9), the liquid WF mass flow writes:

$$\dot{m}_{wf,liq} = \frac{\zeta_{wf} \cdot \kappa_{oil}}{1 - \zeta_{wf}} \, \dot{m}_{tot} \tag{4.13}$$

Inserting Eqs. (4.12) and (4.13) into Eq. (4.11) gives:

$$\dot{m}_{wf,vap} = \left(1 - \frac{\zeta_{wf} \cdot \kappa_{oil}}{1 - \zeta_{wf}} - \kappa_{oil}\right) \dot{m}_{tot} \tag{4.14}$$

On the other hand, from Eqs. (4.6) to (4.9), one has:

$$\dot{m}_{wf,vap} = \dot{m}_{tot} \cdot (1 - \kappa_{oil}) \cdot x_{wf} \tag{4.15}$$

By similarity between Eqs. (4.14) and (4.15), one can write:

$$(1 - \kappa_{oil}) \cdot x_{wf} = 1 - \frac{\zeta_{wf} \cdot \kappa_{oil}}{1 - \zeta_{wf}} - \kappa_{oil} \tag{4.16}$$

From this last equation solved for x_{wf}, the expression of the working fluid quality is derived as a function of κ_{oil} and ζ_{wf} only:

$$x_{wf} = \frac{1 - \zeta_{wf} - \kappa_{oil}}{1 - \zeta_{wf} - \kappa_{oil} + \zeta_{wf} \cdot \kappa_{oil}} \tag{4.17}$$

The oil mass fraction added to the working fluid greatly modifies the saturation equilibrium conditions, while pure cyclopentane has a unique saturation temperature (resp. pressure) for a given pressure (resp. temperature). This deviation, which is a function of the oil concentration, is modelled with various methods in the literature. Theoretical models are defined but very complex to use in practice, so that simpler models based on empirical results are often preferred. The experimental solubility model that is used in this study was firstly presented by *Grebner et al.* in [52] and adapted by *Dickes* in its PhD thesis [51]. This model was developed initially for mixtures between lubricants and refrigerants (R-12 and R-134a), but it can be adapted to hydrocarbons as cyclopentane (C_5H_{10}) thanks to its simple formulation.
At first, for a given temperature T expressed in [K], a dimensionless quantity is defined:

$$\theta^* = \frac{T - T_{sat}(P)}{T_{sat}(P)} \tag{4.18}$$

which has the signification of a superheat above the saturation temperature $T_{sat}(P)$ of pure working fluid. This quantity is expressed by *Grebner et al.* as a function of the working fluid fraction in the liquid phase ζ_{wf} (Eq. 4.9) and the pressure P:

$$\theta^* = (1 - \zeta_{wf}) \cdot (A + B \cdot P) \tag{4.19}$$

where A and B are function of ζ_{wf}:

$$A = a_1 + \frac{a_2}{\zeta_{wf}^{0.5}} \tag{4.20}$$

$$B = a_3 + \frac{a_4}{\zeta_{wf}^{0.5}} + \frac{a_5}{\zeta_{wf}} + \frac{a_6}{\zeta_{wf}^{1.5}} + \frac{a_7}{\zeta_{wf}^{2}} \tag{4.21}$$

The a_i coefficients are fixed to fit this model with empirical results, basically the evolution of the bubble point pressure as a function of the temperature and the working fluid fraction in the mixture (or alternatively the oil fraction). In [52], these coefficients are given for different solutions between R-12 or R-134a and a lubricant (PAG, paraffin, ester or naphthene oil). The work of *Dickes* [51] is focused on a R245fa/oil mixture, so that the model is fitted with empirical results from *Zhelezny et al.* [50] obtained with R245fa and a Planetelf ACD 100FY oil.

Most of the literature dealing with the presence of oil in the working fluid is devoted to refrigerants only, whose solubility with lubricant is often complete [51]. However the solubility between hydrocarbons and oil (especially PAGs) is only partial, as stated by *Totten et al.* in [53]: *The solubility of hydrocarbons is much less in some synthetic lubricants, especially PAGs. This is because, in a typical PAG molecule, each third atom in the polymer backbone, is an oxygen atom, which makes it quite polar. Therefore, hydrocarbons are less soluble in PAGs*. This observation highlights the need for fitting these solubility model with empirical results obtained with hydrocarbons, to ensure a sufficient accuracy.

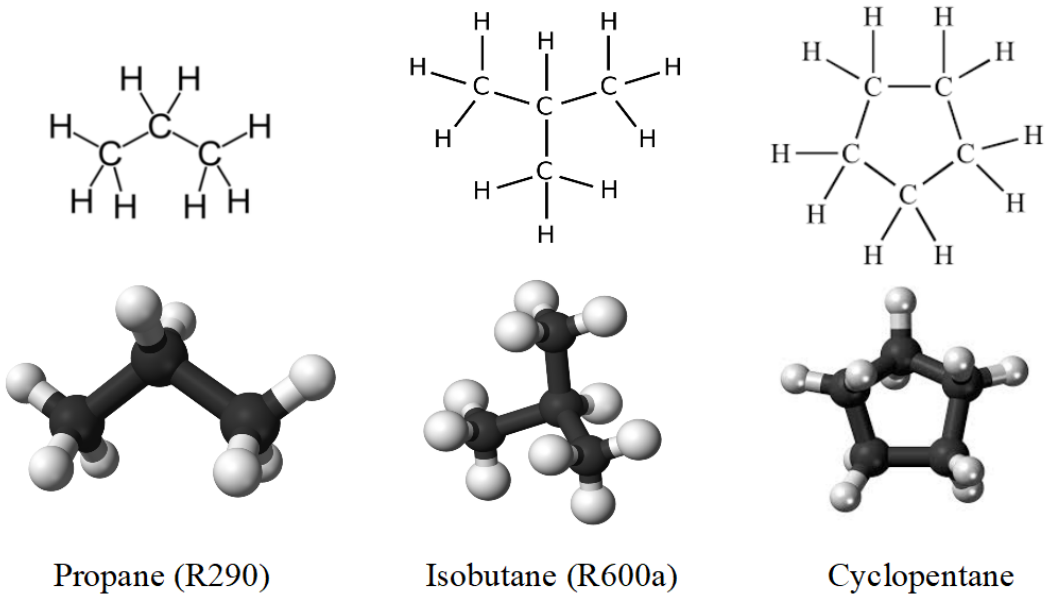

Figure 4.2: Molecules of propane C_3H_8 (R290), isobutane C_4H_{10} (R600a, 2-methylpropane) and cyclopentane C_5H_{10}.

For the present work where cyclopentane is chosen as working fluid, it is impossible to find in the literature appropriate and comprehensive experimental results, and it was unfeasible to perform ourselves such experiments. Indeed, cyclopentane is clearly not a very used working fluid, not only in the field of ORC power systems but also in refrigeration.
As a consequence, it was decided to fit the model presented above with empirical results obtained with another hydrocarbon than cyclopentane (C_5H_{10}). For example, propane R290 (C_3H_8) or (iso-)butane R600(a) (C_4H_{10}) that are commonly used in refrigeration. The molecules of propane, isobutane and cyclopentane are compared in Fig. 4.2.

The thermodynamic properties of mixtures composed of oil and propane or isobutane are studied by *Barbosa et al.* in [54] and [55]. Professor Barbosa and his associates from the Federal University of

Santa Catarina (Brazil) are warmly thanked for having shared with us the complete results of a set of experiments conducted with a mixture composed of propane and an ISO VG 22 PAG oil.
These empirical results are shown in Fig. 4.3: for different temperatures, the bubble point pressure varies with the R290 mass fraction in the liquid (when this fraction is equal to 1, it corresponds to a pure R290 WF). Similarly to other experimental studies, it is observed that the bubble point pressure decreases if the WF mass fraction is reduced (i.e. if the oil mass fraction increases). This observation is amplified if the saturation temperature increases.

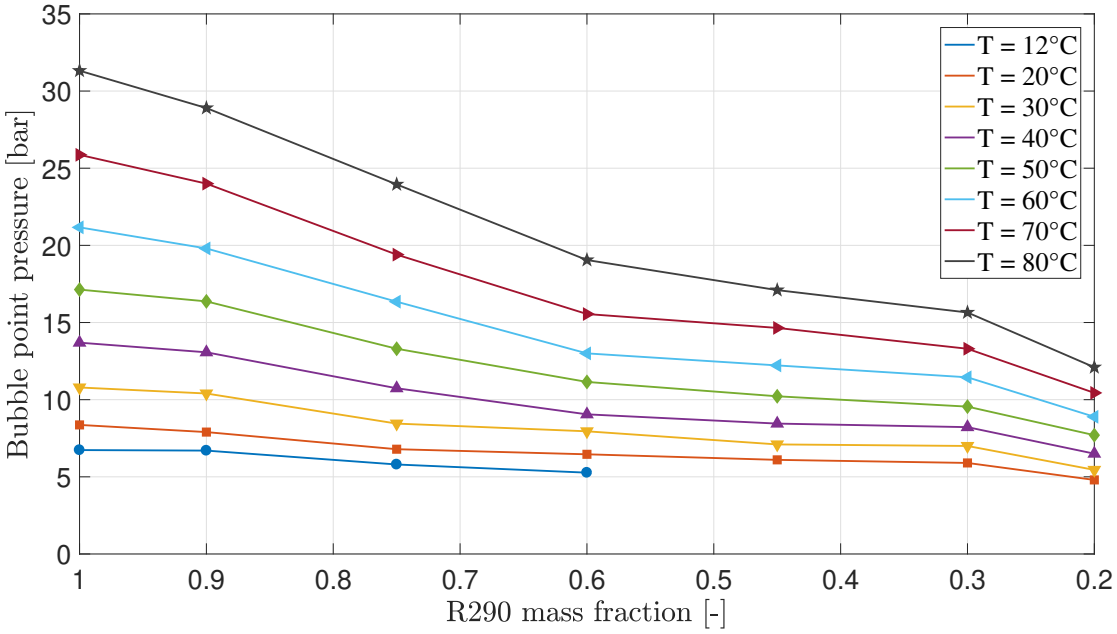

Figure 4.3: Experimental results from *Barbosa et al.*: evolution of the bubble point pressure as a function of the R290 (propane C_3H_8) mass fraction in the R290/oil mixture, for different temperatures.

a_1	a_2	a_3	a_4	a_5	a_6	a_7
0.05434	-0.00787	-0.6052	1.488	-1.324	0.5113	-0.07222

Table 4.2: Values of coefficients appearing in Eqs. (4.20) and (4.21) to fit the solubility model with empirical results from *Barbosa et al.* (Fig. 4.3).

From these empirical results, the solubility model presented in Eqs. (4.18) to (4.21) is fitted using the *Matlab curve fitting toolbox*. The values of the coefficients a_i are presented in Tab. 4.2, and a parity plot comparing empirical results and values obtained with the fitted model is shown in Fig. 4.4. One can conclude from this plot that the fit is relatively precise since nearly all the points are in the confidence interval $\pm 15\%$ around the bisector. This precision is also confirmed by the sum of squares due to error (SSE) between empirical data ($\hat{\theta}_i$) and simulated results (θ_i):

$$SSE = \sum_{i=1}^{n} w_i \left(\hat{\theta}_i - \theta_i\right)^2 \tag{4.22}$$

which is equal to 1.346×10^{-3}, meaning that the random error due to the fit is not significant. In addition, the R-Square statistic of a regression measures how the fitted model is able to explain the experimental

variations of the data. A value close to zero means that the model is not precise, while a value equal to one concludes that the fit explains 100% of the data variations. In this case, the fitting toolbox calculates that R-Square $= 0.9787$, which guarantees a good accuracy.

The solubility model fitted with empirical results from *Barbosa et al.* is thus employed in the following to simulate the Rankine box adapted to deal with the presence of lubricant added to the working fluid. One has to keep in mind that this model is fitted with a mixture of propane and an ISO VG 22 PAG oil, while the Rankine box developed by *Volvo Trucks* operates with a mixture of cyclopentane and an ISO VG 150 PAG oil. Performing directly empirical measurements in the scope of this master thesis would have been more relevant for the results precision, but it was made more difficult due to the particular situation imposed by the Covid-19 pandemic. This empirical part of the study is thus considered as a perspective for further work.

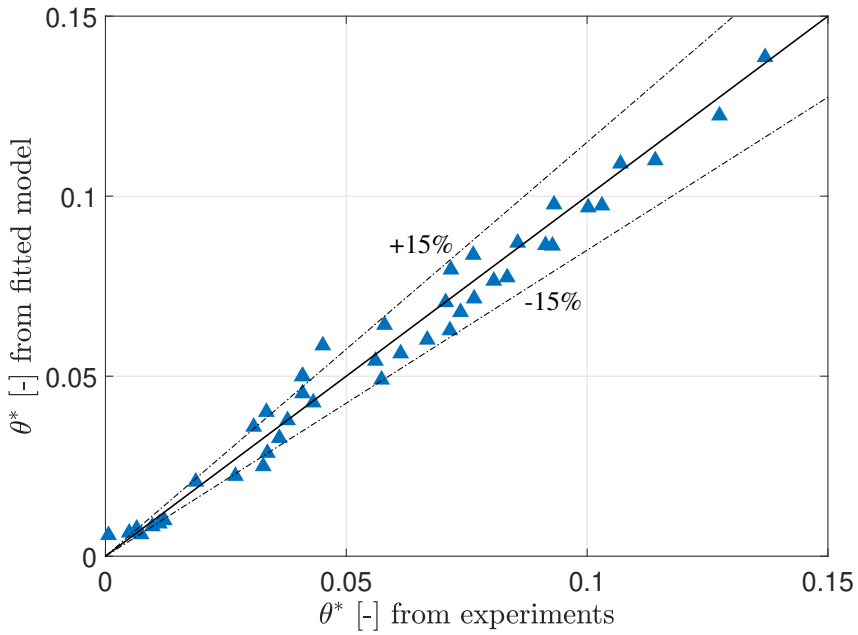

Figure 4.4: Parity plot of the dimensionless superheat θ^* between experimental results from *Barbosa et al.* and simulated results obtained with the fitted solubility model.

4.2.2 Cyclopentane quality and flow composition calculation

From the solubility model presented in the previous section (Eqs. 4.18 to 4.21), the working fluid quality and the flow composition are computed in two steps from the knowledge of the mixture temperature.

1 - Evaluation of the minimum equilibrium temperature:

As said before, if the working fluid is totally in the liquid state, the WF concentration in the liquid phase is maximum:

$$\zeta_{wf,max} = 1 - \kappa_{oil} \tag{4.23}$$

Injecting $\zeta_{wf,max}$ into Eqs. (4.18) and (4.19) gives:

$$T_{eq,min} = T_{sat}(P) \cdot (\theta_{eq,min} + 1) \tag{4.24}$$

With:

$$\theta_{eq,min} = (1 - \zeta_{wf,max}) \cdot \Big[A(\zeta_{wf,max}) + B(\zeta_{wf,max}) \cdot P)\Big] \tag{4.25}$$

The temperature $T_{eq,min}$ is, for a given pressure P, the temperature corresponding to the bubble point (formation of the first bubble of cyclopentane). At this point, the liquid composition is not yet modified, so that: $\zeta_{wf} = \zeta_{wf,max}$. In other words, $T_{eq,min}$ is the minimum equilibrium temperature achievable by a mixture where cyclopentane is partially vaporized.

2 - Comparison with the mixture temperature T:

Once $T_{eq,min}$ is calculated, this temperature is compared to the real mixture temperature T, and two cases are distinguished. It corresponds to the two first possibilities mentioned above, where the different thermodynamic states of the mixture are listed:

- *Liquid state mixture* if $T < T_{eq,min}$: the temperature is below the minimum equilibrium temperature, resulting in a liquid mixture. The working fluid quality is set to zero: $x_{wf} = 0$, and: $\zeta_{wf} = \zeta_{wf,max}$.
- *Liquid-vapor equilibrium* if $T \geq T_{eq,min}$: the temperature is sufficient to reach a liquid-vapor equilibrium, with a vapor phase only composed of cyclopentane. The WF fraction in the liquid phase is computed from the solubility model, by solving Eqs. (4.18) to (4.21) for ζ_{wf}. Finally, x_{wf} is calculated thanks to Eq. (4.17).

The last possibility mentioned above (*liquid oil and vapor working fluid*), where the liquid phase is only composed of oil because cyclopentane would be totally vaporized, is *impossible* to reach in practice. This important conclusion is explained in Fig. 4.5. On this plot, the increase in vapor quality is shown as a function of the mixture temperature with an oil circulation rate equal to 5%. The temperature is compared to the saturation temperature of pure cyclopentane (T_{sat}).

At low temperature, the WF/oil mixture is totally in the liquid state so that $x_{wf} = 0$ and $\zeta_{wf} = \zeta_{wf,max} = 95\%$. If the temperature is increased, one can observe that a temperature higher than T_{sat} is needed to obtain a non-zero quality: the minimum equilibrium temperature $T_{eq,min}$ defined by Eq. (4.24) is above the saturation temperature of pure cyclopentane. The fluid quality further increases with the temperature, and tends asymptotically to $x_{wf} = 1$. It is important to observe that this phase transition is no longer isothermal due to the presence of oil in the working fluid. Simultaneously, the working fluid fraction in the liquid phase tends to zero due to the vaporization of cyclopentane.
In other words, the saturation temperature of the WF/oil mixture increases when ζ_{wf} reduces, meaning that the liquid phase is enriched in oil. This increase in oil fraction in the liquid causes a diminution of the saturation pressure for a fixed temperature (as shown previously in Fig. 4.3), or alternatively an increase in saturation temperature for a given pressure.

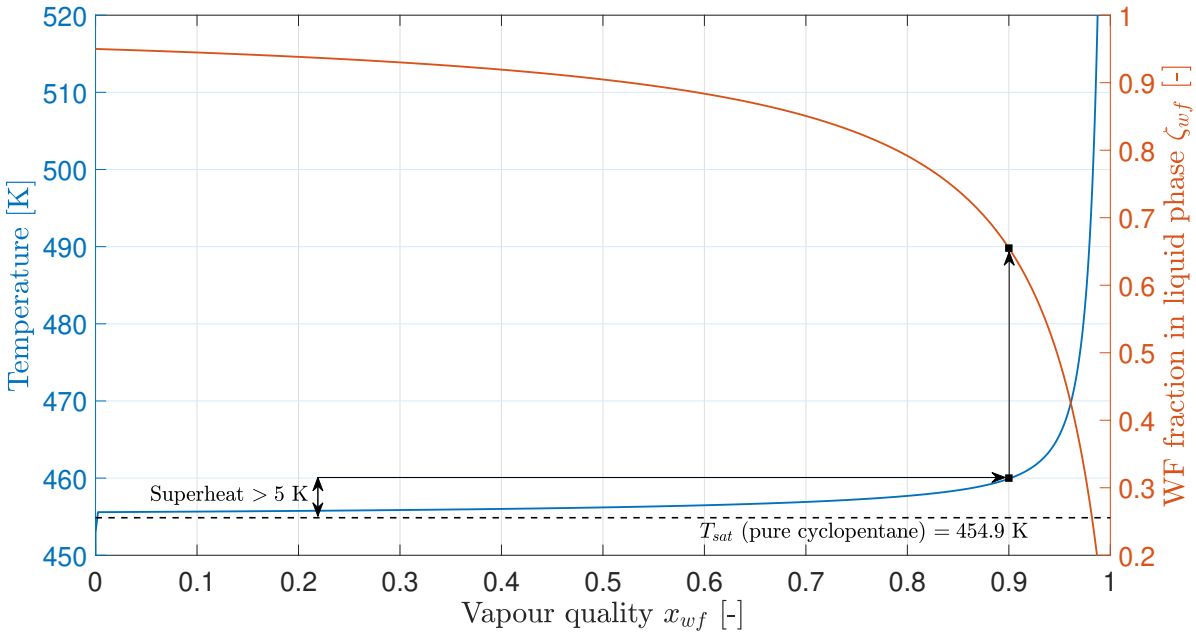

Figure 4.5: Flow composition of the cyclopentane/oil mixture (x_{wf} and ζ_{wf}) as a function of the temperature, with $P = 20$ bars and $\kappa_{oil} = 0.05$.

.

Fig. 4.5 highlights clearly the fact that $x_{wf} = 1$ is achieved for an infinitely large temperature. As a result, this point is *impossible* to observe in practice, even with a large superheat above T_{sat}. The physical explanation of this phenomenon captured by the empirical solubility model is that a small fraction of cyclopentane remains always trapped in the lubricant (liquid bubbles), which prevents from reaching a complete vaporization of WF. This conclusion is of primary importance for the Rankine box simulations, because an observed superheat above the saturation temperature of pure cyclopentane does not signify that the working fluid is totally vaporized. One could also highlight that the definition of the superheat itself, which refers to an increase in temperature above the vapor saturation point, becomes meaningless when lubricant is added in the simulation tool.
For example, the arrows drawn in Fig. 4.5 show that a theoretical superheat equal to 5 K results in a fluid quality only equal to 90%. In this case, the liquid phase still contains 65.5% of cyclopentane.

An important conclusion of this analysis is the need to reach a very large *apparent* superheat above T_{sat} at the expander inlet, in order to maximize x_{wf} before entering the expander, and to decrease as much as possible the liquid mass flow through this component. It is important to maximize the output power produced by the expansion of the vapor phase. But in any case, reaching $x_{wf} = 1$ is impossible as soon as $\kappa_{oil} > 0$. This aspect will be discussed later in the text.

Fig. 4.6 shows the evolution of the fluid composition for several fractions of lubricant in the working fluid (with $P = 20$ bars). The behaviour of the saturation properties observed previously is exacerbated when the oil circulation rate increases. One can observe that for a large lubricant fraction, the saturation properties of the WF/oil mixture are very far from those of pure cyclopentane. However, if $\kappa_{oil} = 1\%$, assuming a fluid composed of cyclopentane only could be relatively accurate. In the case of the Rankine box developed by *Volvo Trucks*, it can be recalled that the oil fraction can rise beyond 10%: relatively large differences are expected between simulation results obtained taking or not into account the presence of lubricant in working fluid.

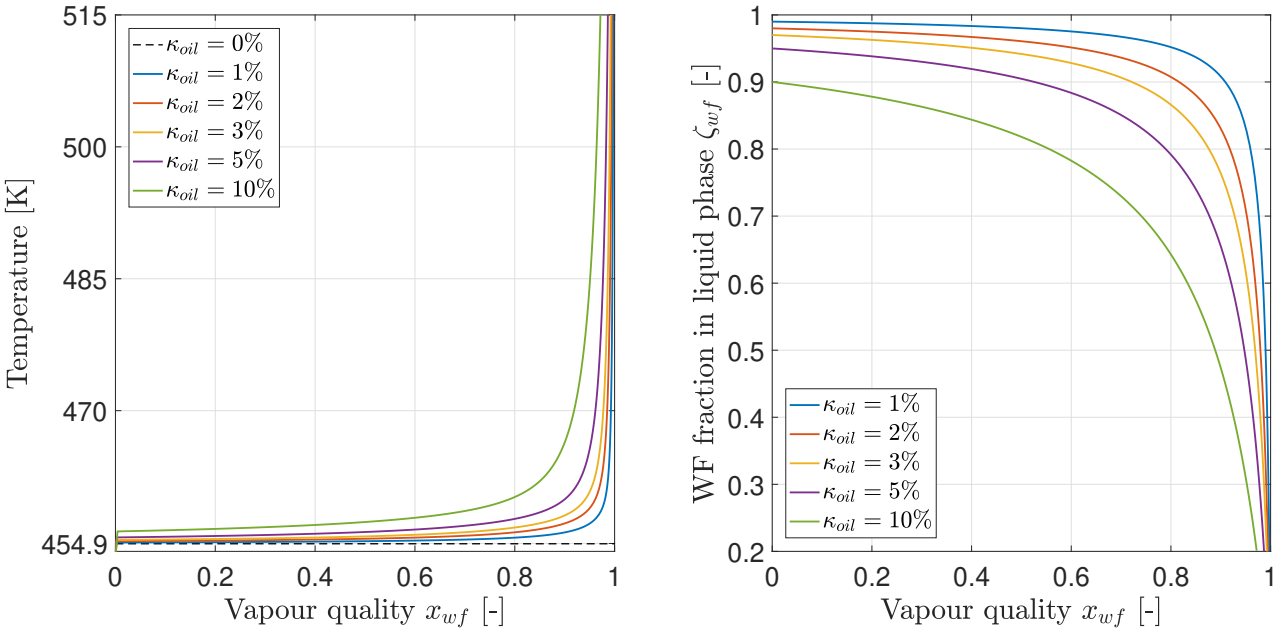

Figure 4.6: Flow composition of the cyclopentane/oil mixture (x_{wf} and ζ_{wf}) for several oil circulation rates, with $P = 20$ bars.

.

4.2.3 Calculation of the mixture enthalpy and density

Among the mixture properties of interest, the enthalpy and the density are not yet specified. If the heat corresponding to the WF/oil mixing is neglected [51], the mixture enthalpy h_{mix} is derived from the energy conservation principle:

$$\dot{m}_{tot} \cdot h_{mix} = \dot{m}_{oil} \cdot h_{oil} + \dot{m}_{wf,liq} \cdot h_{wf,liq} + \dot{m}_{wf,vap} \cdot h_{wf,vap} \tag{4.26}$$

where $h_{wf,liq}$ is the enthalpy of liquid WF, and $h_{wf,vap}$ the one of vapor WF. The oil enthalpy h_{oil} is simply computed from its specific heat capacity cp_{oil}:

$$h_{oil} = cp_{oil} \cdot T \tag{4.27}$$

because any vaporization of the lubricant is taken into account. As a result, the mixture enthalpy writes as a function of its contributions:

$$h_{mix} = \frac{\dot{m}_{oil} \cdot cp_{oil} \cdot T + \dot{m}_{wf,liq} \cdot h_{wf,liq} + \dot{m}_{wf,vap} \cdot h_{wf,vap}}{\dot{m}_{oil} + \dot{m}_{wf,liq} + \dot{m}_{wf,vap}} \tag{4.28}$$

This last expression can be modified as a function of x_{wf} and κ_{oil}:

$$h_{mix} = \kappa_{oil} \cdot cp_{oil} \cdot T + (1 - x_{wf}) \cdot (1 - \kappa_{oil}) \cdot h_{wf,liq} + x_{wf} \cdot (1 - \kappa_{oil}) \cdot h_{wf,vap} \tag{4.29}$$

One could highlight that $h_{wf,vap}$ and $h_{wf,liq}$ are still unknown at this point. The method to compute these enthalpies is introduced later in the text.

From Eq. (4.29), the mixture enthalpy can be computed from the knowledge of the temperature and the pressure only, which also determine completely the fluid composition (κ_{oil}, x_{wf} and ζ_{wf}). As a result, it makes possible to draw the plots shown in Fig. 4.7 and Fig. 4.8. On these plots, the evolution of the enthalpy is observed for different constant pressures as a function of the temperature. However, the enthalpy is chosen as abscissa to obtain figures that are comparable with the literature.
Fig. 4.7 corresponds to $\kappa_{oil} = 1\%$ while Fig. 4.8 is obtained with $\kappa_{oil} = 5\%$. In both cases, the results obtained with the WF/oil mixture (solid lines) are compared to the properties computed assuming pure cyclopentane (dashed lines).

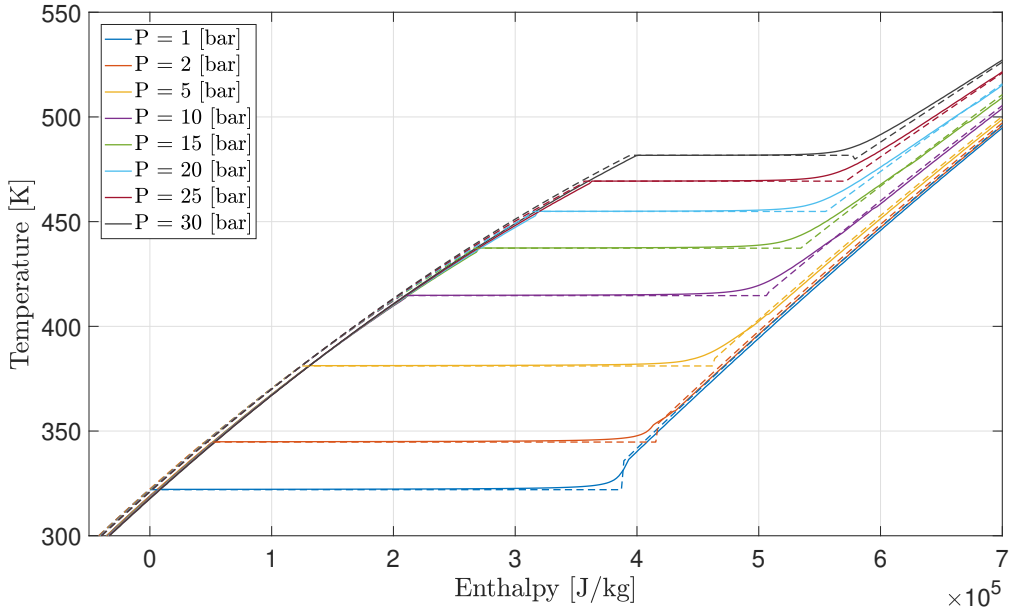

Figure 4.7: Evolution of the mixture temperature as a function of the specific enthalpy for different constant pressures: with an oil circulation rate equal to $\kappa_{oil} = 0.01$ (solid lines) or with pure cyclopentane (dashed lines).

It can be observed that the deviation with respect to pure cyclopentane properties is obviously more important for a higher oil fraction. Moreover, this difference is exacerbated if the pressure increases.
With $\kappa_{oil} = 1\%$ (Fig. 4.7), the deviation is mainly observed for high enthalpies, where the WF/oil mixture model prevents from reaching $x_{wf} = 1$. In addition, the liquid saturation curve is shifted to the right. On the other hand, Fig. 4.8 shows that with $\kappa_{oil} = 5\%$, the mixture properties are far from those obtained with pure WF in the whole enthalpy range. This observation is even more exacerbated with a higher lubricant fraction, so much that this comparison between mixture and pure cyclopentane properties is no more visible on the same plot for different pressure levels.

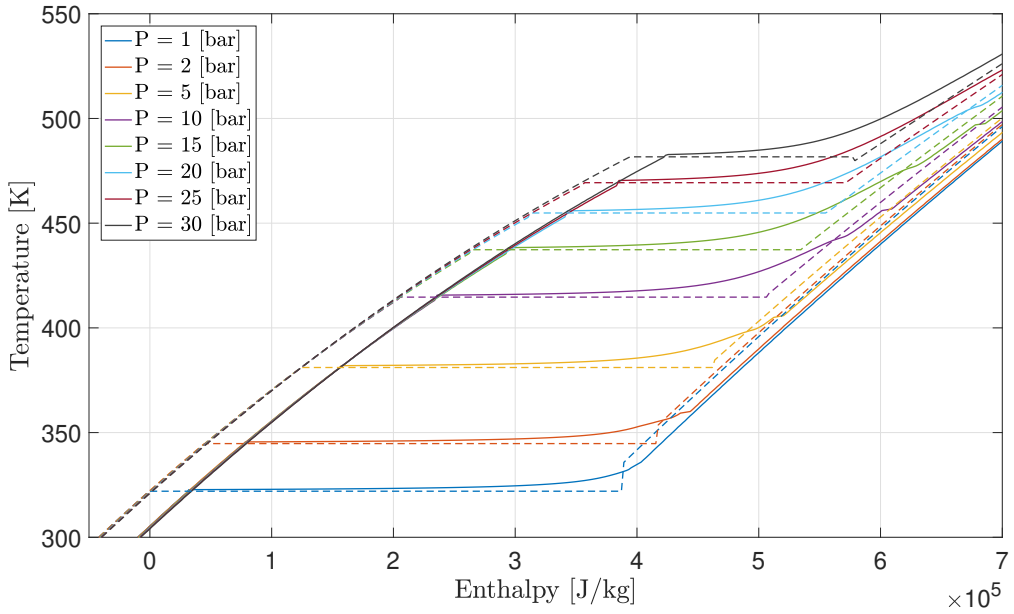

Figure 4.8: Evolution of the mixture temperature as a function of the specific enthalpy for different constant pressures: with an oil circulation rate equal to $\kappa_{oil} = 0.05$ (solid lines) or with pure cyclopentane (dashed lines).

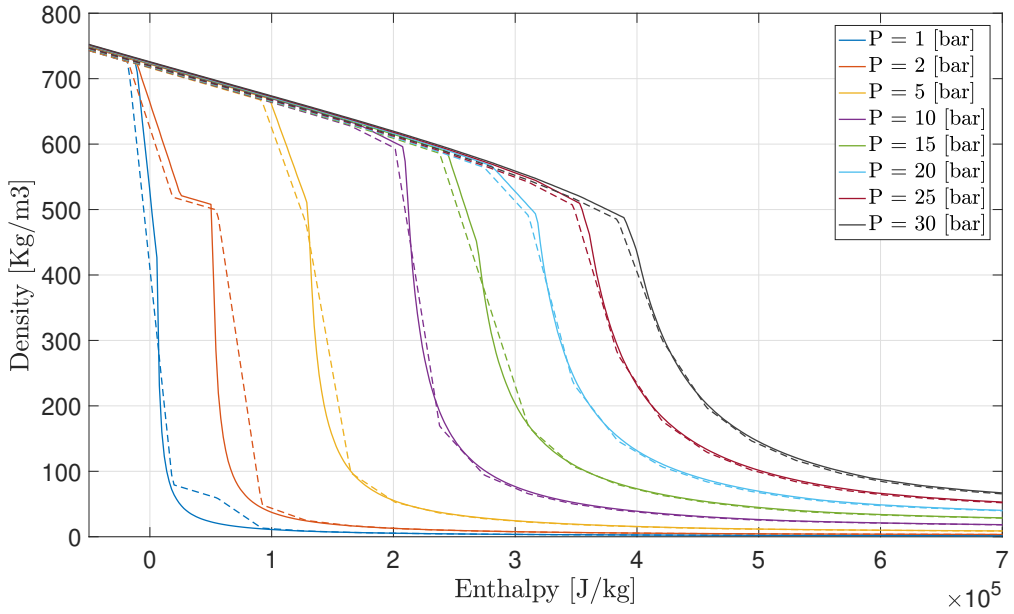

Figure 4.9: Evolution of the mixture density as a function of the specific enthalpy for different constant pressures: with an oil circulation rate equal to $\kappa_{oil} = 0.01$ (solid lines) or with pure cyclopentane (dashed lines).

The mixture density is calculated by conservation of the volumetric flow rate:

$$\frac{\dot{m}_{tot}}{\rho_{mix}} = \frac{\dot{m}_{wf,liq}}{\rho_{wf,liq}} + \frac{\dot{m}_{wf,vap}}{\rho_{wf,vap}} + \frac{\dot{m}_{oil}}{\rho_{oil}} \tag{4.30}$$

which gives:

$$\rho_{mix} = \frac{\dot{m}_{tot}}{\frac{\dot{m}_{wf,liq}}{\rho_{wf,liq}} + \frac{\dot{m}_{wf,vap}}{\rho_{wf,vap}} + \frac{\dot{m}_{oil}}{\rho_{oil}}} \tag{4.31}$$

This equation, combined to the solubility model, is used to compute the mixture density as a function of two other thermodynamic properties. These properties can be for example the temperature and the pressure. To create Fig. 4.9 and Fig. 4.10, the enthalpy and the pressure were chosen to observe the mixture density evolution (with κ_{oil} equal to 1% and 5% respectively).
Once again, the deviation between density computed for the WF/oil mixture or for pure cyclopentane is more important with a higher oil fraction. Moreover, for a given enthalpy, the presence of oil in the working fluid tends to increase the mixture density. This result could be anticipated since the oil density is always higher than the cyclopentane density. In fact, ρ_{oil} is equal to 1025 kg/m^3 (Tab. 4.1), which is higher than the density of liquid cyclopentane at low temperature (around 760 kg/m^3 at $T = 20$°C, depending on the pressure).

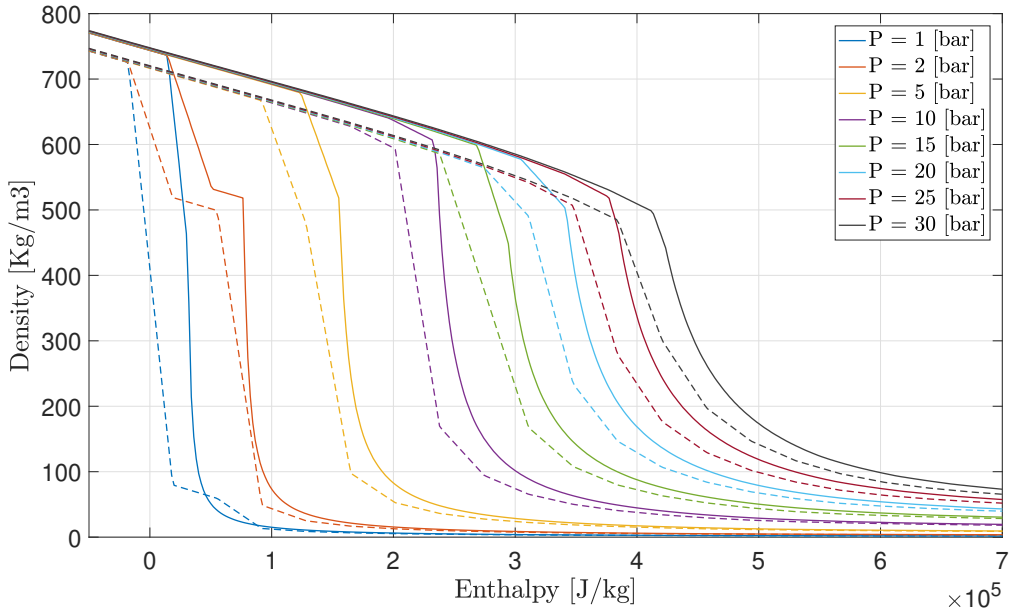

Figure 4.10: Evolution of the mixture density as a function of the specific enthalpy for different constant pressures: with an oil circulation rate equal to $\kappa_{oil} = 0.05$ (solid lines) or with pure cyclopentane (dashed lines).

4.2.4 Iterative algorithm

Equations (4.29) and (4.31), in addition to the solubility model described in the previous sections, complete the set of equations that are needed to compute all the mixture properties of interest, from the knowledge of the temperature T and pressure P: x_{wf}, ζ_{wf}, h_{mix} and ρ_{mix}. However, the new method developed to compute mixture properties aims to be translated into a *Simulink* block, which is integrated to the complete Rankine box model. As said before, the inputs of the current block dealing with pure cyclopentane properties are the pressure and the enthalpy, as shown in Fig. 4.1. By contrast, the solubility model presented in this study considers up to now the pressure and the temperature as main inputs, while the mixture enthalpy is only calculated a posteriori, when the flow composition is already known.

To guarantee an easy integration of this approach to derive the WF properties taking into account the oil circulation rate in the ORC system, a completely new iterative algorithm is developed. This algorithm is presented schematically in Fig. 4.11, and is translated into *Matlab* code to generate the new *Simulink* block responsible for the properties calculation. In accordance with the previous model, the inputs of this new block are P and h_{mix}, as well as the oil circulation rate κ_{oil}. Similarly to Fig. 4.1, the temperature T, the density ρ_{mix} and the cyclopentane quality x_{wf} are now on the output side of the system.

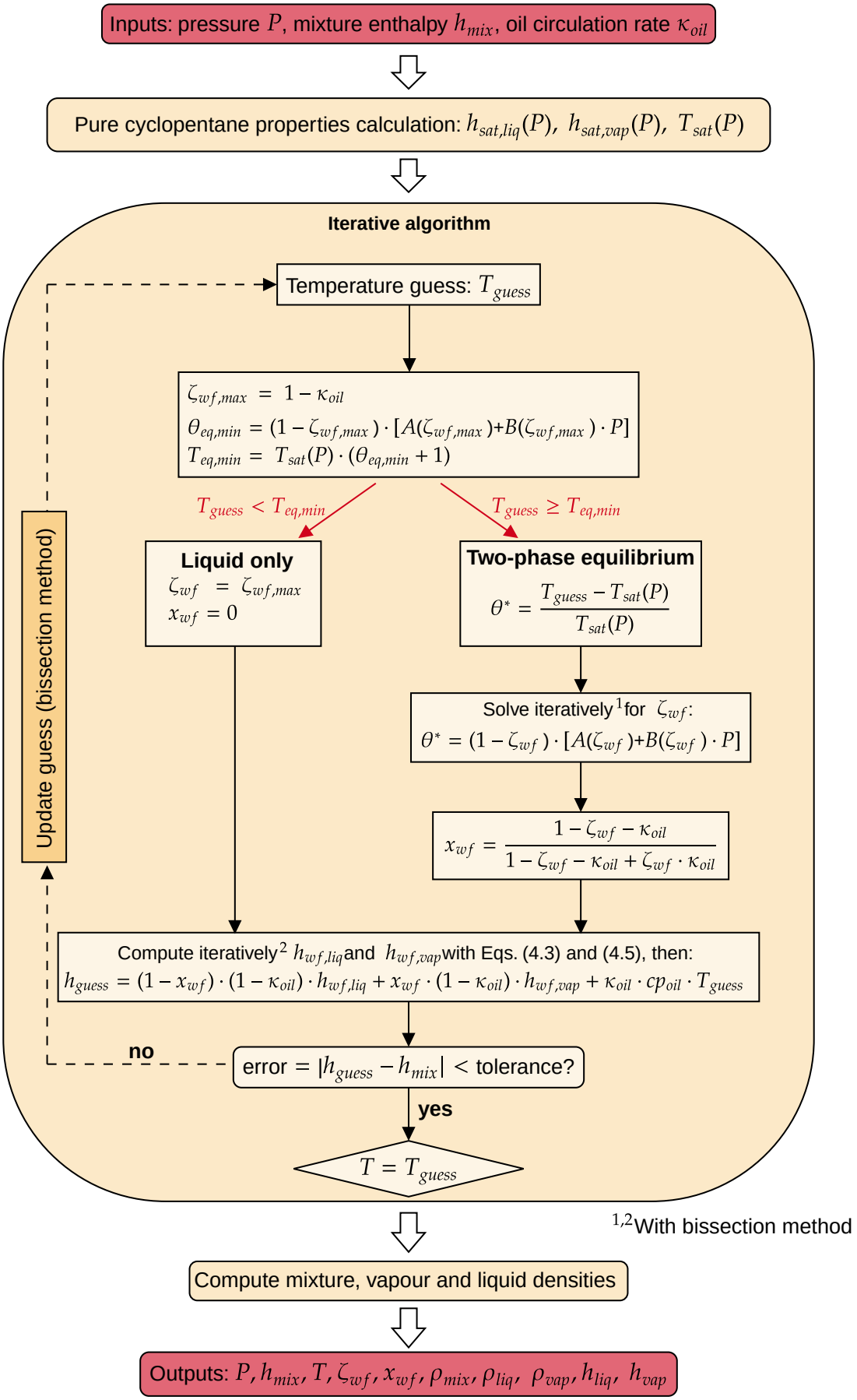

Figure 4.11: Flow chart of the new iterative algorithm which computes all the WF/oil mixture properties as a function of the pressure, the enthalpy and the oil circulation rate.

The iterative algorithm presented in Fig. 4.11 is described in this paragraph. At first, this method computes the saturation properties of pure cyclopentane as a function of the pressure P: $h_{sat,liq}(P)$, $h_{sat,vap}(P)$ and $T_{sat}(P)$, using interpolations between results previously obtained with *Refprop* for different pressure levels. After that, the main goal of this iterative algorithm is replacing the temperature by the mixture enthalpy on the entrance side of the solubility model. As a result, a guess on the temperature value T_{guess} is needed to compensate for the fact that the temperature is not known at the beginning. In a first instance, this assumed temperature is fixed as the mean value between two chosen boundaries $T_{B,low}$ and $T_{B,high}$.

$$T_{guess} = \frac{T_{B,low} + T_{B,high}}{2} \tag{4.32}$$

From this guess, the two-steps method described above can be used. The minimum equilibrium temperature of the mixture $T_{eq,min}$ is derived from Eqs. (4.23) to (4.25) and then compared to T_{guess}.
If $T_{guess} < T_{eq,min}$, it means that the assumed temperature makes impossible to reach a liquid-vapor equilibrium: the WF/oil mixture is totally in the liquid phase, leading to a zero quality.
By contrast, $T_{guess} > T_{eq,min}$ indicates that some cyclopentane is in the vapor state, in equilibrium with a liquid composed of oil *and* liquid cyclopentane. In this case, Eqs. (4.18) to (4.21) are solved iteratively to compute ζ_{wf}, from which x_{wf} is calculated with Eq. (4.17). At this point the flow composition is known, and depends on the oil mass fraction κ_{oil}, the pressure P and the assumed temperature T_{guess}.

The next step of this new algorithm is the computation of the mixture enthalpy h_{guess} corresponding to T_{guess} with Eq. (4.29), either a vapor phase exists or not. For this equation, the values of h_{oil}, $h_{wf,vap}$ and $h_{wf,liq}$ are required. These two last quantities are more complex to compute than the oil enthalpy, which is only function of the temperature ($h_{oil} = cp_{oil} \cdot T$). However, since $h_{wf,vap}$ and $h_{wf,liq}$ correspond to enthalpies of pure cyclopentane, the previous model used to derive WF properties can be exploited. As a result, these two quantities are calculated by solving Eqs. (4.3) and (4.5) for h_{wf}.

At the end of an iteration, the mixture enthalpy h_{guess} (function of the assumed temperature T_{guess}) can be compared to the real value h_{mix} given as input of the block, in order to update the value of T_{guess} until reaching $h_{guess} \simeq h_{mix}$. For this purpose, the bisection method is chosen (also called binary search method or the dichotomy method). This method is suitable to find the zero of a continuous function which is monotonically increasing, such as h_{guess} as a function of T_{guess} for a given pressure and oil circulation rate. As a result, the strategy to update the temperature is the following:

- If $h_{guess} < h_{mix}$, it means that T_{guess} is *lower* than the exact mixture temperature. Therefore, this guess becomes the new lower boundary: $T_{B,low} = T_{guess}$.
- If $h_{guess} > h_{mix}$, it means that T_{guess} is *higher* than the exact mixture temperature. Therefore, this guess becomes the new upper boundary: $T_{B,high} = T_{guess}$.

In both cases, the new guess is computed from Eq. (4.32) with updated values for $T_{B,low}$ and $T_{B,high}$, until reaching a convergence, which means that the error between h_{guess} and h_{mix}:

$$\text{error} = |h_{mix} - h_{guess}| \tag{4.33}$$

becomes lower than a chosen tolerance. At this point, the mixture temperature T is fixed to T_{guess}. In addition, $\rho_{wf,liq}$ and $\rho_{wf,vap}$ are computed thanks to the *Refprop* data corresponding to pure cyclopentane, from the knowledge of $h_{wf,liq}$ and $h_{wf,vap}$ respectively. Finally, Eq. (4.31) is used to derive the density of the WF/oil mixture.

The convergence of this numerical method is ensured if and only if the chosen boundaries at the beginning of the process verify: $T_{B,low} < T < T_{B,high}$. It is easily satisfied by fixing for example $T_{B,low} =$

250 K (lower than the minimum temperature reachable in the system), and $T_{B,high} = 550$ K (above the critical temperature of cyclopentane). Moreover, the bisection method is also used to solve the set of equations (4.18) to (4.21) for ζ_{wf}, as well as Eqs. (4.3) and (4.5) respectively for $h_{wf,liq}$ and $h_{wf,vap}$. For the sake of brevity and because the method is basically the same, these two resolutions are not discussed here.

In order to illustrate the convergence of this algorithm, an example is presented in Fig. 4.12: the sequence of temperature guesses is shown for a pressure $P = 2$ bars, a mixture enthalpy $h_{mix} = 4.5 \times 10^5$ J/kg and a circulation rate $\kappa_{oil} = 5\%$. Each successive guess on the temperature results in an enthalpy h_{guess}, which tends rapidly to h_{mix}. In this case, the final temperature is equal to 366.13 K, the working fluid quality is equal to 0.986 and 12 iterations are needed to satisfy the criterion: $|h_{mix} - h_{guess}| < 10$ J/kg. This tolerance was chosen to guarantee a good precision, without increasing too much the number of required iterations and the computational time. However, one has to keep in mind that $h_{guess} = h_{mix}$ is never reached, so that all the working fluid properties and composition indicators as x_{wf} and ζ_{wf} are only approximated, but with a very good precision.

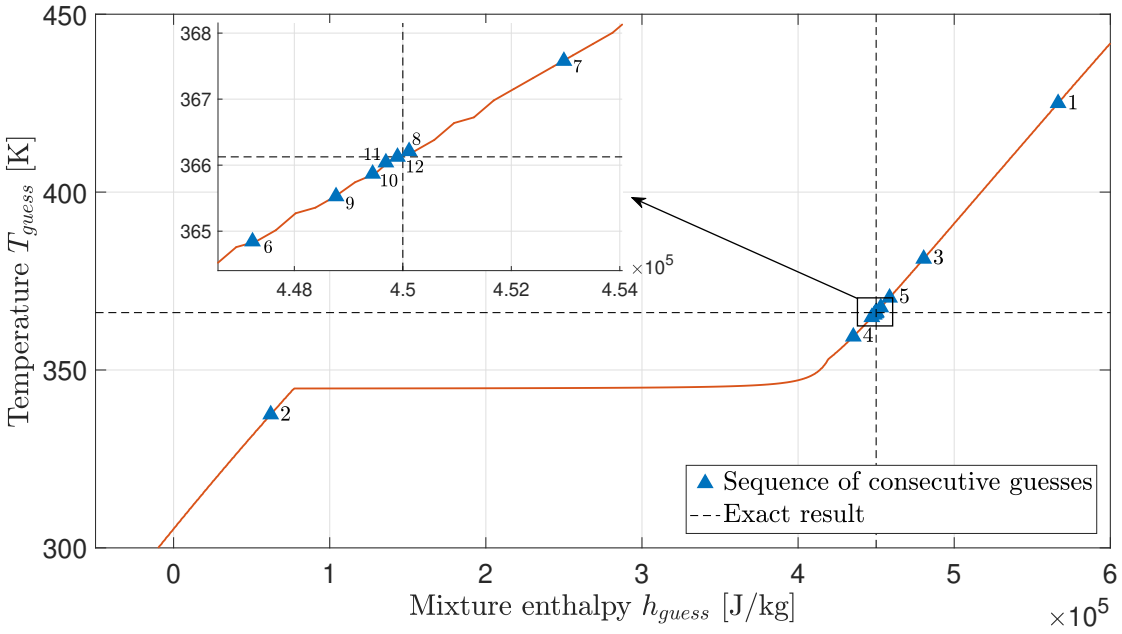

Figure 4.12: Working principle of the bisection method used to find iteratively the fluid temperature for a given mixture enthalpy ($P = 2$ bars and $\kappa_{oil} = 5\%$).

In addition to the mixture enthalpy and density, it is also useful to distinguish the thermodynamic properties of each phase in case of liquid-vapor equilibrium. As said before, the vapor phase is only composed of cyclopentane. Therefore, if this phase exists, its enthalpy is simply:

$$h_{mix,VapourPhase} = h_{wf,vap} \tag{4.34}$$

Similarly, the density of the vapor phase is computed from pure cyclopentane properties:

$$\rho_{mix,VapourPhase} = \rho_{wf,vap} \tag{4.35}$$

On the other hand, the liquid phase contains both cyclopentane and lubricant. The enthalpy of this phase

is obtained from the conservation of energy:

$$\dot{m}_{tot} \cdot h_{mix} = (\dot{m}_{oil} + \dot{m}_{wf,liq}) \cdot h_{mix,LiquidPhase} + \dot{m}_{wf,vap} \cdot h_{mix,VapourPhase} \tag{4.36}$$

so that:

$$h_{mix,LiquidPhase} = \frac{\dot{m}_{tot} \cdot h_{mix} - \dot{m}_{wf,vap} \cdot h_{mix,VapourPhase}}{\dot{m}_{oil} + \dot{m}_{wf,liq}} \tag{4.37}$$

Finally the density of the liquid phase is derived from the conservation of the volumetric liquid flow rate:

$$\rho_{mix,LiquidPhase} = \frac{\dot{m}_{oil} + \dot{m}_{wf,liq}}{\frac{\dot{m}_{oil}}{\rho_{oil}} + \frac{m_{wf,liq}}{\rho_{wf,liq}}} \tag{4.38}$$

The iterative algorithm described in this section, using the solubility model presented above and fitted with empirical data, is thus able to compute all the thermodynamic properties of interest as a function of the pressure, the specific enthalpy and the oil circulation rate in the Rankine box. However, this iterative method requires several iterations at each time step to achieve the convergence (typically between 5 and 15 iterations). Moreover, the block computing fluid properties is used more than twenty times in the *Matlab-Simulink* model of the complete Rankine system. As a result, the increase in computational cost due to this new method to compute mixture properties is huge (more or less a 75% increase in comparison with the model based on pure cyclopentane properties).

The chosen solution to reduce as much as possible the computational time is the tabulation of mixture properties. In order to create this properties database, the new block created in *Matlab-Simulink* is called with a set of different input values (pressure, enthalpy and oil circulation rate). More precisely, 60 different values of pressure are chosen between boundaries that were previously identified by *Volvo Trucks* in the case of cyclopentane, such that the fluid would not be able to reach a pressure outside these limits. The lower boundary is 0.9 bar, and the upper bound is equal to 45 bar. Similarly, 60 values of specific mixture enthalpy are considered between two extreme values ($-1.3 \cdot 10^5$ J/kg and $9.3 \cdot 10^5$ J/kg). In addition, it is assumed that the oil circulation rate would never be higher than 15%: the oil mass fraction evolves from 0 to 15% in steps of 1%, which gives 16 different values.

As a consequence, the new block computing mixture properties is called 57,600 times ($= 60 \times 60 \times 16$) in order to compose a very large set of values covering all the possible thermodynamic states that could be encountered at the different points where mixture properties are calculated in the Rankine system model. The different quantities that are computed for each set of input values are those shown in Fig. 4.11:

- The temperature T [K].
- The working fluid fraction in the liquid phase ζ_{wf} [-] and the cyclopentane quality x_{wf}, defining with κ_{oil} the mixture composition.
- The mixture density ρ_{mix} [kg/m^3] as well as the density of the vapor and liquid phases in the mixture (Eqs. 4.35 and 4.38).
- The enthalpy of the vapor and liquid phases [J/kg] defined by Eqs. (4.34) and (4.37).

In practice, the iterative method is thus not included in the Rankine box model. Instead, linear interpolations between these tabulated results previously computed once and for all are performed on *Simulink*. It makes possible to reduce drastically the computational cost associated to the complete box simulations. In fact, this CPU time becomes even lower than the one necessary for the simulations where pure cyclopentane properties are assumed. As a result, it is possible to perform large sets of simulations, to study the impact of the presence of oil in the working fluid on the Rankine system performances in variable conditions. These simulation results will be shown and discussed later in the text.

One could argue that performing linear interpolations between tabulated mixture properties is less precise than computing these properties for the exact set of input values (P, h_{mix} and κ_{oil}). However, the large number of different values considered for these inputs guarantees a sufficient accuracy. This precision was verified in the scope of this study, by comparing steady-state results of the Rankine box obtained with the initial iterative method or tabulated mixture properties. It was concluded that the error is negligible, and that the drastic reduction in CPU time justifies the small loss in precision.

4.2.5 Expander model

Each component of the Rankine box has to be modified in order to take into account the WF/oil mixture instead of a pure working fluid. Up to now in normal conditions, the mass flow going through the piston expander is only composed of vaporized cyclopentane. However, with a non-zero oil circulation rate and under the assumption that this oil remains totally in the liquid phase, a small liquid mass flow would also go through the expander. As shown before, the presence of oil prevents from reaching $x_{wf} = 1$ even with a large superheat above the saturation temperature of pure cyclopentane. In other words, the working fluid fraction in the liquid phase is always positive due to the small part of WF trapped in lubricant. As a result, the new expander model has to take into account this liquid-vapor equilibrium. The model described below is inspired from the work of *Dickes* [51].

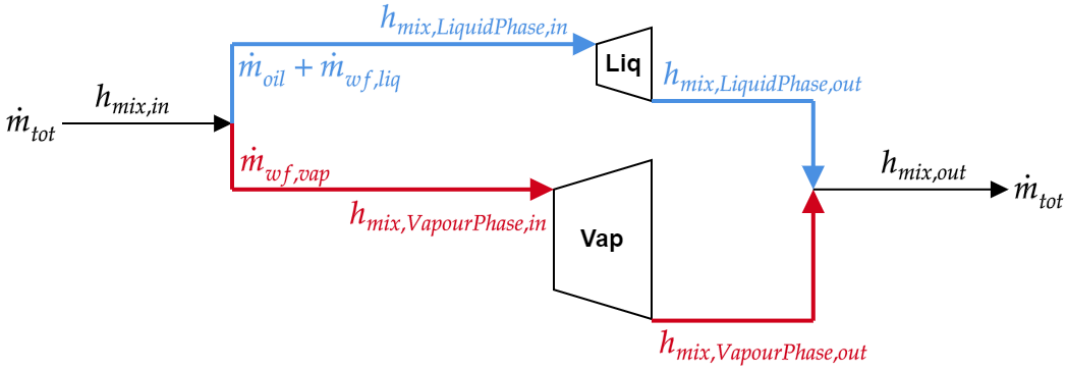

Figure 4.13: Schematic representation of the expander model adapted to take into account the presence of oil in the working fluid.

As shown in Fig. 4.13, the liquid and vapor phases are fictitiously distinguished in the new expander model. The total mixture mass flow is decomposed into two streams at the expander inlet. The expansions of these streams are then considered separately.
From the knowledge of the flow composition, the vapor mass flow composed only of cyclopentane and its corresponding enthalpy derived from Eq. (4.34) are the inputs of the expander model developed for pure working fluid. This standard model of expander is based on the definition of the isentropic efficiency:

$$\eta_{is} = \frac{h_{wf,exp,in} - h_{wf,exp,out}}{h_{wf,exp,in} - h_{wf,exp,out,is}} \tag{4.39}$$

This equation is adapted in accordance with notations used in Fig. 4.13, knowing that the vapor phase is only composed of cyclopentane:

$$\eta_{is} = \frac{h_{mix,VapourPhase,in} - h_{mix,VapourPhase,out}}{h_{mix,VapourPhase,in} - h_{mix,VapourPhase,out,is}} \tag{4.40}$$

where the isentropic outlet enthalpy of the vapor phase is derived from the outlet expander pressure and the inlet entropy of vapor cyclopentane:

$$h_{mix,VapourPhase,out,is} = \text{fct}\left(P_{exp,out}\ ;\ s_{mix,VapourPhase,in}\left(T_{exp,in}\ ;\ \rho_{mix,VapourPhase,in}\right)\right) \tag{4.41}$$

The isentropic efficiency of the piston expander (equipped with 6 pistons) was determined experimentally as a function of the rotation speed and the pressure ratio $r_P = P_{exp,in}/P_{exp,out}$ (Fig. 4.14). It can be observed that generally the efficiency decreases with the rotation speed for a given pressure ratio. Moreover, for a fixed rotation speed, this efficiency reaches a maximum for a certain r_P. The abscissa of this maximum tends to increase with the rotation speed.

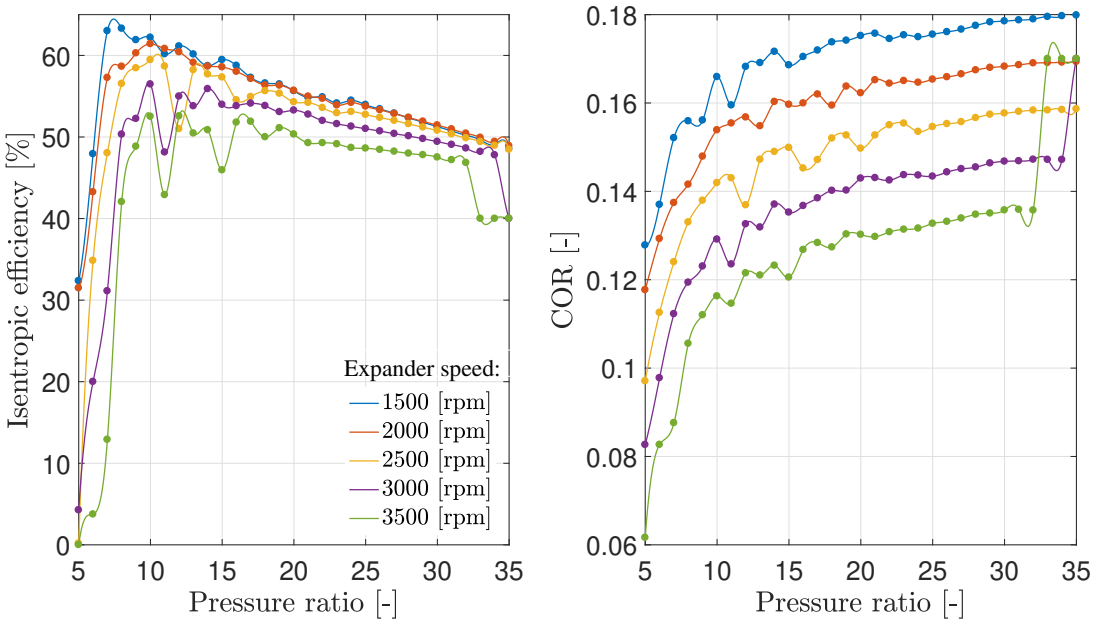

Figure 4.14: Evolution of the isentropic efficiency and cut-off ratio (COR) of the piston expander as a function of the pressure ratio, for different rotation speeds.

In a piston expander, which is a type of positive displacement machine, pistons are moving in the cylinders between the top dead center (TDC) and the bottom dead center (BDC). The cylinder volume at TDC is called the clearance volume V_0. The swept volume during a full stroke between TDC and BDC is noted $V_{s,max}$ (Fig. 4.15). During the suction process (1-2), the cylinder volume progresses between V_0 and $V_0 + V_s$, where V_s is the expander displacement. As a result, the volume that is swept during the expansion (2-3) is not equal to $V_{s,max}$. The cut-off ratio (COR) is defined to represent the relative importance of V_s with respect to $V_{s,max}$:

$$COR = \frac{V_s}{V_{s,max}} \tag{4.42}$$

The cut-off ratio is constant since it depends on construction parameters of the expander. However, in the model developed by *Volvo Trucks*, a fictive cut-off ratio derived experimentally is employed. It is obtained for different rotation speeds and pressure ratios (Fig. 4.14). This variable cut-off ratio can be viewed as a correction of the constant COR defined by Eq. (4.42), to take into account the volumetric efficiency of the expander when the pressure ratio and the rotation speed vary.

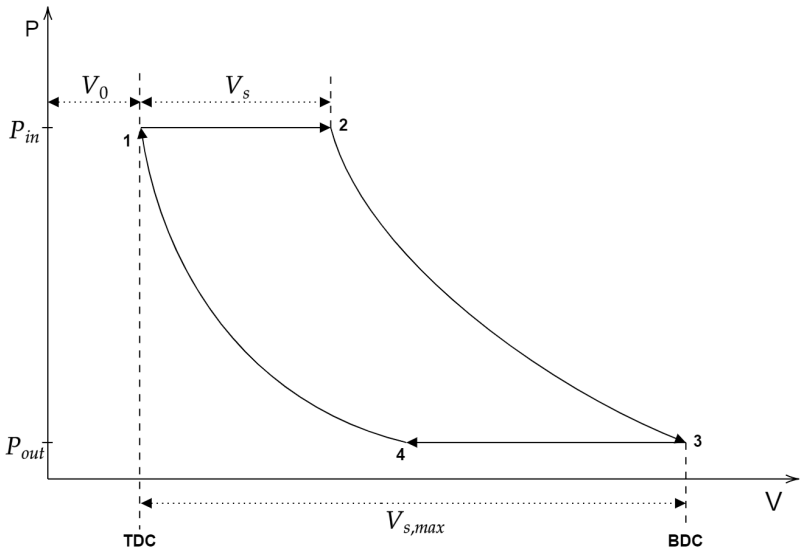

Figure 4.15: Theoretical P-V diagram of a piston expander.

In the complete Rankine box model, the outlet pressure of the expander (condensation pressure) is imposed by the controller depending on the cooling capacities of the condenser. As a result, this outlet pressure is viewed as an input, while the inlet pressure is computed directly by the model. With a positive displacement expander, the pressure ratio depends on the fluid mass flow, the expander rotation speed and the swept volume. To derive $P_{exp,in}$, the vapor density of pure cyclopentane in the expander made up of 6 cylinders is calculated at the end of the suction process (point 2 in Fig. 4.15, when the inlet valve is closed) with:

$$\rho_{exp,in} = \frac{\frac{\dot{m}_{wf,vap} \cdot 60}{N_{exp}}}{6 \cdot (COR \cdot V_{s,max} + V_0)} \tag{4.43}$$

In this equation, N_{exp} is the rotation speed expressed in rotations per minute (varying between 1000 and 3500 rpm in normal operating conditions), $V_{s,max}$ is the cubic capacity of one cylinder (equal to 39 cm^3) and COR is the above-mentioned cut-off ratio. To calculate $\rho_{exp,in}$, only the vapor mass flow composed exclusively of cyclopentane is considered: it is assumed that the liquid mass flow is negligible in the expander. This hypothesis makes possible to compute the inlet pressure $P_{exp,in}$ from the temperature at the expander inlet and the density $\rho_{exp,in}$:

$$P_{exp,in} = \text{fct}\left(T_{exp,in}\ ;\ \rho_{exp,in}\right) \tag{4.44}$$

with tabulated properties computed previously with the *Refprop* database for *pure* cyclopentane, similarly to the previous expander model which does not take into account the presence of oil in the working fluid mass flow.
In order to optimize the isentropic efficiency, the expander rotation speed is controlled. In fact, this speed affects directly the efficiency, but also the inlet pressure and the pressure ratio due to Eqs. (4.43) and (4.44).

Finally, the real outlet enthalpy of the vapor phase ($h_{mix,VapourPhase,out}$) is determined from Eq. (4.40), as well as the power $\dot{W}_{exp,vap}$ produced by the expansion:

$$\dot{W}_{exp,vap} = \dot{m}_{wf,vap} \cdot (h_{mix,VapourPhase,in} - h_{mix,VapourPhase,out}) \tag{4.45}$$

On the other hand, the expansion of the liquid phase is considered separately. This mixture of oil and liquid cyclopentane is viewed as an incompressible fluid which is ideally expanded from the evaporation pressure $P_{exp,in}$ to the condensation pressure $P_{exp,out}$:

$$\begin{aligned} \dot{W}_{exp,liq} &= \left(\dot{V}_{oil} + \dot{V}_{wf,liq}\right) \cdot \left(P_{exp,in} - P_{exp,out}\right) \\ &= \frac{\dot{m}_{wf,liq} + \dot{m}_{oil}}{\rho_{mix,LiquidPhase}} \cdot \left(P_{exp,in} - P_{exp,out}\right) \end{aligned} \tag{4.46}$$

In this formula, the density of the liquid phase $\rho_{mix,LiquidPhase}$ is preliminary computed with Eq. (4.38). Furthermore, the total power produced by the expander is simply the sum of the two contributions:

$$\dot{W}_{exp,tot} = \dot{W}_{exp,vap} + \dot{W}_{exp,liq} \tag{4.47}$$

One can anticipate that $\dot{W}_{exp,liq}$ is nearly negligible compared with $\dot{W}_{exp,vap}$, not only because the expansion of a vapor phase is more powerful but also because the vapor mass flow is much larger than the liquid mass flow. Finally, the enthalpy of the mixture at the outlet of the expander ($h_{mix,out}$) is derived from Eq. (4.29). The mixture properties are then computed from $h_{mix,out}$ and $P_{exp,out}$ with the solubility model largely discussed earlier in the text.
It is important to highlight that this fictive model considers only the *inlet* flow composition to distinguish the liquid fluid from the vapor mass flow. This flow composition is completely described by two of the three parameters κ_{oil}, x_{wf} and ζ_{wf}, and is obviously not the same than the outlet composition since x_{wf} and ζ_{wf} would change during the expansion.

4.2.6 Heat exchangers model

The presence of lubricant in the working fluid of an ORC system has also an impact on the heat exchangers performance. This aspect is discussed extensively by *Shen et al.* in [56] and [57]. Depending on the conditions and the considered exchanger, experiments show that the oil could either increase or decrease the heat transfer coefficient computed for pure working fluid. In any case, there is no general correlations that are commonly adopted in the literature to quantify the HTC variations due to the oil mass fraction. Correlations for pure working fluid are sometimes still employed, neglecting the impact of lubricant [51]. This assumption is plausible for very limited oil mass fraction, which is not the case in this study. In fact, one could remind that the oil circulation rate of the Volvo Rankine box can exceed 10%. As a result, heat transfer correlations of the previous box model are corrected as follows for the evaporation and the condensation.
Beyond these modifications of the convective HTC, the heat exchangers model remains the same. The presence of oil could also have an impact on pressure drops, but these drops are neglected in the model as shown in the chapter dedicated to heat exchanger modelling. It is important to highlight that the FV approach is preferred for the Rankine box model which takes into account the impact of oil, and not the new MB method to model heat exchangers. Indeed, the two main parts of this master thesis were conducted in parallel, so that the MB model was not yet finalized before studying the impact of lubricant

on WF properties. Moreover, the moving boundaries approach cannot be directly used in this context, since the presence of oil affects directly the definition of the liquid and vapor saturation points, so that zone boundaries could not be identified easily.

4.2.6.1 Condensation

The modification of the condenser performances due to the addition of lubricant in the working fluid is addressed in the PhD thesis of *Youbi-Idrissi* [49]. It is concluded that the heat transfer coefficient always decreases if the oil is taken into account. This degradation depends particularly on two parameters: the lubricant mass fraction and the type of lubricant.
Experiments conducted with R134a and a POE oil (Polyolester) show a 7% decrease of the HTC with an oil fraction equal to 2%; this degradation can reach 20% with a 5% oil fraction. Locally, the negative impact of the presence of lubricant is emphasized for elevated working fluid qualities ($x_{wf} > 0.8$). On the other hand, the effect of the type of lubricant is relatively simple: experiments conclude that the HTC degradation is more significant when the oil viscosity is increased.

In the text of *Youbi-Idrissi*, two possibilities are presented to model the impact of lubricant in the calculation of the HTC:

- Correlations for pure working fluid are still employed, using the properties of the WF/oil mixture instead of pure working fluid properties. The viscosity of the fluid is definitely the property of interest that is the most impacted by the oil.
- The heat transfer coefficient is computed for pure working fluid, thereafter this value is corrected by a coefficient C:

$$\alpha_{mix} = \alpha_{PureWF} \cdot C \tag{4.48}$$

  This coefficient takes generally the form of a decreasing exponential:

$$C = exp\left(-a \cdot \kappa_{oil}\right) \tag{4.49}$$

  where κ_{oil} is the oil mass fraction and a is a positive coefficient determined experimentally. As a result, α_{mix} decreases with respect to α_{PureWF} if the oil circulation rate or/and the coefficient a is/are increased.

Because the current correlations chosen to compute the heat transfer coefficient of the cyclopentane do not involve the fluid viscosity, the first of the two methods listed above is impossible to put into practice. As a result, the second possibility described by the decreasing exponential is preferred.

As shown in the chapter dedicated to the heat exchangers modelling, the heat transfer coefficient on the working fluid side of the condenser is computed depending on its thermodynamic state [17]. The only modification of the HTC correlations due to the presence of oil is thus the multiplication by the correction factor C:

$$\alpha_{mix,liq} = \left(\frac{\dot{m}_{mix}}{\dot{m}_{nom}}\right)^{a_{liq}} \cdot \alpha_{liq,nom} \cdot C \tag{4.50}$$

$$\alpha_{mix,vap} = \left(\frac{\dot{m}_{mix}}{\dot{m}_{nom}}\right)^{a_{vap}} \cdot \alpha_{vap,nom} \cdot C \tag{4.51}$$

These correlations are based on a modification of nominal heat transfer coefficients $\alpha_{liq,nom} = 150$ W/m^{2}K and $\alpha_{vap,nom} = 75$ W/m^{2}K according to the working conditions. These modifications depend on the ratio between the fluid mass flow rate (which is now the *total* mixture mass flow rate: $\dot{m}_{mix} = \dot{m}_{wf} + \dot{m}_{oil}$) and a nominal mass flow equal to: $\dot{m}_{nom} = 0.0156$ kg/s (with $a_{liq} = 0.86$ and $a_{vap} = 0.96$).
In the case of a liquid-vapor equilibrium, the biphasic HTC is based on a modification of $\alpha_{mix,liq}$, as already shown in the previous chapter:

$$\alpha_{mix,TwoPhase} = \alpha_{mix,liq} \cdot \Big(X + Y\Big)^{-1/2} \cdot C \tag{4.52}$$

where the quantities X and Y, defined by Eqs. (3.40) and (3.41), are functions of the fluid quality x_{wf}.

It can be highlighted that, due to the presence of oil, it was demonstrated that $x_{wf} = 1$ is not reachable even with a large superheat. As a result, the value of the vapor heat transfer coefficient $\alpha_{mix,vap}$ is never used. In the presence of oil, the switching between correlations is thus simply:

$$\alpha_{mix} = \begin{cases} \alpha_{mix,liq} & \text{if } x_{wf} = 0 \\ \alpha_{mix,TwoPhase} & \text{if } x_{wf} > 0 \end{cases} \tag{4.53}$$

In [49], *Youbi-Idrissi* states that the coefficient a from Eq. (4.49) can have a value between 2.2 and 5, depending on the working fluid and the lubricant.
The principal interest of this study is the evaluation of the fluid properties and flow composition as a result of the lubricant mass fraction. As shown before, one main impact of this fraction is the evolution of the fluid quality x_{wf} as a function of the temperature above the saturation temperature of pure cyclopentane. However, literature devoted to this subject considers the modification of HTC as a secondary impact. As a result, for the Volvo Rankine box, the experimental coefficient of Eq. (4.49) is set to the lowest proposed value (i.e. $a = 2.2$) in order to avoid altering too much the HTC in the condenser, and thus giving an unconsidered importance to this aspect. It is also motivated because simulations could not be compared to HTC derived empirically with cyclopentane and PAG oil: such results are impossible to find in the literature.
For example, with $a = 2.2$, the correction factor computed with Eq. (4.49) is equal to $C = 0.896$ with $\kappa_{oil} = 5\%$, resulting in a 10.4% decrease of the heat transfer coefficient. This diminution is equal to 19.7% with $\kappa_{oil} = 10\%$, which illustrates the non-negligible impact of the oil on the heat transfer coefficient in the condenser of the Rankine box.

4.2.6.2 Evaporation

The single phase heat transfer coefficient on the working fluid side of the exhaust boiler is computed using the well-known Dittus-Boelter equation [39], as already shown in the section devoted to the MB boiler model:

$$\alpha_{wf,liq} = \frac{Nu \cdot k}{L_c} = \Big[0.023 \cdot Re^{0.8} \cdot Pr^{0.4}\Big] \, \frac{k}{L_c} \tag{4.54}$$

where Nu is the Nusselt number, Re the Reynolds number and Pr the Prandtl number. As a reminder, these two last non-dimensional quantities are defined as:

$$Pr = \frac{cp \cdot \mu}{\lambda} \tag{4.55}$$

$$Re = \frac{L_c \cdot \dot{m}_{mix}}{A_{flow} \cdot \mu} \tag{4.56}$$

where cp is the specific heat capacity of the fluid, μ the dynamic viscosity, λ the thermal conductivity, L_c a characteristic length of the fluid flow, and A_{flow} the flow section area. In the case of a liquid-vapor equilibrium, the correlation used to compute the heat transfer coefficient is based on the value of $\alpha_{wf,liq}$:

$$\alpha_{wf,TwoPhase} = \alpha_{wf,liq} \cdot \left[1 + \left(\frac{3.8}{P_{red}^{0.38}} \cdot \left(\frac{x_{wf}}{1 - x_{wf}} \right)^{0.76} \right) \right] \tag{4.57}$$

As a reminder, this equation is a modified version of the correlation initially proposed by *Shah et al.* [43].

To take into account the presence of oil, it is impossible to use a simple correction factor, similar to Eq. (4.49). In fact, the heat transfer coefficient associated to the evaporation can either be increased or decreased due to the oil fraction. In [49], *Youbi-Idrissi* states that for a moderate quality ($0.1 < x_{wf} < 0.6$), a low lubricant mass fraction ($< 2\%$) induces generally a considerable increase of the HTC for any type of refrigerant. However, when $x_{wf} > 0.7$ the HTC is considerably reduced. As a result, the approach chosen to model the Rankine box is comparable to the first possibility listed above for the condenser model: the correlations for pure cyclopentane are still employed (Eqs. 4.54 to 4.57) but are now associated to the properties of the WF/oil mixture. The properties that have to be calculated are the ones appearing in the definition of Reynolds and Prandtl numbers: thermal conductivity, specific heat capacity and dynamic viscosity.

The literature provides only one simple correlation to calculate the specific heat capacity of a mixture, considering an ideal mixing [49]:

$$cp_{mix} = (1 - \kappa_{oil}) \cdot cp_{wf} + \kappa_{oil} \cdot cp_{oil} \tag{4.58}$$

The value of cp_{wf} is derived from the cyclopentane properties using *Refprop*, and cp_{oil} is given by the PAG oil datasheet (2000 J/kg/K, see Tab. 4.1). One can note that cp_{wf} and cp_{oil} are of the same order. The situation is not the same for the thermal conductivity, since the conductivity of the lubricant λ_{oil} ($= 0.15$ W/m/K) is several times higher than the one of the working fluid λ_{wf} (between 1×10^{-5} and 8×10^{-4} W/m/K). In this case, *Baustian et al.* in [58] propose the following correlation to derive the mixture conductivity λ_{mix}:

$$\lambda_{mix} = (1 - \kappa_{oil}) \cdot \lambda_{wf} + \kappa_{oil} \cdot \lambda_{oil} - 0.72 \cdot \kappa_{oil} \cdot (1 - \kappa_{oil}) \cdot (\lambda_{oil} - \lambda_{wf}) \tag{4.59}$$

where the third term represents the correction applied due to the large difference between λ_{oil} and λ_{wf}. The last property of interest to compute the HTC in the exhaust boiler is the dynamic viscosity of the mixture μ_{mix}. One again, the selected correlation was proposed by *Baustian et al.* in [58]:

$$\mu_{mix} = \left[\kappa_{oil} \cdot \mu_{oil} + (1 - \kappa_{oil}) \cdot \mu_{wf} \right]^{1.38} \tag{4.60}$$

Finally, the heat transfer coefficient on the working fluid side of the exhaust boiler is computed with Eqs. (4.54) to (4.57), integrating mixture properties derived from Eqs. (4.58) to (4.60), with:

$$\alpha_{mix} = \begin{cases} \alpha_{wf,liq} & \text{if } x_{wf} = 0 \\ \alpha_{wf,TwoPhase} & \text{if } x_{wf} > 0 \end{cases} \tag{4.61}$$

Fig. 4.16 shows the evolution of the three properties of interest as a function of the oil circulation rate κ_{oil}, with fixed pressure and mixture enthalpy. As the specific heat of the oil is lower than the one of cyclopentane, cp_{mix} decreases with κ_{oil}. However, the thermal conductivity and the viscosity of the mixture increase with κ_{oil}. As said previously, the increase in viscosity is obviously the most significant impact of the presence of oil.

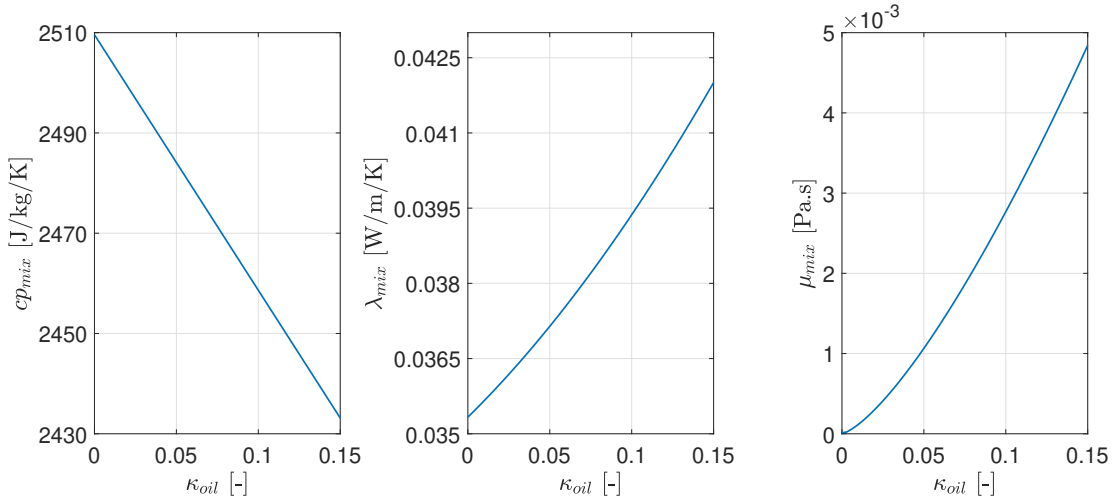

Figure 4.16: Evolution of the specific heat capacity, the thermal conductivity and the dynamic viscosity of the mixture as a function of the oil circulation rate, for $h_{mix} = 5 \times 10^5$ J/kg and $P = 20$ bars.

From the analysis of Eqs. (4.54) to (4.57), one can observe that a decrease of cp_{mix} induces a reduction of the heat transfer coefficient. In the same way, the increase of the mixture viscosity due to the presence of oil also causes a degradation of the heat transfer. However, the enhancement of the thermal conductivity observed if κ_{oil} increases is beneficial for the HTC. These opposite trends highlight the complex impact of the lubricant on exhaust boiler performances.

4.2.7 Pump model

The pump model is also modified due to the presence of oil in the working fluid, but this improvement is less significant than the modification of the other components. In fact, the mixture going through the pump in normal operating conditions is totally in the liquid phase: $x_{wf} = 0$ and $\zeta_{wf} = \zeta_{wf,max}$. As a result, considering separately the vapor and liquid steams is not necessary and the current pump model can still be employed. Properties of pure liquid cyclopentane are thus simply replaced by those of the WF/oil mixture. This model is based on a constant isentropic efficiency of the pump η_{is} equal to 60%, and a mechanical efficiency η_{mech} fixed to 90% to compute the pump power demand:

$$\dot{W}_{pump} = \frac{\dot{m}_{mix} \cdot (h_{mix,out,is} - h_{mix,in})}{\eta_{is} \cdot \eta_{mech}} \tag{4.62}$$

As shown before, the evaporation pressure is imposed by the expander model, and the condensation pressure is fixed by the controller depending on the cooling capacities of the direct air condenser. This pressure ratio is thus an input of the pump model, which computes the mixture mass flow as a function of the mixture density, the pump rotation speed and its internal displacement C_{pump}:

$$\dot{m}_{mix} = \rho_{mix} \cdot N_{pump} \cdot C_{pump} \tag{4.63}$$

The pump rotation speed (ranging from 150 to 2500 rpm) is controlled to adapt the working fluid mass flow, in order to track a superheat set-point at the outlet of the exhaust boiler.

4.3 Impact of oil on ORC performances

The impact of the oil circulation rate on the Rankine box performances is evaluated in two stages. At first, steady-state simulations are performed: the exhaust mass flow, exhaust temperature and ambient air temperature are set to constant values, and ORC performances are computed as a function of the oil mass fraction. Furthermore, the Frankfurt-Koblenz (FK) road cycle is simulated for different oil circulation rates, to assess the impact of lubricant on transient performances.

4.3.1 Steady-state results as a function of κ_{oil}

In the Rankine box, the set-point value of the super-heating at the expander inlet is the result of an optimization process, which aims to maximize the net ORC power. When cyclopentane is chosen as WF, this set-point varies typically between 20 and 40 K. On the other hand, it was already shown in the section dedicated to the empirical solubility model that a large *apparent* superheat above the saturation temperature of pure cyclopentane is required to maximize the WF quality at the expander inlet (Fig. 4.5). In fact, the fraction of working fluid trapped into liquid oil bubbles decreases logically when superheat is increased. As a result, in the Rankine box model that takes into account the presence of oil added to WF, the set-point value of super-heating is fixed to the upper bound of the above-mentioned interval (40 K), in order to maximize the vapor mass flow in the expander and the produced mechanical power. Steady results presented below are thus obtained with this super-heating at the outlet of the exhaust boiler. As a reminder, the controller tracks this set-point by acting on the pump rotation speed to vary the WF mass flow.
The set-point of the sub-cooling at the outlet of the condenser is fixed to 9 K, similarly to simulations that do not consider the impact of lubricant.

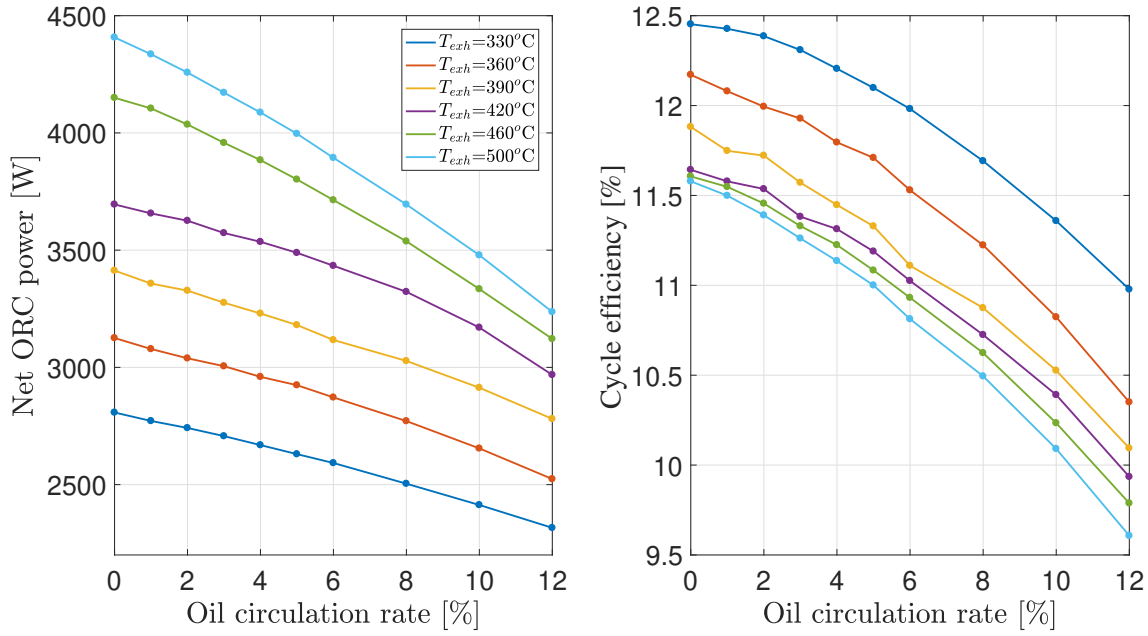

Figure 4.17: Evolution of net ORC power and cycle efficiency as a function of the oil circulation rate, for different exhaust temperatures and a constant exhaust mass flow (0.1 kg/s), with $T_{air} = 300$ K.

Figs. 4.17 to 4.24 show the results of steady-state simulations characterized by an ambient air temperature equal to 300 K. The exhaust mass flow is fixed to 0.1 kg/s (typical value at moderate engine load), and on each plot the different curves correspond to different exhaust temperatures. Physical quantities of

interest are plotted as a function of the oil circulation rate (κ_{oil}) in the Rankine box (ranging from 0 to 12%). The simulation time is set to 1500 seconds to ensure that steady conditions are reached.

One can observe in Fig. 4.17 that the net power produced by the ORC system decreases considerably when the oil circulation rate is increased. With a fixed exhaust mass flow, this observation is exacerbated if the exhaust temperature (i.e. the heat input) is large. With $\kappa_{oil} = 10\%$, the relative decrease in net power with respect to the simulation assuming pure cyclopentane ($\kappa_{oil} = 0\%$) is equal to 17% with $\dot{m}_{exh} = 0.1$ kg/s and $T_{exh} = 330$°C. This relative decrease reaches 26% with $\dot{m}_{exh} = 0.1$ kg/s and $T_{exh} = 500$°C. These results demonstrate clearly that the impact of lubricant is not negligible. The evolution of the cycle efficiency, defined as the ratio between the net produced power and the heat input, follows logically the same trend. For a given oil mass fraction, this efficiency is higher when the heat input is low.

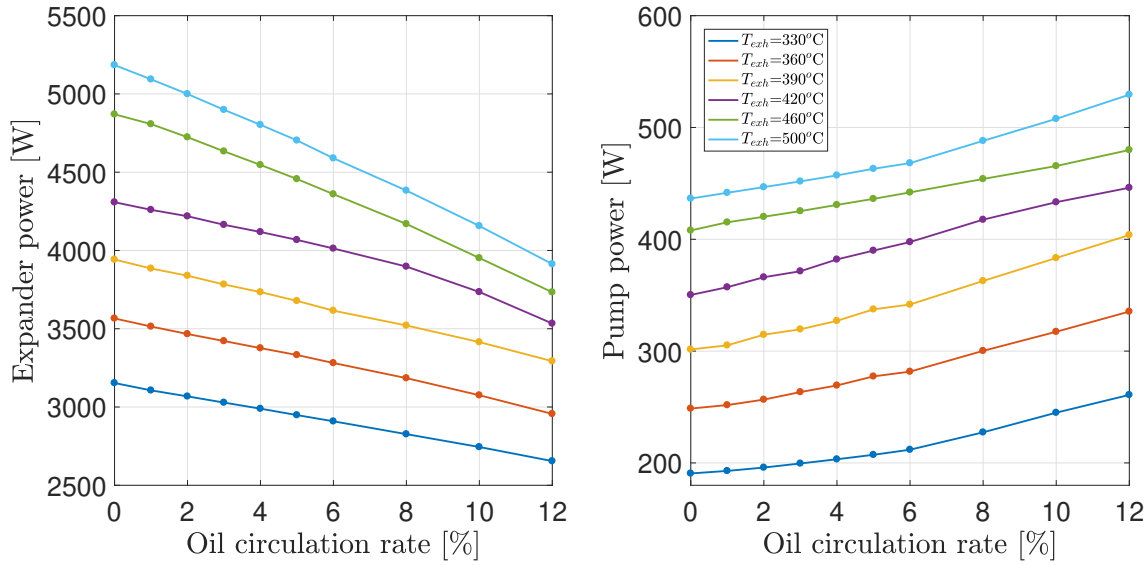

Figure 4.18: Evolution of expander and pump powers as a function of the oil circulation rate, for different exhaust temperatures and a constant exhaust mass flow (0.1 kg/s), with $T_{air} = 300$ K.

As a reminder, the ORC net power is defined as the expander gross power minus the power consumption of the feed pump and fans providing the air mass flow in the condenser. As shown in Fig. 4.18, the expander power decreases dramatically with the oil circulation rate. This decrease is the main aspect leading to the large reduction in net power. In addition, the pump power increases with κ_{oil}, which further decreases the ORC net power. By contrast, the power consumption of electrically-driven fans is nearly independent from the oil circulation rate.

The decrease in expander power is manly caused by the evolution of the WF quality at the expander inlet (Fig. 4.19). Indeed, one can conclude by comparing Figs. 4.18 and 4.19 that the relative decrease in expander power when κ_{oil} increases is nearly equal to the relative decrease in WF quality at the expander inlet. In fact, this quality represents the relative importance of the vapor mass flow with respect to the whole cyclopentane mass flow. Knowing that the expansion of the liquid phase is nearly negligible (this aspect is discussed later in the text), the decrease in WF quality represents an irretrievable loss in expander power. In other words, the produced power mainly depends on the vapor mass flow through the expander, which is greatly altered at high oil mass fraction.
In parallel, this loss of expander power is also illustrated by the WF fraction remaining in the liquid phase (Fig. 4.19), which increases at the expander inlet when κ_{oil} increases.

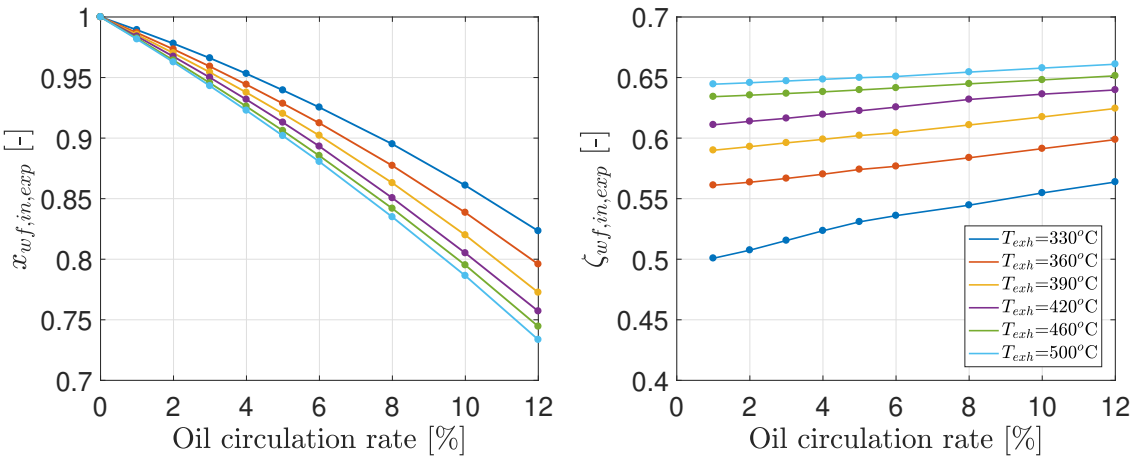

Figure 4.19: Evolution of the WF quality and WF fraction in the liquid phase at the expander inlet, as a function of the oil circulation rate, for different exhaust temperatures and a constant exhaust mass flow (0.1 kg/s), with $T_{air} = 300$ K.

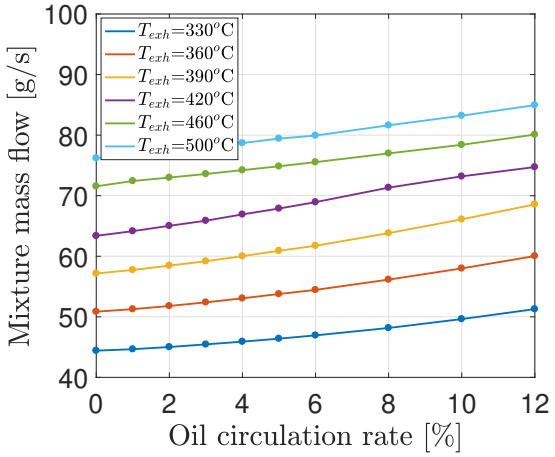

Figure 4.20: Evolution of the mixture mass flow as a function of the oil circulation rate, for different exhaust temperatures and a constant exhaust mass flow (0.1 kg/s), with $T_{air} = 300$ K.

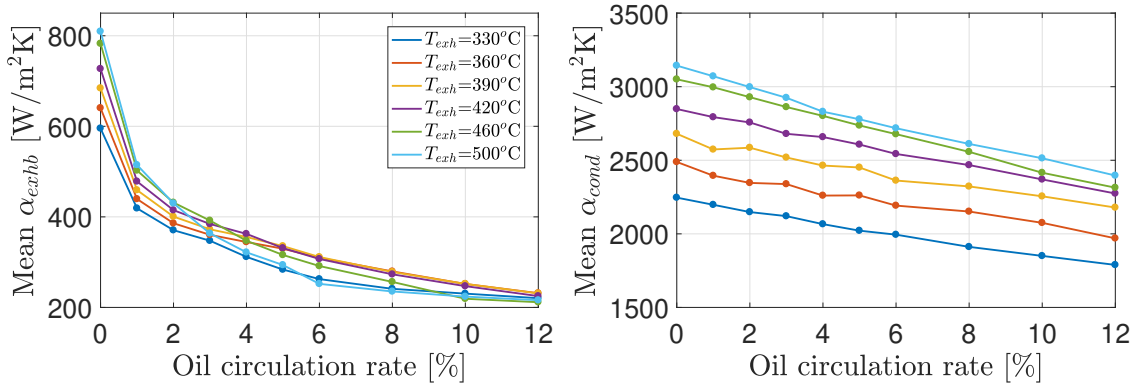

Figure 4.21: Evolution of the averaged HTC (exhaust boiler and condenser) as a function of the oil circulation rate, for different exhaust temperatures and a constant exhaust mass flow (0.1 kg/s), with $T_{air} = 300$ K.

The increase in pump power due to the presence of oil in the working fluid, which also causes a decrease in net power, comes simply from the fact that the mixture mass flow (cyclopentane + lubricant) increases with the oil circulation rate (Fig. 4.20). However, this increase in mixture mass flow does not mean that the cyclopentane mass flow is also increased. For example, the mixture mass flow obtained at $T_{exh} = 330°C$ (blue curve in Fig. 4.20) is equal to 44.4 g/s when $\kappa_{oil} = 0$, and equal to 49.6 g/s when $\kappa_{oil} = 10\%$ (difference equal to 5.2 g/s). And one can calculate that in the second case, the oil mass flow is equal to 4.96 g/s, which is almost equal to the difference between these two mixture mass flow rates. In other words, the increase in mixture mass flow comes simply from the added oil mass, while the cyclopentane mass flow is nearly independent from κ_{oil}. This result is important to highlight, but in any case the oil mass flow induces an increase in pump power demand.

In addition to the expander power and the pump power consumption, performances of heat exchangers are also altered by the presence of lubricant. For the exhaust boiler and the air condenser, an averaged heat transfer coefficient on the WF side is computed for each simulation (Fig. 4.21). Taking into account the mixture properties instead of pure cyclopentane characteristics induces a large decrease in mean HTC with κ_{oil} for the exhaust boiler. As a reminder, the presence of oil tends to increase the mixture thermal conductivity, which is beneficial for the HTC, but it also increases the mixture viscosity, which tends to decrease the HTC. As shown previously in Fig. 4.16, this increase in mixture viscosity is significant since the chosen PAG oil for the Rankine box is very viscous. As a result, the effect of viscosity is predominant, and the HTC in the boiler is reduced when the lubricant is modelled.
On the other hand, the averaged HTC on the WF side of the condenser also decreases with κ_{oil}, but less significantly. This decrease was anticipated due to the correction factor applied to the HTC computed by assuming pure cyclopentane properties (Eq. 4.48).

In addition to the results presented in this document, several simulations were performed without taking into account the negative impact of lubricant on the heat transfer coefficients. The result is that the decrease in HTC does not have a significant impact on ORC net power. It can be explained by two reasons. Firstly, in each heat exchanger, the thermal resistance is mainly dependent on the secondary side (gas side of the exhaust boiler, and air side of the condenser). Indeed, the heat transfer coefficient on the WF side remains much larger than the one corresponding to the secondary side, even with large κ_{oil}. As a result, the decrease in HTC on the WF side does not modify drastically the total thermal resistance.
Secondly, it is mainly the decrease in expander power that is responsible for the reduced ORC net power, so that simulations performed with or without modified HTC do not lead to significant discrepancies.

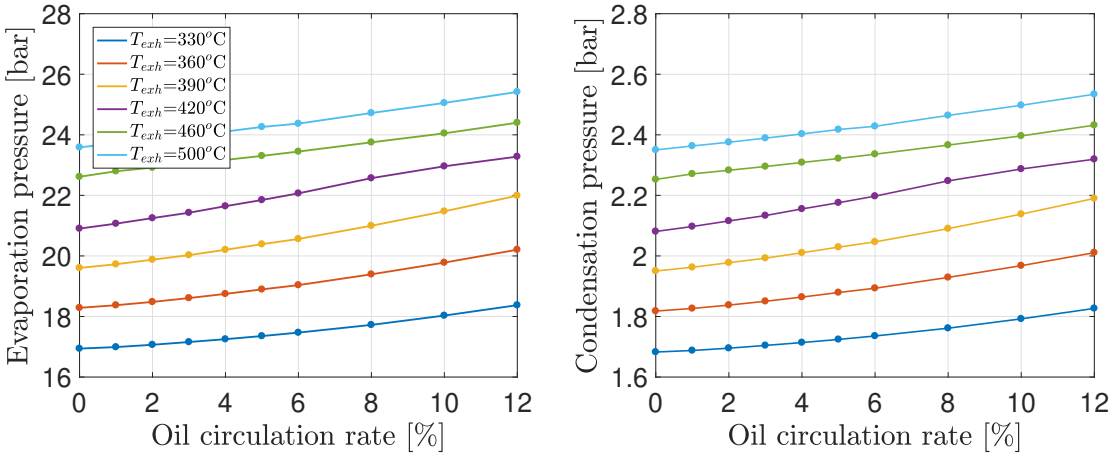

Figure 4.22: Evolution of evaporation and condensation pressures as a function of the oil circulation rate, for different exhaust temperatures and a constant exhaust mass flow (0.1 kg/s), with $T_{air} = 300$ K.

As said before, the decrease in expander power seems to be mainly explained by the reduced vapor mass flow through the expander when the oil circulation rate increases. One could suggest that this loss of power could also be explained by variable inlet and outlet expander conditions when κ_{oil} is modified. Indeed, both pressure levels (evaporation and condensation pressures) increase for given exhaust conditions when the oil circulation rate increases, as shown in Fig. 4.22. However, the pressure ratio between inlet and outlet pressures of the expander (Fig. 4.23) is nearly independent from κ_{oil}, and even from exhaust conditions more generally. As a result, the pressure ratio cannot be considered as a reason explaining the decrease in ORC power. In addition, Fig. 4.23 shows also that the temperature at the expander inlet tends to increase with the oil circulation rate, which should be beneficial for the expander power. But the opposite evolution is observed, and one can highlight that inlet fluid temperature is not responsible for the decrease in expander power.
As a conclusion, reduced ORC performances (net power) due to the presence of lubricant are mainly explained by the severe decrease in expander power, and to a lesser extent by the increase in pump power. More precisely, the decrease in expander gross power is mainly caused by the decrease in vapor mass flow through this component (i.e. decrease in WF inlet quality when κ_{oil} increases), and not by modified fluid conditions at the expander inlet and/or outlet. Furthermore, the impact of oil on WF heat transfer coefficients is not negligible, but it does not alter significantly the ORC net power.

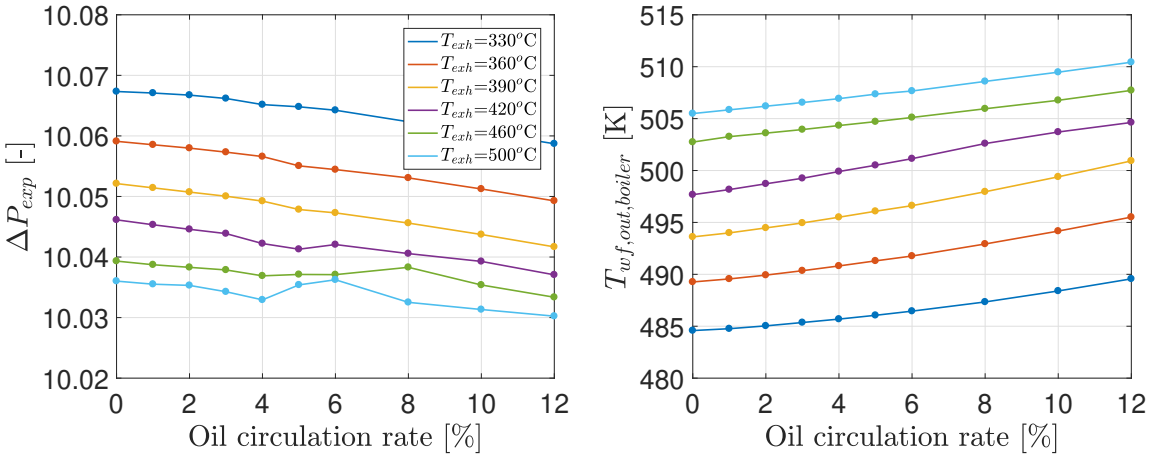

Figure 4.23: Evolution of the pressure ratio and mixture temperature at the expander inlet, as a function of the oil circulation rate, for different exhaust temperatures and a constant exhaust mass flow (0.1 kg/s), with $T_{air} = 300$ K.

Two other quantities are important to observe as a function of the oil circulation rate (Fig. 4.24). The first one comes directly from the expander model adapted to take into account the presence of lubricant (Fig. 4.13); it is the ratio between the power produced by the expansion of the vapor phase and the total expander power:

$$\frac{\dot{W}_{exp,vap}}{\dot{W}_{exp,tot}} = \frac{\dot{W}_{exp,vap}}{\dot{W}_{exp,liq} + \dot{W}_{exp,vap}} \tag{4.64}$$

The evolution of this power ratio can be observed on the left side of Fig. 4.24. Starting logically from 1 when $\kappa_{oil} = 0$, this quantity decreases with the oil circulation rate, which means that the power from the expansion of the liquid phase increases with respect to the total expander power. However, this power ratio is never far below 1, so that the expansion of the liquid phase could be neglected for the majority of exhaust conditions, especially if the exhaust temperature is moderate. This observation was already anticipated during the presentation of the new expander model.

The second quantity of interest is also a ratio between powers. If the power demands corresponding to the pumping of oil and liquid WF (cyclopentane) are fictitiously distinguished, one can consider the quotient between the power coming from the oil mass flow and the total pump power:

$$\frac{\dot{W}_{pump,oil}}{\dot{W}_{pump,tot}} = \frac{\dot{W}_{pump,oil}}{\dot{W}_{pump,oil} + \dot{W}_{pump,wf}} \tag{4.65}$$

As shown on the right side of Fig. 4.24, this ratio increases slower than κ_{oil}, meaning that the relative increase in pump power demand due to the oil mass flow is lower than the oil circulation rate.

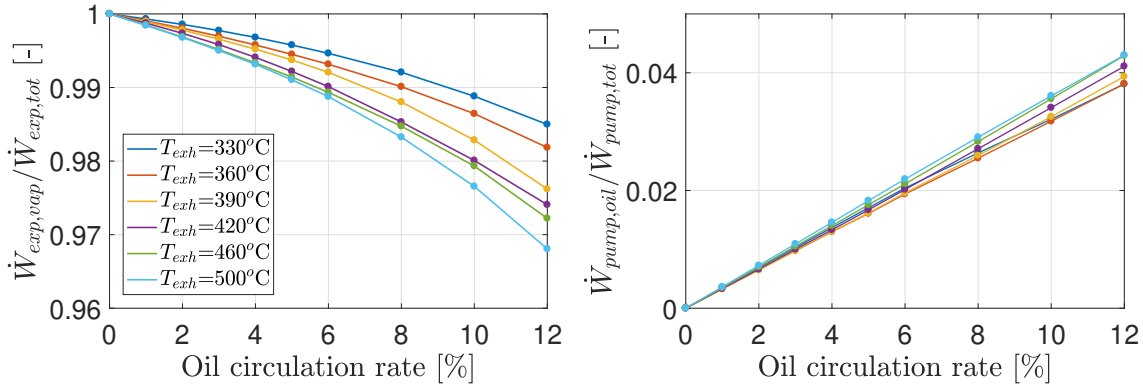

Figure 4.24: Evolution of power ratios (expander and pump) as a function of the oil circulation rate, for different exhaust temperatures and a constant exhaust mass flow (0.1 kg/s), with $T_{air} = 300$ K.

4.3.2 Relative decrease in net power depending on steady exhaust conditions

In the previous section, results of steady-state simulations are presented as a function of the oil circulation rate, associated to a fixed exhaust mass flow and several exhaust temperatures. In order to study more precisely the impact of oil on net ORC power with all the possible exhaust conditions, a very large set of simulations are performed by varying both exhaust temperature (from 260°C to 500°C) and exhaust mass flow rate (from 0.1 to 0.5 kg/s), with a constant oil circulation rate $\kappa_{oil} = 5\%$. The results are shown in Fig. 4.25, where each contour plot corresponds to a different ambient air temperature (15, 27 or 40°C). Similarly to the previous section, these simulations are obtained with a super-heating set-point equal to 40 K, and a sub-cooling set-point fixed to 9 K (simulation time = 1500 s).
To construct these plots, the ORC net power is computed for all the different external conditions with $\kappa_{oil} = 5\%$, but also with $\kappa_{oil} = 0\%$ (pure cyclopentane). Since the goal of these simulations is studying the impact of lubricant, it is the *relative decrease in net power* obtained with $\kappa_{oil} = 5\%$ that is plotted in Fig. 4.25, with respect to the net power computed by considering pure cyclopentane properties.

One can observe that the decrease in net power due to the 5% oil mass fraction is larger when the heat input increases (i.e. when the exhaust mass flow and/or the exhaust temperature increase). This observation is in accordance with the results shown in the previous section, and is particularly true with $T_{air} = 15$°C and $T_{air} = 27$°C. In the case where the ambient air temperature is fixed to 40°C, an important power loss is noted at high exhaust temperature and $\dot{m}_{exh} \simeq 0.2$ kg/s, which is not explicable physically. This particular result comes probably from the behavior of the controller in these conditions.
In any case, the decrease in net power due to the presence of oil is relatively large, even with only a 5% oil mass fraction. This decrease tends to be more important when the ambient air temperature is reduced.

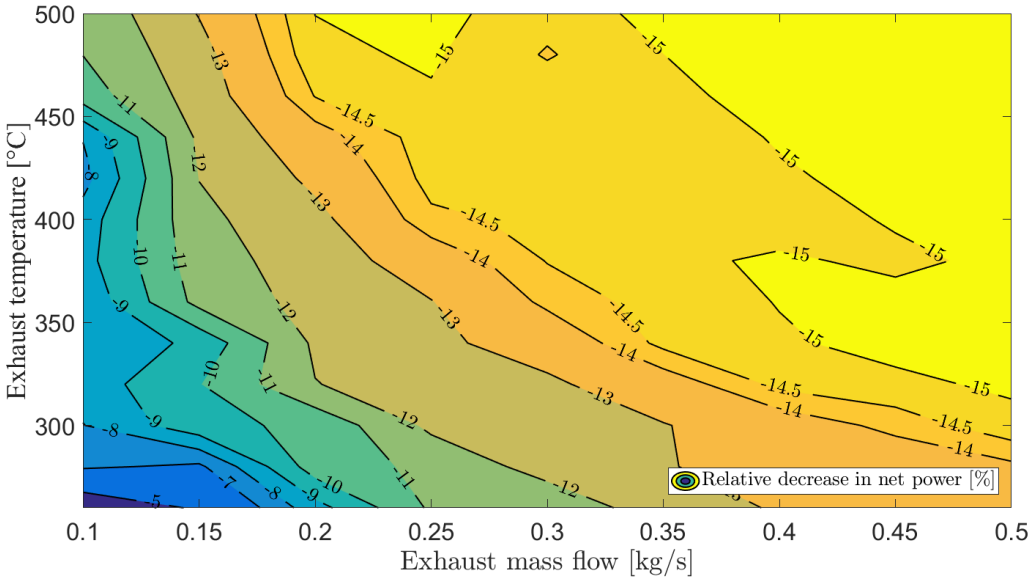

(a) Air temperature = 15°C

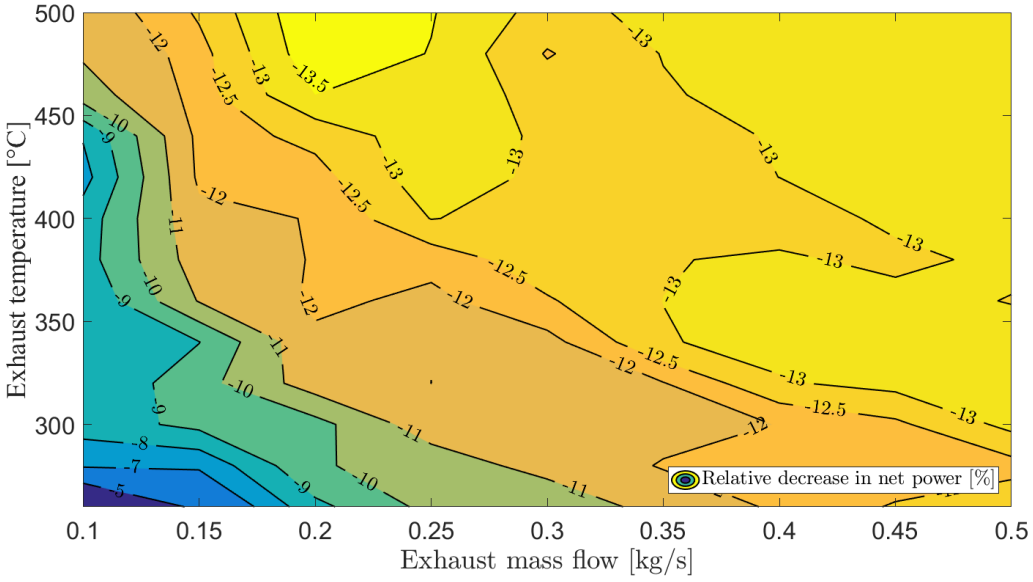

(b) Air temperature = 27°C

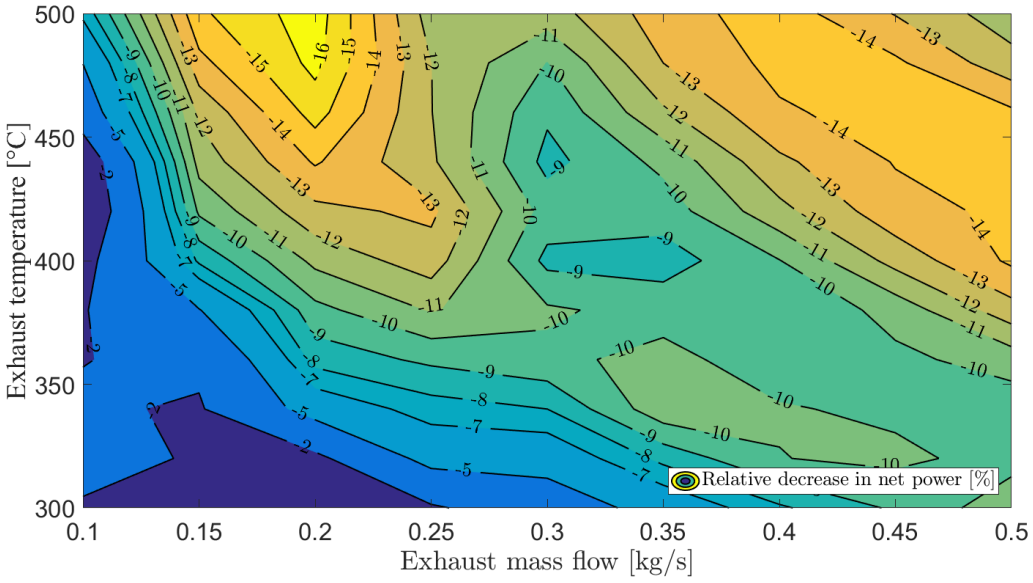

(c) Air temperature = 40°C

Figure 4.25: Relative decrease in net power obtained with $\kappa_{oil} = 5\%$, in comparison with net power calculated by assuming a pure working fluid ($\kappa_{oil} = 0\%$) as a function of exhaust conditions.

4.3.3 Evolution of steady performances with the super-heating set-point

In the steady-state simulations presented in the two previous sections, the set-point value of the super-heating (SH) at the expander inlet is fixed to 40 K. This large value is chosen to maximize the WF quality before entering the piston expander, to counteract the effect of lubricant which traps some liquid cyclopentane in liquid oil bubbles. However, it is interesting to study the impact of this set-point value on ORC performances. To this end, simulation results presented in this section are obtained with fixed exhaust conditions ($\dot{m}_{exh} = 0.2$ kg/s and $T_{exh} = 330$°C) and $T_{air} = 27$°C. The sub-cooling set-point is fixed to 9 K, and the simulation time remains equal to 1500 seconds.

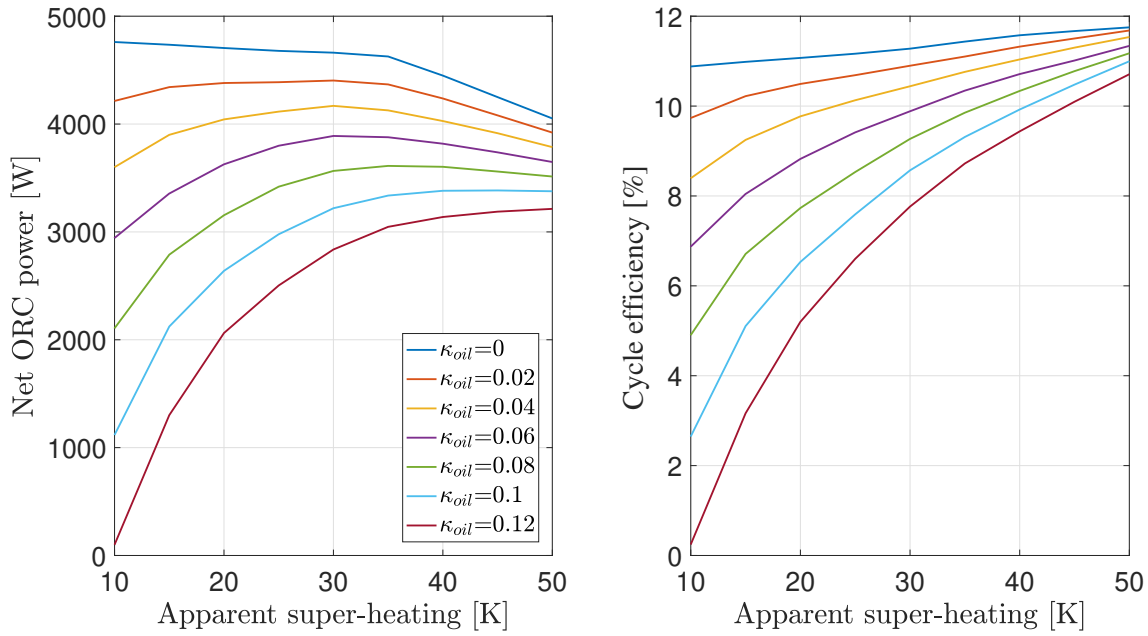

Figure 4.26: Evolution of net ORC power and cycle efficiency as a function of the apparent super-heating at the expander inlet, with $T_{exh} = 330$°C, $\dot{m}_{exh} = 0.2$ kg/s and $T_{air} = 300$ K.

The net ORC power and the cycle efficiency are represented in Fig. 4.26 for different oil circulation rates, as a function of the super-heating ranging from 10 to 50 K. However, one has to remind that these SH values, defined as the temperature rise above the saturation temperature of *pure* cyclopentane, corresponds only to an *apparent super-heating*. In fact, it is impossible to reach a WF quality equal to 1 as soon as the oil circulation rate is non-zero.

For each value of κ_{oil}, the cycle efficiency increases monotonically with the super-heating. However, it is rather the net power that is important to maximize in the case of ORC power systems, and one can observe that its evolution is more complex. In fact, when the super-heating is increased, the net power increases and tends to reach a maximum whose abscissa is different for each value of κ_{oil}. With pure WF, the maximum net power is already reached with the lowest set-point value. If κ_{oil} increases, the maximum of each net power curve moves to the right. For example, the maximum net power is obtained with a super-heating equal to 30 K if $\kappa_{oil} = 4\%$, and with a super-heating fixed to 35 K if $\kappa_{oil} = 8\%$. In other words, it is beneficial to increase the super-heating set-point as a function of the oil circulation rate, in order to maximize the net power produced by the Rankine box.

One can observe that the plot showing the evolution of the expander power (Fig. 4.27) is similar to the one presenting the net power: each curve exhibits a maximum which moves to the right if κ_{oil} increases. This result could be anticipated, since it has already been demonstrated that the expander power accounts for the most part of the net power evolution when the oil mass fraction varies. By contrast, the pump power decreases monotonically with the SH value.

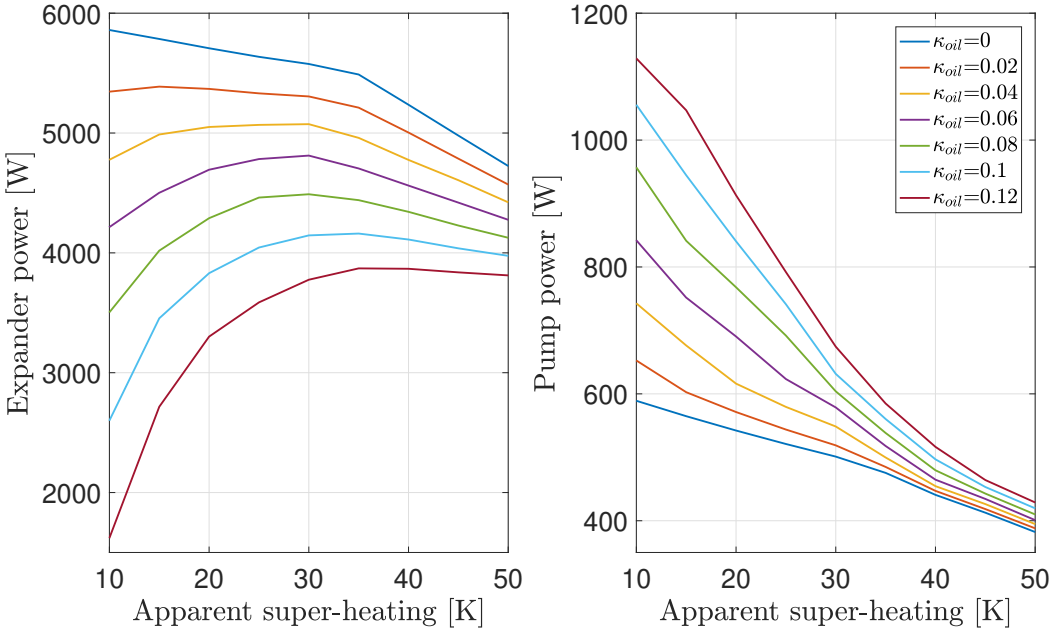

Figure 4.27: Evolution of expander and pump powers as a function of the apparent super-heating at the expander inlet, with $T_{exh} = 330°C$, $\dot{m}_{exh} = 0.2$ kg/s and $T_{air} = 300$ K.

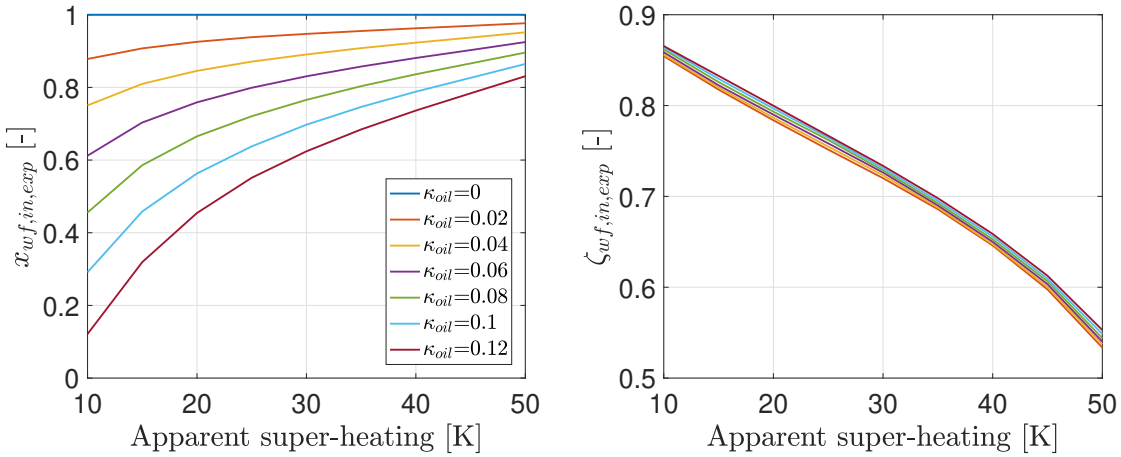

Figure 4.28: Evolution of the WF quality and WF fraction in the liquid phase at the expander inlet, as a function of the apparent super-heating at the expander inlet, with $T_{exh} = 330°C$, $\dot{m}_{exh} = 0.2$ kg/s and $T_{air} = 300$ K.

It can be verified that the WF quality at the inlet of the piston expander (Fig. 4.28) increases with the super-heating set-point, which is obviously the objective (i.e. increasing the WF quality aims to maximize the vapor WF mass flow through the expander). This outstanding increase is important to highlight, since it demonstrates that the WF quality can be drastically modified by varying the SH set-point, depending on the oil circulation rate.
However, it is not interesting to maximize the WF quality at the expander inlet since Figs. 4.26 and 4.27 shows that both expander and net powers reach a maximum for a given SH value, depending on κ_{oil}. In other words, the WF quality is not the only parameter that explains the evolution of the expander power. In fact, the total mixture mass flow (Fig. 4.29) has also an important impact: a decreasing total mass flow rate causes a reduction of the produced gross power.

As a consequence, the evolution of the expander power as a function of the SH value is the result of two opposite trends. The first one is the WF quality, which is monotonically increasing with the super-heating (Fig. 4.28). This phenomenon is beneficial for the expander power, since the expansion of the vapor mass flow is much more powerful than the one of the liquid flow. The second trend is the evolution of the mixture mass flow, which decreases monotonically with the SH value (Fig. 4.29) and leads to a reduced expander power. These two opposite trends, observed when the SH is increased, explain why it would be interesting to adjust the super-heating set-point as a function of the oil circulation rate, in order to maximize the ORC net power (Fig. 4.26).

The evolution of the mixture mass flow also causes the decrease in pump power (Fig. 4.27) when the SH value is increased: if the mixture mass that needs to be pumped per unit time decreases, the pump power is logically reduced.
As a reminder, the SH set-point at the outlet of the exhaust boiler is tracked by the controller which acts on the pump rotation speed, and thus can vary the mixture mass flow. For given exhaust conditions, the heat input that can be transferred in the boiler from exhaust gases to the WF is fixed. As a result, a larger super-heat at the boiler outlet is not possible without decreasing the mixture mass flow, which is illustrated by the left plot in Fig. 4.29.

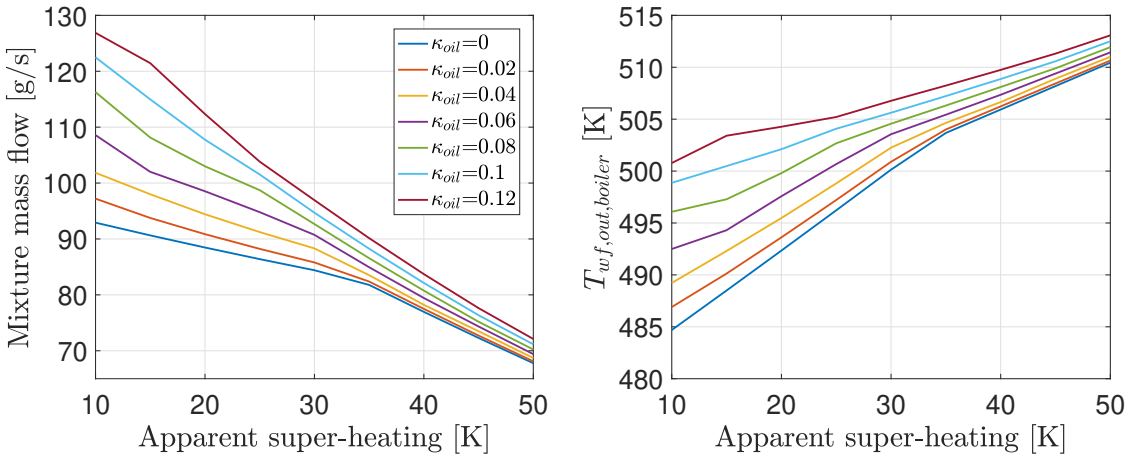

Figure 4.29: Evolution of mixture mass flow and mixture temperature at the expander inlet, as a function of the apparent super-heating at the expander inlet, with $T_{exh} = 330°C$, $\dot{m}_{exh} = 0.2$ kg/s and $T_{air} = 300$ K.

As shown on the right chart in Fig. 4.29, increasing the SH value induces logically an increase in mixture temperature at the outlet of the boiler (expander inlet). However, this temperature grows more slowly than the SH set-point because the evaporation pressure, and as a consequence the saturation temperature of pure WF, decrease when the SH value increases. It is in fact an indirect effect: the evaporation pressure is directly fixed proportionately to the total mass flow rate. As a result, the high-pressure level follows the same trend that this mass flow, which is reduced if the super-heating is increased.

Finally, Fig. 4.29 also suggests that the value of the SH set-point cannot be only fixed in order to maximize the net Rankine box power. In fact, the maximum temperature of cyclopentane is equal to 550 K, and its critical point temperature is 511.72 K. One can observe that this second temperature is easily reached with SH = 50 K. Moreover, the piston expander requires that the inlet fluid temperature does not exceed 530 K to guarantee safe operating conditions. But this temperature could be reached with certain exhaust conditions and an elevated SH set-point. As a result, the need to maximize the net power produced by the Rankine box is facing other technical requirements. In practice, the super-heating set-point would not be higher than 40 K (in accordance with previous studies conducted by *Volvo Trucks*), even with a very high oil circulation rate.

4.3.4 Transient simulations (FK road cycle)

In addition to steady-state results, the Frankfurt-Koblenz (FK) road cycle is simulated with a super-heating set-point equal to 40 K (and a sub-cooling fixed to 20 K) for different values of κ_{oil}. This road cycle was already introduced in Section 3.6.2 (Figs. 3.19 and 3.20), where transient simulations obtained with the new MB model are presented.

Fig. 4.30 shows the evolution of the net ORC power produced during a part of the FK cycle (from 1000 to 3000 seconds, which represents around 33 minutes). The result obtained by considering pure cyclopentane properties is compared to the simulations corresponding to $\kappa_{oil} = 5\%$ and 10%.

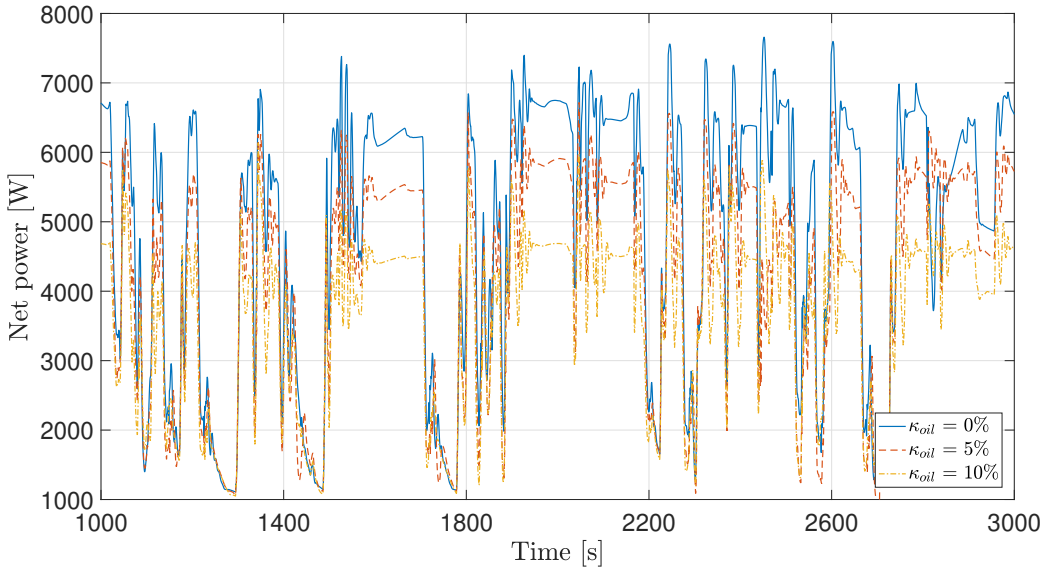

Figure 4.30: Evolution of the ORC net power during a part of the FK road cycle, for different κ_{oil}.

It can be observed that the decrease in net power is considerable if the lubricant added to WF is taken into account, especially if $\kappa_{oil} = 10\%$. However, the temporal evolution of the ORC net power seems to follow the same trend with or without lubricant, so that the transient behavior of the Rankine box is not particularly modified by the presence of oil in the working fluid.
The primary reason of the decrease in net power is obviously the reduced expander gross power when the oil circulation rate increases (Fig. 4.31). In addition, the increase in pump power consumption (Fig. 4.32) also causes a net power decrease, while the fan power consumption does not vary significantly with the value of κ_{oil}. These observations are in accordance with steady simulations presented in Section 4.3.1.

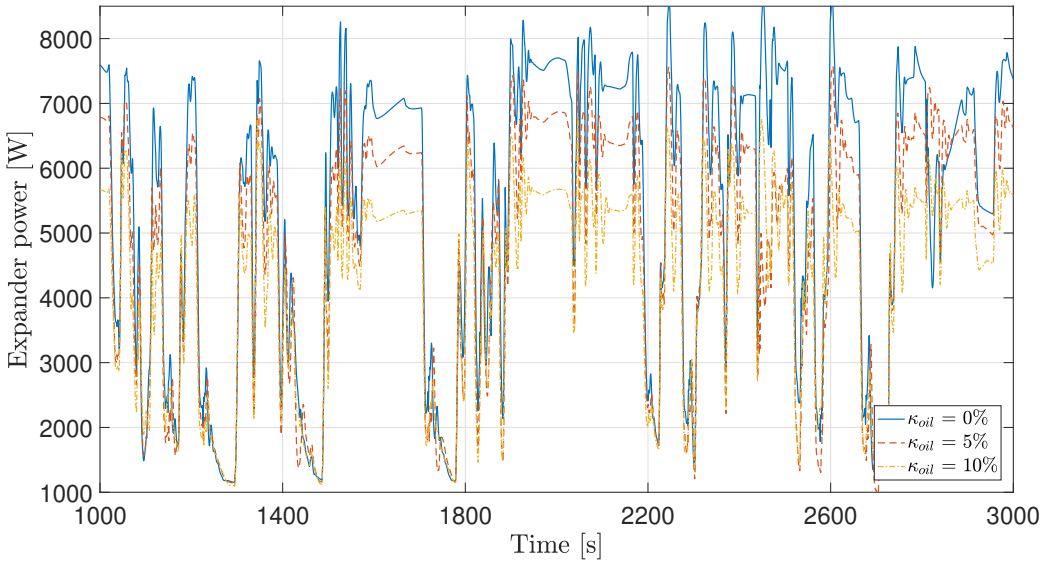

Figure 4.31: Evolution of the expander power during a part of the FK road cycle, for different κ_{oil}.

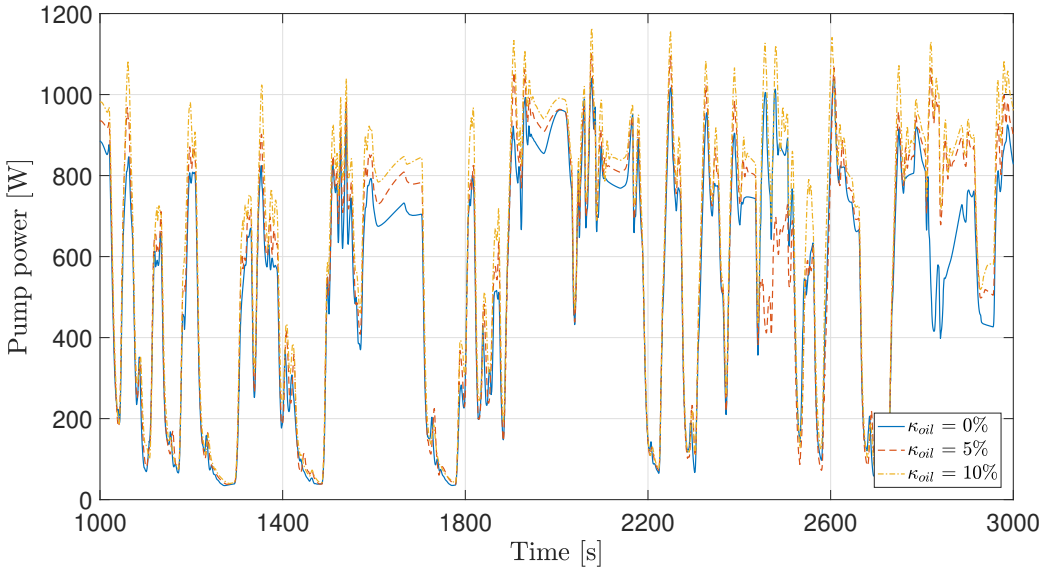

Figure 4.32: Evolution of the pump power during a part of the FK road cycle, for different κ_{oil}.

Similarly to steady simulations, the decrease in expander power is caused in part by the reduced WF quality at the expander inlet when the oil circulation rate increases (Fig. 4.33). On this figure, it can be seen that the fluid quality rarely exceeds 0.9 during the road cycle simulated with $\kappa_{oil} = 5\%$. Even with this relatively low oil mass fraction, the WF quality is thus greatly altered. This observation highlights once again the main negative impact of the lubricant added to the working fluid.
In order to reach the super-heating set-point (40 K) regardless the value of κ_{oil}, the mixture mass flow is higher if κ_{oil} increases (Fig. 4.34). This increase in mixture mass flow causes the higher pump power demand shown in Fig. 4.32.

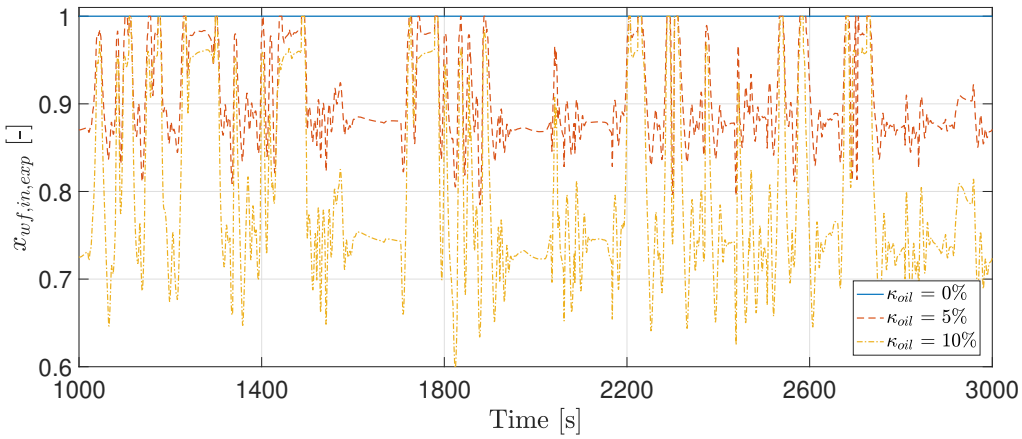

Figure 4.33: Evolution of the WF quality at the expander inlet during a part of the FK road cycle, for different κ_{oil}.

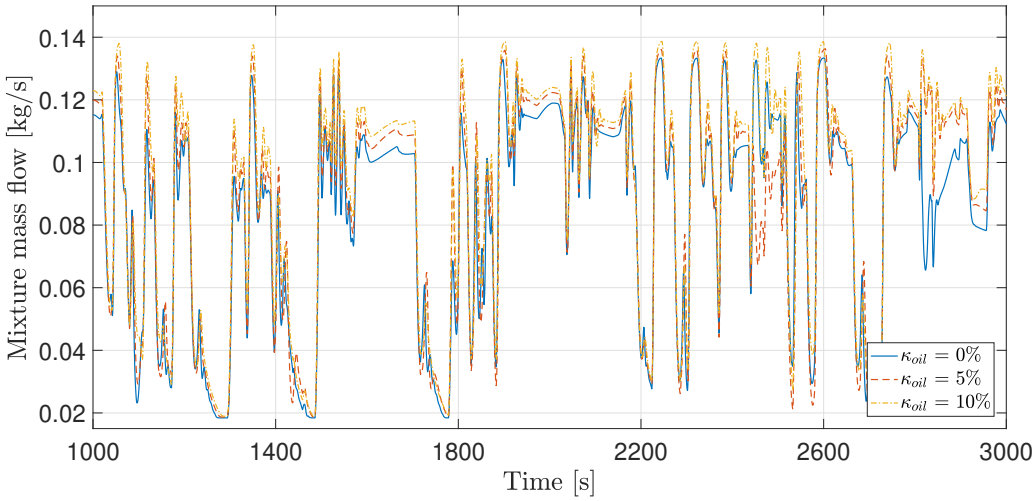

Figure 4.34: Evolution of the mixture mass flow during a part of the FK road cycle, for different κ_{oil}.

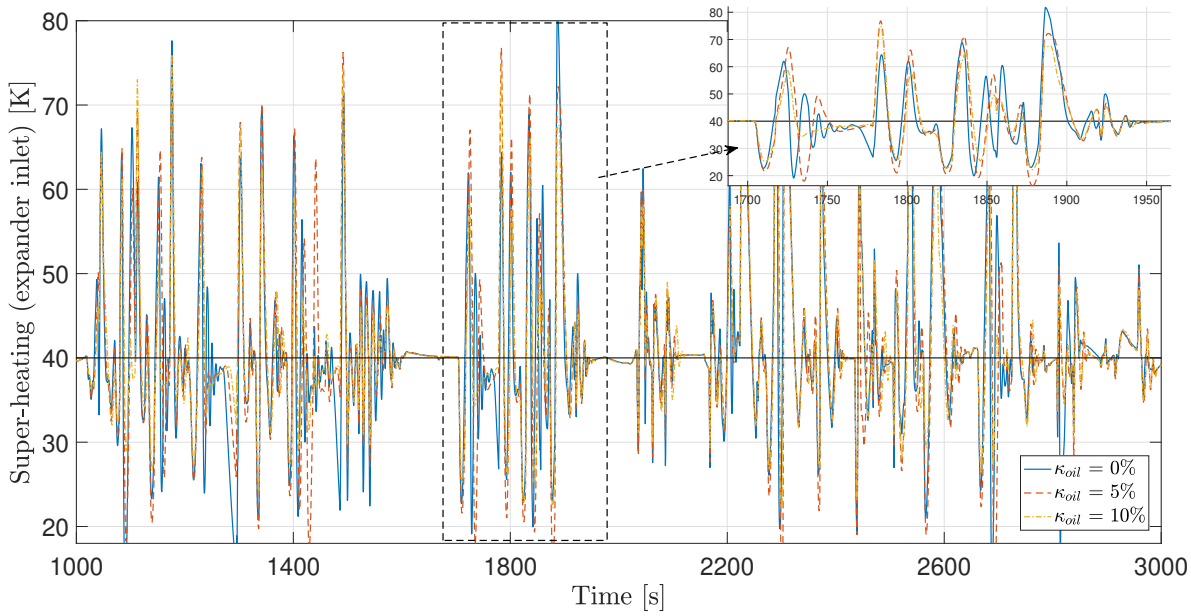

Figure 4.35: Evolution of the super-heating at the expander inlet (set-point = 40 K) during a part of the FK road cycle, for different κ_{oil}.

Simulation results presented in this section do not show that the presence of lubricant in the model modifies significantly transient characteristics of the Rankine box, especially concerning the expander and pump powers, as well as the fluid mass flow rate. In addition, it is interesting to analyze the tracking of the SH set-point at the expander inlet during the road cycle, with or without lubricant. This comparison is shown in Fig. 4.35.
Due to highly transient exhaust conditions during the FK cycle, SH is sometimes very far from the set-point value (40 K). But one can observe that, in general, the set-point is followed with the same precision regardless the value of κ_{oil}. However, one can see on the zoom (performed around $t = 1800$ s) that the temporal evolution of the super-heating is not exactly the same with $\kappa_{oil} = 0\%$, 5% or 10%. Variations around SH= 40 K are similar but exhibit certain differences at some points. However, it is impossible to conclude that the controller operates better with or without lubricant: some peaks are steeper with lubricant, but others are steeper without lubricant. As a result, it can be considered that transient simulations presented in this section do not show that modelling precisely the WF/oil mixture in the Rankine system induces significant modifications regarding transient behaviors of the box.

4.4 Conclusion

In the second part of this master thesis, the impact of lubricant added to the working fluid to ensure the lubrication of the piston expander is studied in detail. In fact, the Rankine model considers up to now thermodynamic properties of pure cyclopentane, while the oil circulation rate in the Rankine box can reach 10%. The need to model this lubricant is thus easily understood.
At first, the empirical solubility model used in this study is presented. Due to the Covid-19 pandemic, it was unfortunately impossible to fit this model with empirical results obtained directly by *Volvo trucks*. Moreover, empirical results are impossible to find in the literature for a mixture of cyclopentane and PAG oil. As a result, the empirical model is fitted with measurements corresponding to another hydrocarbon (propane R290) and a PAG oil that is less viscous than the one used by *Volvo Trucks* (empirical data from *Barbosa et al.*). This model, associated to an iterative algorithm, is exploited to compute thermodynamic properties of the cyclopentane/oil mixture from the knowledge of the pressure, the mixture enthalpy and the oil circulation rate in the Rankine box.

In addition to the mixture properties calculation, each component of the Rankine box model is improved to take into account the presence of oil. Heat transfer coefficients in the exchangers are modified according to correlations found in the literature. It is important to precise that the FV approach is chosen here to model heat exchangers, and not the new MB model presented in the previous chapter. Indeed, the direct impact of lubricant on saturation properties would complicate significantly the definition of zone boundaries. But a MB method modified to take into account the presence of oil is possible to develop, and could be the subject of further work.
Finally, the expander model is drastically revised in order to distinguish fictitiously the vapor and liquid mass flow rates through this component.

The complete Rankine box model adapted to deal with the presence of lubricant in WF is then exploited to perform steady-state and transient simulations. It is shown that the decrease in ORC net power when the oil circulation rate increases is significant and higher than anticipated. For example with $\kappa_{oil} = 5\%$, this relative decrease varies between 2% and 16%, depending on the exhaust conditions and the ambient air temperature. This loss of net power is mainly due to the dramatic decrease in expander power, but also to the increase in pump power. In fact, the expander gross power is reduced because the presence of oil prevents from reaching a WF quality equal to 1 at the expander inlet. Even with a large apparent superheat, a small part of cyclopentane remains trapped into liquid oil bubbles and cannot be vaporized. The vapor WF mass flow rate through the expander is thus reduced, and as a consequence

the expander power decreases. Obviously, this phenomenon is emphasized when the oil circulation rate increases, so that Rankine box performances deteriorate rapidly if a large amount of lubricant is added to cyclopentane.
On the other hand, the increase in pump power comes simply from the fact that the mixture mass flow rate increases with κ_{oil}. However, even if lubricant alters negatively the heat transfer coefficient on the WF side of each heat exchanger, simulations have shown that this impact does not have a significant effect on ORC performances.

The large set of steady simulations, performed for different exhaust conditions and ambient air temperature, has shown that the relative decrease in net power due to the presence of lubricant is higher if the heat input (proportional to the exhaust mass flow multiplied by the exhaust temperature) is large. Moreover, Rankine box performances are more deteriorated if the ambient air temperature is low.
Simulations carried out by varying the value of the super-heating set-point at the expander inlet highlight that, for a given oil circulation rate, it exists a set-point value which maximizes the net power produced by the Rankine box. In fact, the ideal set-point is a trade-off between to opposite trends: a low superheat enables to increase the mixture mass flow, while a large superheat tends to maximize the WF quality at the expander inlet. As a conclusion, it would be interesting to modify the Rankine box controller, in order to adjust the set-point value as a function of the oil mass fraction added to cyclopentane. This improvement is a perspective for further work. However, the super-heating set-point is also fixed in practice according to technical requirements regarding the expander, but also the working fluid itself.
Finally, transient simulations performed during the FK road cycle for different values of oil circulation rate have demonstrated that the lubricant does not have a notable impact on the transient behavior of the Rankine system.

It is important to highlight that the significant impact of lubricant on ORC performances is probably overestimated. In fact, the decrease in net power due to the presence of oil is generally much higher than anticipated. Indeed, the precision of simulation results presented in this study is not guaranteed: the Rankine box model is based on the empirical solubility model (to compute thermodynamic properties of the WF/oil mixture) that is fitted with empirical data coming from experiments conducted by *Barbosa et al.*. Their work is based on a mixture made of R290 (propane) and an ISO VG 22 PAG oil, while the Rankine system simulated here operates with cyclopentane and a more viscous lubricant (ISO VG 150 PAG oil). Even if propane and cyclopentane are both hydrocarbons, their physical characteristics are not similar. As a result, it is probable that mixture properties and composition are not precisely evaluated in the model, which could explain large decreases in net power, mainly coming from the working fluid quality at the expander inlet which is surprisingly very low when κ_{oil} is large. However, it was unfortunately impossible to perform ourselves experiments to fit the model with cyclopentane and the ISO VG 150 PAG oil.

To conclude, the Rankine box model developed in this study to model precisely the impact of lubricant on the system performances gives coherent results. However, it cannot be exploited without forgetting that the empirical solubility model is not calibrated with the good pair of working fluid and lubricant. Obviously, it would be very interesting in the future to improve this model by fitting it with empirical results obtained directly by *Volvo Trucks* with cyclopentane and PAG oil. Moreover, a comparison between the net power computed by simulations and performances obtained experimentally are necessary to validate definitely this new model, but it was unfortunately impossible in the scope of this master thesis. These perspectives are thus left for future work.

5 | Global conclusion

This internship at *Volvo Trucks* was dedicated to the modelling of the waste heat recovery system by means of organic Rankine cycle. This add-on component, called *Rankine box*, aims to recover thermal energy from exhaust gases to produce electricity on board. It is developed in the scope of the *Rankine Generation 3* project, in which this internship takes part. The complete Rankine system is modelled on *Matlab-Simulink*. The goal of this master thesis was to improve this model on two major aspects. This study is thus composed of two distinct parts conducted in parallel, presented in Chapters 3 and 4. Beforehand, Chapter 2 proposes a state of the art on ORC power systems for waste heat recovery.

At first, a new model of heat exchanger is developed using the moving boundaries approach. This method aims to be computationally more efficient than the previous model developed by *Volvo Trucks*, which is based on a spatial discretization of the exchangers into a large number of control volumes. In fact, the new MB model only considers at most three distinct zones that are defined as a function of the working fluid state in the exchanger (liquid, two-phase or vapor). This new model is then used to model the exhaust boiler as well as the air condenser in the complete ORC model. In addition, the controller associated to the Rankine system is also adapted, since the new model does not have exactly the same transient behavior than the previous one.
It is shown that the MB approach gives good results regarding both steady-state and transient simulations. Moreover, this model is very efficient: it enables to decrease by 72% the CPU time required to perform simulations along a driving cycle.

The second part of this master thesis is dedicated to the modelling of the mixture composed of cyclopentane and lubricant which performs the Rankine cycle. Indeed, pure cyclopentane properties were assumed up to now in the model, while the oil circulation rate in this system could exceed 10% in practice. This study shows that the impact of lubricant on ORC performances is significant. Indeed, when the fluid is vaporized, a small part of liquid cyclopentane remains always trapped into the liquid oil bubbles. As a result, it is impossible to reach a fluid quality equal to 1 at the expander inlet, which causes a large decrease in expander power. An increase in pump power when oil is added to the fluid is also observed, so that the net produced power is considerably altered. For example, an oil circulation rate equal to 5% causes a decrease in net power varying between 2% and 16%, depending on exhaust conditions and ambient air temperature.
This study also demonstrates the interest of varying the super-heating set-point at the expander inlet as a function of the oil circulation rate, in order to maximize the expander power.

These two topics studied in parallel during this master thesis represent significant improvements of the Rankine box model. It was unfortunately impossible to exploit empirical results due to the Covid-19 pandemic, so that this internship is totally focused on simulations. However, comparison between the simulation results presented in this study and empirical measurements would be a very interesting perspective for further work. At first, the new MB heat exchanger model could be validated definitely. In addition, the solubility model chosen to represent the mixture between working fluid and lubricant could

be fitted with empirical data obtained directly by *Volvo Trucks*. Indeed, the precision of this model would be improved if empirical results corresponding to cyclopentane and PAG oil are exploited, instead of the results used in this study that were obtained with propane.

The two parts of this work could also be combined in the same Rankine box model, where heat exchangers are modelled with the moving boundaries approach and the presence of lubricant into the working fluid is also taken into account. To this end, it is necessary to adapt the MB heat exchanger model developed in this study. Indeed, this one is only able to deal with a pure working fluid, and not a WF/oil mixture. It was not necessary to perform these modifications in the scope of this master thesis, so that this improved model is considered as a perspective for future work. However, it is already possible to highlight some aspects of this MB model that would be adapted to consider the mixture.
At first, the zone where WF is in the vapor state will be no more necessary, since the presence of oil prevents from vaporizing completely the working fluid. It means that the exchanger model will be only composed of two zones (liquid and two-phase). Moreover, the definition of the boundary between these two zones should also be modified. Indeed, the lubricant impacts saturation properties so that the bubble point is reached for a temperature higher than the saturation temperature of pure cyclopentane. In addition, the mixture enthalpy defining the transition between liquid and two-phase zones would become a function of the oil circulation rate in the Rankine box.
This new model would also compute the convective heat transfer coefficient depending on the lubricant mass fraction. For this purpose, correlations presented in this study and applied in the FV heat exchanger model could be still employed. Moreover, equations describing mass and energy exchanges between adjacent zones would also be modified to take into account the oil circulation rate.

Bibliography

[1] "European Commission for Energy, Climate change and Environment - reducing co2 emissions from heavy-duty vehicles." https://ec.europa.eu/clima/policies/transport/vehicles/heavy_en. Accessed: 2020-03-25.

[2] F. Rodriguez and O. Delgado, "Co2 emissions and fuel consumption standards for heavy-duty vehicles in the european union," 05 2018.

[3] B. Xu, D. Rathod, A. Yebi, Z. Filipi, S. Onori, and M. Hoffman, "A comprehensive review of organic rankine cycle waste heat recovery systems in heavy-duty diesel engine applications," *Renewable and Sustainable Energy Reviews*, vol. 107, pp. 145–170, 03 2019.

[4] A. Legros, G. Ludovic, M. Diny, Z. Hamid, and V. Lemort, "Comparison and impact of waste heat recovery technologies on passenger car fuel consumption in a normalized driving cycle," *Energies*, vol. 7, pp. 5273–5290, 08 2014.

[5] N. Espinosa, M. Lazard, L. Aixala, and H. Scherrer, "Modeling a thermoelectric generator applied to diesel automotive heat recovery," *Journal of Electronic Materials*, vol. 39, pp. 1446–1455, 09 2010.

[6] J. Liu, J. Fu, C. Ren, L. Wang, Z. Xu, and B. Deng, "Comparison and analysis of engine exhaust gas energy recovery potential through various bottom cycles," *Applied Thermal Engineering*, vol. 50, no. 1, pp. 1219 – 1234, 2013.

[7] R. Saidur, M. Rezaei, W. Muzammil, M. Hassan, S. Paria, and M. Hasanuzzaman, "Technologies to recover exhaust heat from internal combustion engines," *Renewable and Sustainable Energy Reviews*, vol. 16, no. 8, pp. 5649 – 5659, 2012.

[8] D. Arias, T. Shedd, and R. Jester, "Theoretical analysis of waste heat recovery from an internal combustion engine in a hybrid vehicle," 04 2006.

[9] S. Quoilin, M. V. D. Broek, S. Declaye, P. Dewallef, and V. Lemort, "Techno-economic survey of organic rankine cycle (orc) systems," *Renewable and Sustainable Energy Reviews*, vol. 22, pp. 168 – 186, 2013.

[10] S. Quoilin, *Sustainable Energy Conversion Through the Use of Organic Rankine Cycles for Waste Heat Recovery and Solar Applications.* PhD thesis, Energy systems Unit, Aerospace and Mechanical engineering departement, University of Liege, 2011.

[11] T. Horst, W. Tegethoff, P. Eilts, and J. Koehler, "Prediction of dynamic rankine cycle waste heat recovery performance and fuel saving potential in passenger car applications considering interactions with vehicles' energy management," *Energy Conversion and Management*, vol. 78, p. 438–451, 02 2014.

[12] F. Bettoja, A. Perosino, V. Lemort, G. Ludovic, T. Reiche, and T. Wagner, "Nowaste: Waste heat re-use for greener truck," *Transportation Research Procedia*, vol. 14, pp. 2734–2743, 12 2016.

[13] V. Chintala, S. Kumar, and J. K. Pandey, "A technical review on waste heat recovery from compression ignition engines using organic rankine cycle," *Renewable and Sustainable Energy Reviews*, vol. 81, pp. 493 – 509, 2018.

[14] V. Grelet, T. Reiche, V. Lemort, M. Nadri, and P. Dufour, "Transient performance evaluation of waste heat recovery rankine cycle based system for heavy duty trucks," *Applied Energy*, vol. 165, pp. 878 – 892, 2016.

[15] F. Galuppo, M. Nadri, P. Dufour, T. Reiche, and V. Lemort, "Assessment of rankine wast heat recovery potential on heavy duty trucks using direct condensation," *5th International Seminar on ORC Power Systems, Athens, Greece*, 2019.

[16] H. Marlok, A. Pfeifer, M. Hotger, and M. Bucher, "White paper: Modular waste heat recovery system with electric power output," tech. rep., Mahle - ATZ Heavyduty worldwide, February 2019.

[17] V. Grelet, V. Lemort, M. Nadri, P. Dufour, and T. Reiche, "Waste heat recovery Rankine cycle based system modeling for heavy duty trucks fuel saving assessment," in *Proceedings of the 3RD International Seminar on Organic Rankine Cycle (ORC) Power Systems*, vol. paper 67, (Brussels, Belgium), ASME ORC Brussels, 2015.

[18] F. Galuppo, M. Nadri, P. Dufour, T. Reiche, and V. Lemort, "Evaluation of a coupled organic rankine cycle mild hybrid architecture for long-haul heavy-duty truck ∗∗the french ministry of higher education and research is acknowledged for the financial support of this cifre phd thesis 2016/1205.," *IFAC-PapersOnLine*, vol. 52, no. 5, pp. 478 – 483, 2019. 9th IFAC Symposium on Advances in Automotive Control AAC 2019.

[19] N. Espinosa, L. Tilman, V. Lemort, S. Quoilin, and B. Lombard, "Rankine cycle for waste heat recovery on commercial trucks: approach, constraints and modelling," 05 2010.

[20] D. Di Battista, M. Di Bartolomeo, C. Villante, and R. Cipollone, "On the limiting factors of the waste heat recovery via orc-based power units for on-the-road transportation sector," *Energy Conversion and Management*, vol. 155, pp. 68–77, 01 2018.

[21] C. Katsanos, D. Hountalas, and E. Pariotis, "Thermodynamic analysis of a rankine cycle applied on a diesel truck engine using steam and organic medium," *Energy Conversion and Management*, vol. 60, pp. 68 – 76, 2012. Special issue of Energy Conversion and Management dedicated to ECOS 2011 - the 24th International Conference on Efficiency, Costs, Optimization, Simulation and Environmental Impact of Energy Systems.

[22] T. Tartière and M. Astolfi, "A world overview of the organic rankine cycle market," *Energy Procedia*, vol. 129, pp. 2 – 9, 2017. 4th International Seminar on ORC Power Systems.

[23] A. Desideri, *Dynamic modeling of Organic Rankine cycle power systems*. PhD thesis, University of Liege, Thermodynamics Laboratory, Aerospace and Mechanical engineering departement, 2016.

[24] R. Dickes, O. Dumont, R. Daccord, S. Quoilin, and V. Lemort, "Modelling of organic rankine cycle power systems in off-design conditions: an experimentally-validated comparative study," *Energy*, vol. 123, pp. 710 – 727, 2017.

[25] A. Desideri, B. Dechesne, J. Wronski, M. Van den Broek, S. Gusev, V. Lemort, and S. Quoilin, "Comparison of moving boundary and finite-volume heat exchanger models in the modelica language," *Energies*, vol. 9, p. 339, 05 2016.

[26] R. Majumdar, S. Singh, and S. K. Saha, "Quasi-steady state moving boundary reduced order model of two-phase flow for orc refrigerant in solar-thermal heat exchanger," *Renewable Energy*, vol. 126, pp. 830 – 843, 2018.

[27] E. Feru, B. de Jager, F. Willems, and M. Steinbuch, "Two-phase plate-fin heat exchanger modeling for waste heat recovery systems in diesel engines," *Applied Energy*, vol. 133, pp. 183 – 196, 2014.

[28] B. Rasmussen, R. Shah, A. Musser, A. Alleyne, C. Bullard, P. Hrnjak, and N. Miller, "Control-oriented modeling of transcritical vapor compression systems," 01 2004.

[29] R. Sangi, P. Jahangiri, and D. Mueller, "A combined moving boundary and discretized approach for dynamic modeling and simulation of geothermal heat pump systems," *Thermal Science and Engineering Progress*, vol. 9, 12 2018.

[30] D. Kim, D. Ziviani, J. E. Braun, and E. A. Groll, "A moving boundary modeling approach for heat exchangers with binary mixtures," *Energy Procedia*, vol. 129, pp. 466 – 473, 2017. 4th International Seminar on ORC Power SystemsSeptember 13-15th 2017 Politecnico di Milano, Italy.

[31] C. Cuevas, J. Lebrun, V. Lemort, and P. Ngendakumana, "Development and validation of a condenser three zones model," *Applied Thermal Engineering*, vol. 29, no. 17, pp. 3542 – 3551, 2009.

[32] V. Grelet, *Rankine cycle based waste heat recovery system applied to heavy duty vehicles: topological optimization and model based control*. PhD thesis, Universy of Lyon and University of Liege, Aerospace and Mechanical engineering departement, 2016.

[33] I. Vaja, *Definition of an object oriented library for the dynamic simulation of advanced energy systems: Methodologies, Tools and Applications to Combined ICE-ORC Power Plants.* PhD thesis, University of Parma, 2009.

[34] M. Graber, N. C. Strupp, and W. Tegethoff, "Moving boundary heat exchanger model and validation procedure," *1TU Braunschweig, Inst. f. Thermodynamik*, 2010.

[35] H. Qiao, C. Laughman, V. Aute, and R. Radermacher, "An advanced switching moving boundary heat exchanger model with pressure drop," *International Journal of Refrigeration*, vol. 65, pp. 154–171, 05 2016.

[36] T. Horst, H. Rottengruber, M. Seifert, and J. Ringler, "Dynamic heat exchanger model for performance prediction and control system design of automotive waste heat recovery systems," *Applied Energy*, vol. 105, p. 293–303, 05 2013.

[37] I. H. Bell, S. Quoilin, E. Georges, J. E. Braun, E. A. Groll, W. T. Horton, and V. Lemort, "A generalized moving-boundary algorithm to predict the heat transfer rate of counterflow heat exchangers for any phase configuration," *Applied Thermal Engineering*, vol. 79, pp. 192 – 201, 2015.

[38] D. Li, K. Luo, and J. Dang, "A moving boundary model for two-phase flow heat exchanger incorporated with relative velocities between boundaries and fluid," *International Journal of Heat and Mass Transfer*, vol. 95, pp. 35 – 44, 2016.

[39] F. P. Incropera and D. P. DeWitt, *Fundamentals of Heat and Mass Transfer*. New York City, New York: John Wiley & Sons, Inc., 4th edition ed., 1996.

[40] S. Zivi, "Discussion: "Estimation of Steady-State Steam Void-Fraction by Means of the Principle of Minimum Entropy Production" (Zivi, S. M., 1964, ASME J. Heat Transfer, 86, pp. 247–251)," *Journal of Heat Transfer*, vol. 86, pp. 251–252, 05 1964.

[41] J. Jensen, *Dynamic Modeling of ThermoFluid Systems*. PhD thesis, 2003.

[42] M. Kærn, B. Elmegaard, and L. Larsen, "Experimental comparison of the dynamic evaortor response using homogeneous and slip flow modeling," pp. 246–255, 06 2011.

[43] M. Shah, "A general correlation for heat transfer during film condensation inside pipes," *International Journal of Heat and Mass Transfer*, vol. 22, no. 4, pp. 547 – 556, 1979.

[44] S. Skogestad, "Tuning for smooth pid control with acceptable disturbance rejection," *Industrial & Engineering Chemistry Research - IND ENG CHEM RES*, vol. 45, 10 2006.

[45] R. Dickes, O. Dumont, and V. Lemort, "Lubricating oil entrainment in an orc system and its impact on performance rating," 09 2018.

[46] P. Popovic, *Investigation and analysis of lubricant effects on the performance of an HFC-134a refrigeration system*. PhD thesis, Iowa State University, 1999.

[47] J. Yang, B. Yu, Z. Ye, J. Shi, and J. Chen, "Experimental investigation of the impact of lubricant oil ratio on subcritical organic rankine cycle for low-temperature waste heat recovery," *Energy*, vol. 188, p. 116099, 2019.

[48] "Refprop, nist reference fluid thermodynamic and transport properties database." `https://www.nist.gov/srd/refprop`. Accessed: 2020-05-11.

[49] M. Youbi-Idrissi, *Impact de l'huile de lubrification sur les performances thermodynamiques des pompes à chaleur réversibles*. PhD thesis, Conservatoire national des arts et metiers - CNAM, 2003.

[50] V. Zhelezny, Y. Semenyuk, S. Ancherbak, A. Grebenkov, and O. Beliayeva, "An experimental investigation and modelling of the solubility, density and surface tension of 1,1,1,3,3-pentafluoropropane (r-245fa)/synthetic polyolester compressor oil solutions," *Journal of Fluorine Chemistry*, vol. 128, no. 9, pp. 1029 – 1038, 2007.

[51] R. Dickes, *Charge-sensitive methods for the off-design performance characterization of organic Rankine cycle (ORC) power systems*. PhD thesis, Thermodynamics Laboratory, Aerospace and Mechanical engineering departement, University of Liege, 2019.

[52] J. Grebner, "The effects of oil on the thermodynamic properties of dichlorodifluoromethane (r-12) and tetrafluoroethane (r-134a)," 01 1992.

[53] R. S. Ge Totten, Sr Westbrook, *Fuels and lubricants handbook: technology, properties, performance and testing*. George E. Totten edition, 2003.

[54] M. A. Marcelino Neto and J. Barbosa Jr, "Solubility, density and viscosity of a mixture of r-600a and polyol ester oil," *International Journal of Refrigeration*, vol. 31, pp. 34–44, 01 2008.

[55] M. A. M. Neto and J. R. Barbosa, "Solubility, density and viscosity of mixtures of isobutane (r-600a) and a linear alkylbenzene lubricant oil," *Fluid Phase Equilibria*, vol. 292, no. 1, pp. 7 – 12, 2010.

[56] B. Shen and E. A. Groll, "Review article: A critical review of the influence of lubricants on the heat transfer and pressure drop of refrigerants, part 1: Lubricant influence on pool and flow boiling," *HVAC&R Research*, vol. 11, no. 3, pp. 341–359, 2005.

[57] B. Shen and E. A. Groll, "Review article: A critical review of the influence of lubricants on the heat transfer and pressure drop of refrigerants—part ii: Lubricant influence on condensation and pressure drop," *HVAC&R Research*, vol. 11, no. 4, pp. 511–526, 2005.

[58] J. Baustian and M. Pate, "Properties of oil-refrigerant mixtures with application to oil concentration measurement: Part i: Thermophysical and transport properties," *ASHRAE Trans*, vol. 92, pp. 55–73, 1986.

[59] S. Quoilin, A. Desideri, J. Wronski, I. Bell, and V. Lemort, "Thermocycle - a modelica library for the simulation of thermodynamic systems," *University of Liège, Energy Systems Research Unit, Belgium*, 2010.

[60] D. Luong and T. Tsao, "Transient dynamics modeling and control for waste heat recovery of heavy duty diesel powertrain," *Volvo-UCLA Research group*, 2010.